

Use of *SOLIS* Satellite-based Solar Spectral
Irradiance for Characterization of Thin Film
Photovoltaic Modules

by

Diego Alejandro Sanchez Herrera

Date and Place of Birth:

July 18 1978 in Bucaramanga, Colombia

Master Thesis

Requisite for the Obtention of the MSc. Title in the
POSTGRADUATE PROGRAMME RENEWABLE ENERGY

Energy and Semiconductor Research Laboratory (EHF)
Department of Physics
Faculty of Mathematics & Natural Sciences
Carl von Ossietzky Universitaet Oldenburg
Oldenburg, Germany

Date of Examination: July 2007

1. Examiner: Dr. Prof. Hans Georg Beyer
2. Examiner: Dr. Konrad Blum

I HEREBY STATE THAT

this thesis entitled

*Use of SOLIS Satellite-based Solar Spectral Irradiance for
Characterization of Thin Film Photovoltaic Modules*

is the result of my work, using only the quoted resources.

Diego Alejandro Sanchez Herrera

Augsburg, Germany

July 18 2007

Table of Contents

1	Introduction	1
2	The Satellite-based Spectral Data: <i>SOLIS</i>	5
2.1	The Clear Sky Module	5
2.1.1	The Radiative Transfer Model: <i>libRadtran</i>	7
2.2	The Cloud Module	9
2.3	The Quality of the Data	9
3	Photovoltaic Modules Used and the I_{sc} Measurements	11
3.1	The Photovoltaic Modules	11
3.1.1	<i>a-Si Tianjin Jinneng</i>	12
3.1.2	<i>CdTe First Solar FS-62</i>	12
3.1.3	<i>c-Si Hyundai HiS-M188SF</i>	15
3.2	The Ground Measurements	16
3.2.1	Temperature Effects on the I_{sc} and G Measurements	18
3.2.2	Other Considerations about the Measurements	21
4	The Spectral Parameters <i>SPARs</i>	23
4.1	The Data Used for the <i>SPARs</i> Analysis	24
4.2	Average-Photon Energy <i>APE</i>	26
4.2.1	Calculation of <i>APE</i> with <i>SOLIS</i> Spectral Data.	28
4.2.2	Understanding <i>APE</i>	30

4.2.3	Plots of <i>SOLIS</i> Spectra and <i>SOLIS APE</i>	34
4.3	<i>Used Fraction or Broad Band Photoelectrical Efficiency UD</i>	38
4.3.1	<i>Used Fraction UD</i> Analysis	42
4.4	Modified Irradiances	48
4.4.1	Modified Irradiances and Linearity	51
4.5	Proposed Spectral Models	54
5	RESULTS: The Short Circuit Current Models	59
5.1	I_{sc} Temperature Model	61
5.1.1	Results of the Application of the Temperature Model	62
5.2	Spectral Effects	68
5.3	Application of the I_{sc} Spectral Models	77
6	CONCLUSIONS	83
6.1	The Spectral Parameters <i>UD</i> and <i>APE</i>	83
6.2	Modified Irradiances	86
6.3	Spectral Effects on <i>PV</i> Devices	86
6.3.1	Predictions Based on <i>SOLIS</i> Spectral Irradiance	86
6.3.2	Spectral Effects on the Measured Data	87
6.4	<i>SOLIS</i>	89
6.5	Final Comments and Suggestions	90
A	Short Recapitulation on the Solar Spectrum	91
A.1	Standard Spectra	93
B	Other Plots for the Data Sets Used for the Short Circuit Current Modeling	95
C	Abbreviations	103

List of Figures

2.1	Modified Lambert-Beer curves	8
3.1	Spectral Response Used for <i>a-Si</i> Modules	13
3.2	Spectral Response of <i>CdTe</i> Modules	15
3.3	Spectral Response Used for <i>c-Si</i> Module	16
3.4	Relative Spectral Responses Overlapped	17
3.5	Measurement Setup	18
3.6	Data Acquisition Setup	19
3.7	Panoramic of Measurement Site with Sun's Path	20
3.8	Abnormal Behaviour April 2007	22
4.1	Global Irradiance Time Series: <i>SOLIS</i> and <i>SOLIS</i> Integrated	25
4.2	Solar Elevation vs UTC.	25
4.3	Solar Azimuth φ_s vs UTC.	25
4.4	Irradiance dependence on Sun Elevation and Sun Azimuth.	27
4.5	<i>APE</i> Calculation.	29
4.6	<i>APE</i> vs G_{solis} groups k^*	36
4.7	<i>APE</i> vs γ_s	36
4.8	<i>APE</i> vs γ_s and φ_s	37
4.9	<i>APE</i> vs G_{solis} groups γ_s	37
4.10	Different <i>SOLIS</i> Spectra for fixed Global Broad Band Irradiance	39
4.11	Different <i>SOLIS</i> Spectra for fixed Clear Sky Index	39

4.12 UD vs G_{solis} and APE for $a\text{-Si}$, $CdTe$ and $c\text{-Si}$	43
4.13 Sun as Black Body and Spectral Responses	45
4.14 <i>SOLIS</i> Spectra with Spectral Responses Overlapped	46
4.15 Modified Irradiances $APExG$ and $UDxG$	50
5.1 Data Flow in I_{sc} Modeling	60
5.2 I_{sc} vs G Applying Temperature Model.	62
5.3 I_{sc}/G vs G Applying Temperature Model.	63
5.4 I_{sc25}/G vs T and γ_s Measured Irradiance.	65
5.5 I_{sc} vs G_{solis} Applying Temperature Model.	66
5.6 I_{sc}/G vs G Applying Temperature Model	67
5.7 I_{sc25}/G and I_{sc25}/G_{solis} vs UD	73
5.8 Data Bins for I_{sc25}/G and I_{sc25}/G_{solis} vs UD	74
5.9 UD vs APE	75
5.10 I_{sc25} vs G_{ud}	76
5.11 I_{sc25}/G_{ud} vs G and $I_{sc25}/G_{udsolis}$ vs G_{solis}	79
A.1 Extraterrestrial Solar spectrum.	92
A.2 Influence of Atmosphere on Solar Spectrum.	92
A.3 <i>ASTM 1.5D</i> and <i>ASTM 1.5G</i> Spectra.	94
B.1 γ_s Time series	96
B.2 G_{solis} vs G	97
B.3 APE and UD vs G and G_{solis}	98
B.4 G_{ud} vs G	99
B.5 $APExG$ vs G	100
B.6 I_{sc25}/G and I_{sc25}/G_{solis} vs APE	101
B.7 Data Bins for I_{sc25}/G and I_{sc25}/G_{solis} vs APE	102

List of Tables

3.1	<i>PV</i> -Modules' electro-technical features	12
4.1	Influence of Wavelength Integration Limits on <i>APE</i> values	30
4.2	<i>APE</i> Reddening of Spectra for Fixed G	40
4.3	<i>APE</i> Reddening of Spectra for Fixed k^*	40
4.4	<i>UD</i> Reddening of Spectra for Fixed G	45
4.5	<i>UD</i> Reddening of Spectra for Fixed k^*	45
4.6	Fits for model $APE \times G$ vs G and $UD \times G$ vs G for <i>a-Si</i>	55
4.7	Fits for models $UD \times G$ vs G for <i>CdTe</i> and for <i>c-Si</i>	55
4.8	Calculated Relative Dispersion of k^* Groups due to Spectral Effects	55
5.1	Fits I_{sc} vs G and I_{sc} vs G_{solis} k^* groups for <i>a-Si</i>	71
5.2	Fits I_{sc} vs G and I_{sc} vs G_{solis} k^* groups for <i>c-Si</i>	71
5.3	Goodness of Fits for Modeled I_{sc} for <i>a-Si</i> . Measured irradiance.	80
5.4	Goodness of Fits for Modeled I_{sc} for <i>a-Si</i> . <i>SOLIS</i> irradiance	80
5.5	Goodness of Fits for Modeled I_{sc} for <i>c-Si</i> . Measured irradiance.	80
5.6	Goodness of Fits for Modeled I_{sc} for <i>c-Si</i> . <i>SOLIS</i> irradiance	80
A.1	Attenuation Processes in Atmosphere	93
A.2	Standard Spectra According to <i>CIE</i> and <i>ASTM</i>	94

Abstract

The aim of this thesis is the outdoor characterization of *PV* modules using spectral irradiance data. This data is calculated on the basis of the coupling of satellite meteorological information with a radiative transfer model. Measurements of the characteristic curves of a poly-crystalline Silicon *c-Si* and an amorphous Silicon module *a-Si* are performed on horizontal surface. A third intermediate technology *CdTe* is characterized theoretically. Measurements of global broad band irradiance are performed also on horizontal surface. The characterization of the modules is based on the modeling of the short circuit current I_{sc} as function global broad band irradiance and the inclusion of spectral parameters.

For spectral analysis we have at hand two spectral parameters in the form of positive real numbers: The *Average Photon Energy APE* and the *Used Fraction UD*. The first parameter is a pure descriptor of the spectral variations of the spectrum of the Sun, while the second considers the influence of the spectral fluctuations coupled to the spectral response of the *PV* device under investigation. The *APE* parameter is calculated only with the satellite-based spectral irradiance, while *UD* requires the spectral irradiance and the spectral response of the *PV* device. Another parameter, which resulted particularly useful for understanding the previous parameters is the *Clear Sky Index k** calculated from the satellite based *Cloud Index n*.

In this first attempt to use satellite-based irradiance for modeling short circuit current, many relevant aspects were investigated, which will help to define future approaches to model *PV* devices, not only in the cases of using irradiance data based on satellite information.

Acknowledgements

I want to express my gratitude to several persons who collaborated in the completion of this thesis:

To *Meteocontrol GmbH* for supporting this research project, especially to Dipl. Ing. (FH) Stefan Bofinger. In Oldenburg University to Dr. Elke Lorenz for her devoted assistance and fruitful discussions; equally to Dr. Annette Hammer. Also to my colleague MSc. Mauricio Rojas and Dipl. Phys. Udo Kulchewski for their willingness to discuss basic aspects of this work. To *First Solar GmbH* for kindly providing the *CdTe* modules.

Chapter 1

Introduction

The efficiency of *photovoltaic (PV)* modules changes depending on the operating conditions. Therefore it is worth to dedicate efforts to understanding at what extent and how these variations occur.

Many factors alter the operation of the *PV* devices: Irradiance, temperature of the device, angle of incidence, Air Mass, cloud conditions and ratio of diffuse and direct irradiance. In this work we will concentrate on the effects on the short circuit current values, because this parameter is the one related to power production which results mostly affected by varying operating conditions. Differently, the voltage is much more stable.

Up to now the effects of irradiance and temperature have been considered as the most significant. The well known linear model between broad band irradiance and short circuit current is used nowadays, as well as the model describing fractional variations on the short circuit current value for varying temperatures. However these models are beginning to be insufficient for emerging technologies and for the growing need of confidence in the design of power plants. This need has its origin in the need for satisfying the everyday growing demand for energy *, which drives advances

*The focus of this work is pure technical; however the social-economical context is relevant and I am convinced that we should not only look for more and cleaner ways to obtain the energy, but reconsider why so much energy is being required. A significant reduction of the energy demand worldwide can only occur under rational use of the resources, which is interlinked with a change in the habits of living and production. These changes are only possible if the present economical models make room for them.

in different fields of natural sciences. In this way the so-called *Thin Film* technologies land in our discussion: Briefly this is a *PV* technology developed in the last two decades, which differs in four main aspects from the traditional Silicon crystalline technologies [7]:

1. Thin and long cells with high rate of photon-electron conversion. The cells are about $1\mu m - 6\mu m$ thick, while *c-Si* cells are about $200\mu m - 300\mu m$.
2. Low consumption of material per peak power unit produced: $0.2kg/kW_p$ vs $16kg/kW_p$.
3. Lower consumption of primary energy per peak power unit: $5MWh/kW_p$ vs $14MWh/kW_p$.
4. *Better* performance under low irradiance conditions and high diffuse fractions.

The points two, three and four in our list of advantages talk about potential economical benefits of using *thin film* technologies. Points two and three are related to the *module's production side* while point four is related to the *module's energy yield side*. However what could look like a double-sided gain, may or may not be like that: *Thin film* devices are *normally*[†] less efficient than crystalline Silicon devices; however they may be cheaper to produce. So it seems we have a reduction of costs in one side and a reduction of the energy yield in the other. The question is whether the overall balance will be better, worse or equal than the one of the crystalline technologies when spectral considerations are made.

Besides the costs of production, the prices of *PV* modules are determined by their *STC* performance values. However these conditions are extremely seldom found outdoors. On the other side of the economical balance, the energy yield depends on the *real life* conditions. Therefore a *PV* device with a superior *Performance Ratio (PR)* and lower costs of production looks like a promising technology. According to point four it may happen that this is the case for *thin film* technologies under cloudy and low irradiance conditions. This is what we would like to find out. A long way is ahead before getting there: We have basic new stuff included: Spectral irradiance data modeled

[†]Under Standard Test Conditions: $1000W/m^2$, $25^\circ C$ cell temperature, *AM1.5G*

from satellite information coupled with ground measurements. Many other targets will appear in between, related to the recognition of the possibilities of this scheme of spectral characterization.

The experiences characterizing *thin film* technologies with the variables global broad band irradiance and temperature have suggested that something is missing in the analysis (due to poorer results). Examples of *PV* modules characterizations can be found in [11] [10] [8] [9]. A pioneer work using ground measured spectral irradiance has been performed by T.R. Betts [2] at *Loughborough University* in the *UK* in recent years (2004). This work constitutes a reference for the present research.

Along this document we will get a comprehensive view of the work performed. We will start in **chapter 2** with a brief introduction to the scheme *satellite - radiative transfer model (SOLIS)* used for the calculation of the spectral irradiance. In **chapter 3** we will know about the ground measurements and the technical details of the *PV* modules used in the research. In the **chapter 4** the spectral parameters used in this work will be introduced and analyzed by using *SOLIS* irradiance data. In this chapter the short circuit current spectral models will be proposed. In **chapter 5** we will analyze how the spectral variations manifest in the data and how the use of ground measured data together with *SOLIS* data interferes with the observation of the spectral effects. Finally the proposed spectral models will be applied. In the last chapter the relevant conclusions will be summarized together with suggestions for further analysis of spectral effects on *PV* devices.

Chapter 2

The Satellite-based Spectral Data: *SOLIS*

SOLIS is an acronym for *SOlar Irradiance Scheme*. It is a method for the calculation of the solar irradiance on Earth's surface (on horizontal plane) based on satellite images with cloud information and data containing information about the aerosols, water vapor and ozone of the atmosphere. *SOLIS* has the capability to resolve spectral irradiance in 26 bands and its output is available in hourly values and slot values (every fifteen minutes) for a location on Earth specified by latitude, longitude and altitude above mean sea level.

SOLIS works through the linkage of two modules: the clear sky module and the cloud module.

2.1 The Clear Sky Module

The calculation of the irradiance for defined regions on Earth's surface is made with information from the following satellites:

MSG-2 O_3 , water vapor

ERS-2/ENVISAT Aerosols, O_3

This information allows the calculation of the irradiance in W/m^2 for a given time on a given place on Earth in 26 wavelength bands starting at 306.8 nm and ending at 3001.9 nm [13]. The broadband irradiance corresponds to the sum of the values of the 26 bands.

The clear sky module uses as special feature the combination of a radiative transfer model (*RTM*) and a fitting function called the *Modified Lambert-Beer* function (*MLB*). The spatial coverage requirements of the *SOLIS* scheme require that all the calculations are performed on short times. However using the *RTM* for all the calculations would take too long. This is the reason why the *RTM* is used only a few times per day for the determination of the *MLB* functions for irradiance. The way in which the clear sky module works is depicted in the following paragraphs.

The simple relationship that describes the attenuation of monochromatic light by matter of attenuation coefficient or optical depth τ is given in equation 2.1.

$$I = I_0 \cdot e^{-\tau} \quad (2.1)$$

In our case, the irradiance is evidently dependent on the hour of the day, it is, on the solar zenith angle of the sun (*SZA*). A modified expression taking into account this fact is equation 2.2, in which a modified optical depth varying with *SZA* and a multiplicative factor also dependent on *SZA* are implemented.

$$I(\theta_z) = I_0 \cdot e^{(-\tau/\cos \theta_z)} \cdot \cos \theta_z \quad (2.2)$$

The corresponding equation for polychromatic light corresponds to equation 2.3; this is the so called *Modified Lambert-Beer* function (*MLB*) and can be found in [14]. τ_0 is the optical depth at *SZA* of 0° and a is a correction parameter calculated at a *SZA* of 60° . This equation is the fundament of the calculation of the clear sky irradiance in polychromatic bands and broad band and holds for

direct and diffuse components (therefore also for global irradiance). The a parameter accounts for the polychromatic character of the light and is necessary due to the non-additivity of the attenuation coefficients τ for monochromatic light. The values of this parameter differ for each case: direct, diffuse and global components. It should be noted that the *MLB* is a fitting function although its roots are in the well known exponential attenuation of radiation by matter.

$$I = I_0 \cdot e^{(-\tau_0 / \cos^a(\theta_z))} \cdot \cos \theta_z \quad (2.3)$$

This means that after calculation of τ_0 and a , a function for the calculation of clear sky irradiance on Earth's surface for any time of the day is available. This means that the radiative transfer model will be only used twice (0° and 60° SZA) for one day and the rest of the values will be calculated using the *MLB* relationship. Notice that with τ_0 and a fixed, the *MLB* is only a function of SZA. In figure 2.1 plots of solar irradiance curves calculated with the *MLB* function are displayed and compared to several points obtained with the *RTM*. The spatial resolution of the clear sky data is $50km \times 50km$.

2.1.1 The Radiative Transfer Model: *libRadtran*

The *RTM* used is called *libRadtran* and consists in a library of *C* and *FORTRAN* code for the calculation of solar radiation in the Earth's atmosphere. This model considers not only the turbidity of the atmosphere but the aerosol composition separated from the water vapor. This is a requirement for the reliability of the spectral distribution of the irradiance. The *libRadtran RTM* is compatible with the *Kato spectral bands*, the ones selected for *SOLIS*. For more information on this model please refer to [14] and [1].

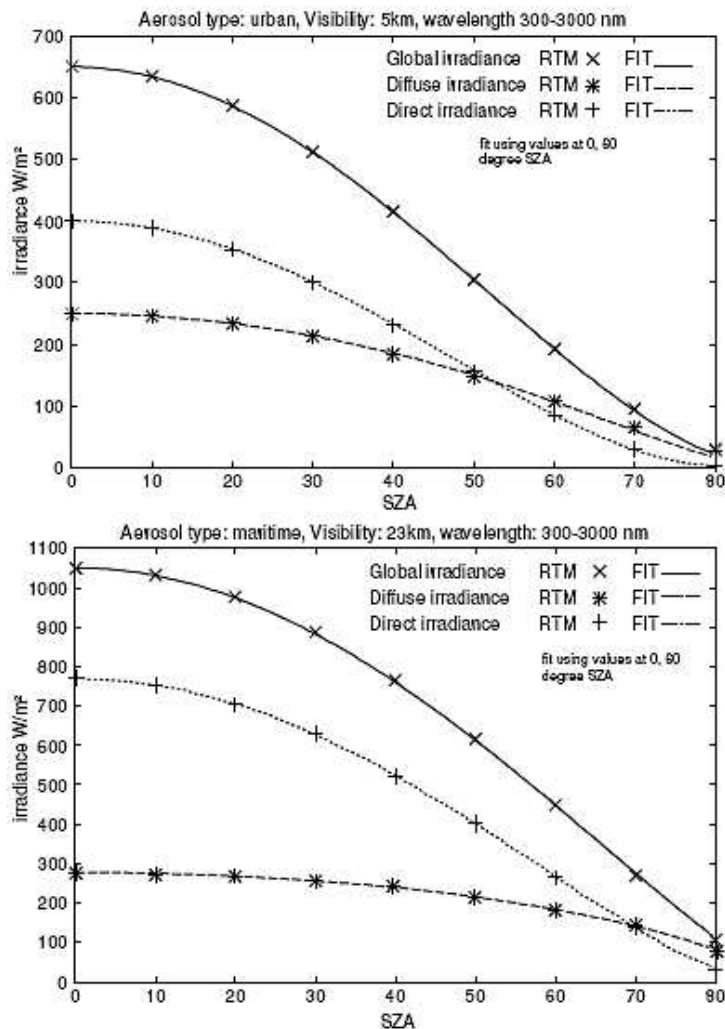


Figure 2.1: Comparison of solar irradiance calculations as function of SZA based only on RTM and based on RTM and MLB for two different atmospheric clear sky conditions [14].

2.2 The Cloud Module

The cloud module completes the solar irradiance scheme and calculates the irradiance on Earth' surface according to equation 2.4. In this equation k^* is the *Clear Sky Index*, whose values are calculated from the *Cloud Index* values n . The values of clear sky irradiance are obtained from the Clear Sky module.

$$G = k^* \cdot G_{ClearSky} \quad (2.4)$$

The cloud module works based on the cloud information supplied by the satellite *MSG-2*; with a temporal resolution of 15 minutes and a spatial one of $1km \times 1km$. The n values are derived from normalized cloud reflectivity and the k^* values are calculated from the $n-k^*$ relationship (see equation 2.5).

$$k^* = \begin{cases} 1.2 & n \leq 0.2 \\ 1 - n & 0.2 < n \leq 0.8 \\ 1.6667n^2 - 3.6667n + 2.0667 & 0.8 < n \leq 1.1 \\ 0.05 & n > 1.1 \end{cases} \quad (2.5)$$

2.3 The Quality of the Data

Validation of the *SOLIS* data is only available for broad band irradiance. The errors depend on the location, the time of the year and the time scale of the data (hourly, monthly values, etc). In general it has been observed that the absolute error in the calculation of global broad band irradiance is higher for summer than for winter. On the other hand the relative error is higher in winter (30%-40%) than in summer (15%-25%) due to lower values of irradiance. An example on the variation with the time scale for a location in Germany in summer supply the following values:

- 1min: rmse=35%

- 5min: rmse=32%
- 10min: rmse=28%
- 30min: rmse=22%
- 60min: rmse=19.5%

For more information about the errors of the *SOLIS* broad band irradiance data please refer to [12].

Validation of the *SOLIS* spectral data with ground measurements of spectral irradiance is not available yet, but it is expected that it will be performed soon.

Chapter 3

Photovoltaic Modules Used and the I_{SC} Measurements

In this chapter the technical description of the *PV* modules under investigation is given. Also relevant information concerning the ground measurements of short circuit current and global broadband irradiance.

3.1 The Photovoltaic Modules

Three types of *PV* modules have been used in this work. The reference technology is a poly-crystalline module and the *thin film* technologies are represented by amorphous Silicon and Cadmium-Telluride modules. In total we have 9 modules distributed like this:

1. Two already used *a-Si* modules *Tianjin- Jinneng*.
2. Four brand new *CdTe FS-62* modules provided by *First Solar*.
3. One used poly-crystalline module *Hyundai HiS-M188SF*.

Module Type	<i>a-Si</i>	<i>c-Si</i>	<i>CdTe</i>
P_{MPP} [W]	38 ± 1	$188 \pm 4\%$	62.5 ± 3.1
V_{MPP} [V]	45	26.2	64
I_{MPP} [A]	0.84	7.20	0.95
V_{OC} [V]	60	33.0	91
I_{SC} [A]	1	7.87	1.14
P_{MPP} T coefficient	-	$-0.32\%/\text{ }^{\circ}\text{C}$	$-0.25\%/\text{ }^{\circ}\text{C}$
V_{OC} T coefficient	$-0.28\%/\text{ }^{\circ}\text{C}$	$-0.30\%/\text{ }^{\circ}\text{C}$	$-0.29\%/\text{ }^{\circ}\text{C}$
I_{SC} T coefficient	$+0.09\%/\text{ }^{\circ}\text{C}$	$+0.08\%/\text{ }^{\circ}\text{C}$	$+0.04\%/\text{ }^{\circ}\text{C}$
Cell type	<i>a-Si</i>	6" poly <i>c-Si</i>	<i>CdTe</i>
Number of cells		54	116
Cell efficiency [%]	-	14.3	-
Module efficiency [%]	-	13.0	-

Table 3.1: Electro-technical data of the PV-modules used in the experiment. The data is supplied for one module at STC conditions ($1000\text{W}/\text{m}^2$, $\text{AM}1.5\text{G}$ and module temperature of $25\text{ }^{\circ}\text{C}$).

The electro-technical data of these modules are presented in table 3.1.

The spectral response curves of the devices were sampled and average values were calculated according to the wavelength bands used by *SOLIS* for delivery of the spectral irradiance data.

3.1.1 *a-Si Tianjin Jinneng*

For the measurements the two modules available were connected in parallel in order to increase the current output.

The spectral response curve for this model was not found, so we took a curve from [18]. This is an early study on the spectral effects on the power production of photovoltaic modules carried out at the *Fraunhofer Institut fuer Solar Energiesysteme (ISE)* in Freiburg, Germany. See Fig. 3.1 on page 13.

3.1.2 *CdTe First Solar FS-62*

These four brand new modules were kindly provided by *First Solar GmbH*. Two of them were used in parallel to increase the current output. The other two were kept under dark conditions in order to

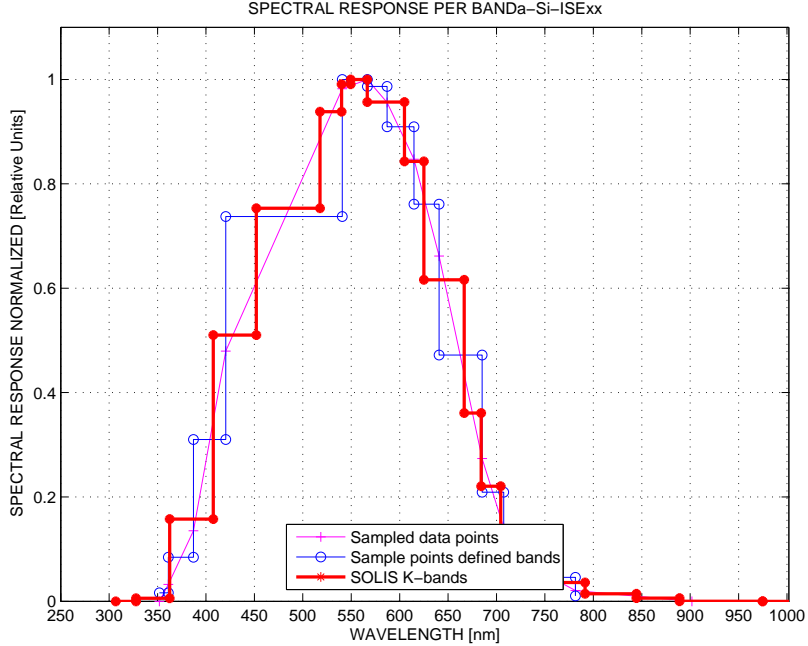


Figure 3.1: Spectral response assumed for *a*-Si. Three curves are displayed: 1. The sampled curve. 2. The mean values for the bands defined by the sampled points. 3. The mean spectral response for the *SOLIS Kato-bands*. This last curve will be used for the calculation of *device-dependent* spectral parameters. Taken from [18].

be able to perform a later comparison of the effects of the semiconductor degradation process that takes place in thin film modules during the first months of operation.

Each module is (1200mmx600mmx6.8mm) with a mass of 11.4kg and has 116 *CdTe* cells. These modules are of the type *frameless laminate*.

For these modules, the manufacturer supplied a quantum efficiency curve which was taken as the spectral response of the modules [5] (See Fig. 3.2 on page 15). Taking the quantum efficiency as the spectral response implies an error because the amount by which both quantities differ depends on the inverse of the wavelength of the light considered. This can be seen in equation 3.1 on page 14. Here EQE_{λ_0} is the *External Quantum Efficiency* of the device at a fixed wavelength λ_0 in $A/(photon/s)$ or *electron/photon*; i.e. the electrical current output divided by the photon flux ϕ_{λ_0} . SR_{λ_0} is the corresponding spectral response in A/W .

$$EQE_{\lambda_0} = \frac{\text{measured.current}}{\text{photon.flux}} = \frac{I_{\lambda_0}}{\phi_{\lambda_0}}$$

and

$$SR_{\lambda_0} = \frac{\text{measured.current}}{\text{incident.power}} = \frac{I_{\lambda_0}}{P_{\lambda_0}}$$

because

$$\phi_{\lambda_0} = \frac{\lambda_0 P_{\lambda_0}}{hc}$$

follows :

$$EQE_{\lambda_0} = hc \frac{SR_{\lambda_0}}{\lambda_0}$$

Because we are interested in the relative spectral responses, the magnitude of this error for a fixed wavelength (which is in the order of *lambda*) is not important. What account for errors in our calculations is the artificial scaling introduced for different wavelengths. In equation 3.2 we have an explicit expression for the ratio of the spectral response values at two wavelengths as function of the ratio of the corresponding quantum efficiency values. This expression let us see that as the wavelength difference increase, the error introduced increases. In the case of *CdTe* the most significant case would be to calculate the error at about 500nm and 850nm. In this case we have that the ratio of spectral responses is about 1.7 times the ratio of quantum efficiencies. This means that the shape of the *EQE* and *SR* curves differ: the latest has its maximum about 850nm while the first at about 500nm.

Despite taking the quantum efficiency curve as the spectral response curve is a childish error, it was detected at a later phase of the work and therefore **the results displayed for *CdTe* in this document have not been corrected.** This does not mean actually that the calculations for *CdTe* are wrong, but can not be interpreted in the same fashion as the results for *a-Si* and *c-Si*. This is the case for the parameter *UD* introduced in chapter 4 which depend on the spectral response of the device.

$$\frac{SR_{\lambda_2}}{SR_{\lambda_1}} = \frac{EQE_{\lambda_2}}{EQE_{\lambda_1}} \frac{\lambda_2}{\lambda_1} \quad (3.2)$$

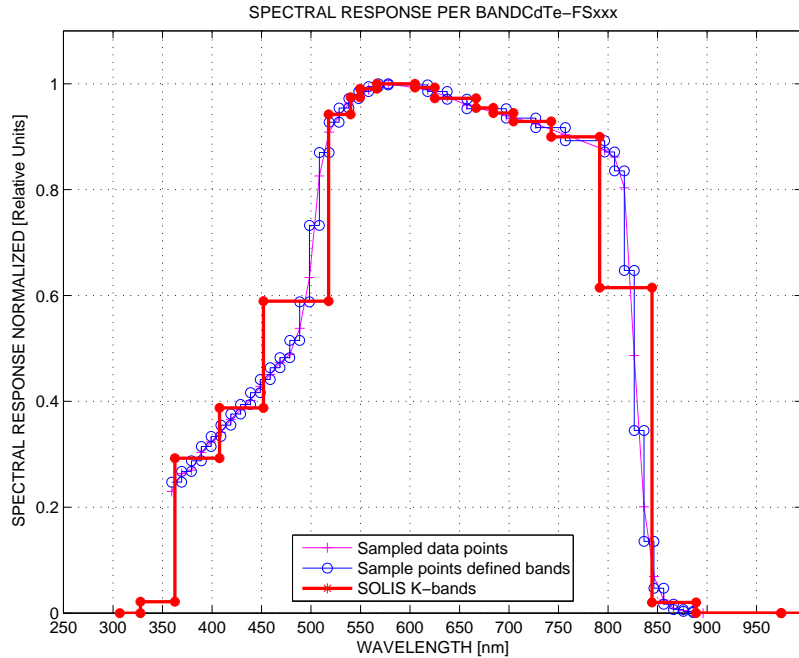


Figure 3.2: Spectral response of the *CdTe* modules. The curve was obtained from the producer as a quantum efficiency curve. Three curves are displayed: 1. The sampled curve. 2. The mean values for the bands defined by the sampled points. 3. The mean spectral response for the *SOLIS Kato-bands*. This last curve will be used for the calculation of *device-dependent* spectral parameters. Taken from [5].

3.1.3 c-Si Hyundai HiS-M188SF

This is the reference module. For crystalline photovoltaic technologies the influence of different light spectra is expected to be very low. In the experiment we used a single module given that the current output is high enough for a proper measurement. The module has 56 cells connected in series in a matrix of 9cells \times 6cells. Its dimensions are (1476mmx983mmx35mm) and its weight is around 17kg.

For this module the actual spectral response could not be found, so we used a curve from [4]. See Fig. 3.3 on page 16.

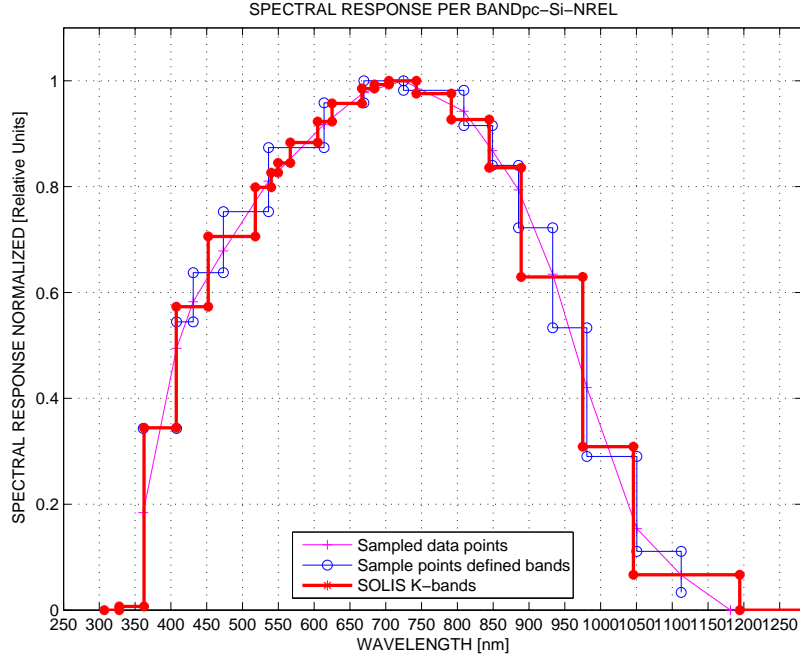


Figure 3.3: Spectral response assumed for the *c-Si* module. Three curves are displayed: 1. The sampled curve. 2. The mean values for the bands defined by the sampled points. 3. The mean spectral response for the *SOLIS Kato-bands*. This last curve will be used for the calculation of *device-dependent* spectral parameters. Taken from [4].

3.2 The Ground Measurements

The measurements of short circuit current and other parameters were performed with the device *PVPM-1000C* [15]. This device includes a *combi sensor* which consists in an irradiance sensor and a temperature sensor. A mono-crystalline Silicon cell measures the irradiance and the temperature on this cell is measured by a *PT-1000* sensor. It is easy to see that these measurements have 2 drawbacks:

1. The irradiance value is measured with the same type of device whose behaviour is to be investigated. This means that its readings will contain spectral effects.
2. We don't know how precise it is to assume that the temperature of the modules is equal to the measured temperature of the sensor cell. Even more, possibly the temperature of the modules

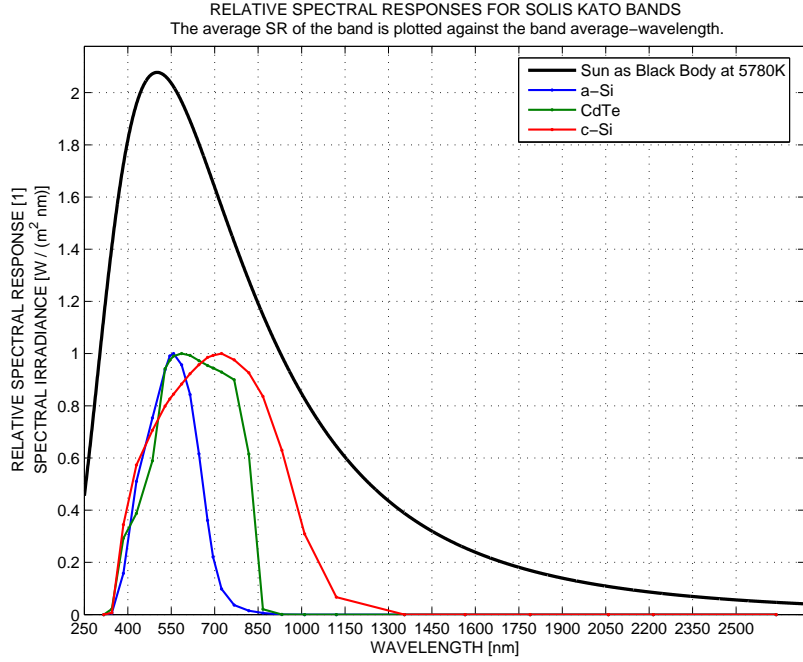


Figure 3.4: Relative spectral responses for the 3 modules under investigation and spectral irradiance for a *black body* at 5780K at the distance Sun-Earth from the Sun. The average values of the spectral responses have been plotted against the wavelength average value of each *SOLIS Kato-band*.

cannot be defined with the measurement of temperature at a single point. In the measurement setup The modules were set in such a way that air can easily flow below them for cooling purposes. Likewise for the sensor cell which is enclosed in a plastic box.

Every measurement of this device consists in the calculation of the characteristic curve of the module under the irradiance and temperature conditions at the moment. In this way a list of parameters is obtained after each measurement, which lasts about 2 seconds. The most relevant parameters are:

1. Global broad band Irradiance G [W/m^2]
2. Cell temperature T [$^\circ C$]
3. Open circuit voltage U_{oc} [V]
4. Short Circuit Current I_{sc} [A]



Figure 3.5: Picture of the measurement setup. When the picture was taken (December 7 2006) the 2 $CdTe$ modules and the $c-Si$ module were mounted. The *combi sensor* is in the lower-left corner of the picture. The rest of solar modules with no-null inclination have nothing to do with this research and are part of a grid connected power plant.

All the measurements were performed on horizontal surface.

Because most of the time we had only one measurement device, we had to alternate the measurements for the different modules. After measuring a few weeks the 3 module types, we decided to measure only for $a-Si$ and $c-Si$ given that in the group, they are the modules with the biggest difference in the spectral responses. In this way we *sacrificed* the only module for which we had a spectral response supplied by the manufacturer but gained more measurements for the chosen technologies under similar conditions. In general measurements were performed for one week for a module type and then we changed to the other.

3.2.1 Temperature Effects on the I_{sc} and G Measurements

Unfortunately much of the collected data had to be rejected for analysis because of problems which are or seem to be related to the temperature measurements. In the first place, in the last week of year



Figure 3.6: A characteristic curve measurement was carried out every 5 minutes and the data was stored in a *PC* connected to the measurement device. In May 2007 data was measured simultaneously with two similar measurement devices for *a-Si* and *c-Si*.

2006, it seems that a short circuit occurred in the sensor. All the temperatures registered for one week correspond to the lower limit of the sensed range of sensor, i.e. -50°C . After that we started to have problems with the measurement device: The continuous measurements were interrupted automatically after a few hours. The measurement device was sent for reparation and calibration twice, which stopped the measurements for about two months altogether. As the measurements were restarted on the abnormal hot and sunny days of April 2007, the data points for clear sky conditions displayed a strange behaviour which has not been understood completely but is related to temperature. This behaviour was observed for measurements of both module types *a-Si* and *c-Si* and is not recognizable with *SOLIS* irradiance. An example of this phenomenon is found in figure Fig. 3.8 on page 22. In this plot the data points for clear sky conditions are branched and form something similar to an ellipse. The upper branch corresponds to the *before noon* points and the lower branch to the *afternoon* data. In the afternoon the temperature values for a fixed irradiance value are higher than in the morning and nearly all the points are above 25°C . In the morning not all the points are above this reference temperature, just the points above about 300W/m^2 . Because this



Figure 3.7: The Sun's path in the sky was calculated according to the geographical coordinates of the site. In this way the Sun elevation *horizon line* was calculated and the data points under this angle were ignored in the modeling analysis.

phenomenon occurs in the plots of *temperature corrected* and *non-corrected* short circuit current*, it seems that what we observe is an overestimation of the irradiance values. This overestimation may be due to two different reasons related to temperature:

1. The temperature coefficient used by the measuring device for calculating the *temperature corrected* values of global broad band irradiance seem to be underestimated. By checking the calibration of the device, a value of $5.8 \times 10^{-4} / {}^\circ\text{C}$ was estimated.
2. Differences between the temperature of the sensor cell and the actual temperature of the modules. In this case it would mean that the temperature of the sensor is higher than the one of the modules. A look to the wind data of a meteorological station nearby may help to see whether this hypothesis makes sense or not.

3.2.2 Other Considerations about the Measurements

In Fig. 3.7 on page 20 we have a panoramic picture of the site of the measurements in Augsburg, in southern Germany. In this picture lines are drawn with the path of the Sun for different months of the year. The program used for that allows also the calculation of horizon line of the site, it is the Sun elevation angle above which no shadows due to surrounding objects exist. For most of the azimuthal directions, this value is 5° , however on the west side a building rises the horizon line to 12° for the azimuth angles in the range $265^\circ - 280^\circ$ †. These horizon line values are used for filtering the data by Sun elevation values, which are calculated according to the norm *DIN 5034*.

*For an explanation about the temperature model applied to short circuit current data, please refer to chapter 5 on page 59.

†The azimuth angle is 0° on the north, 90° in the East and 270° on the west.

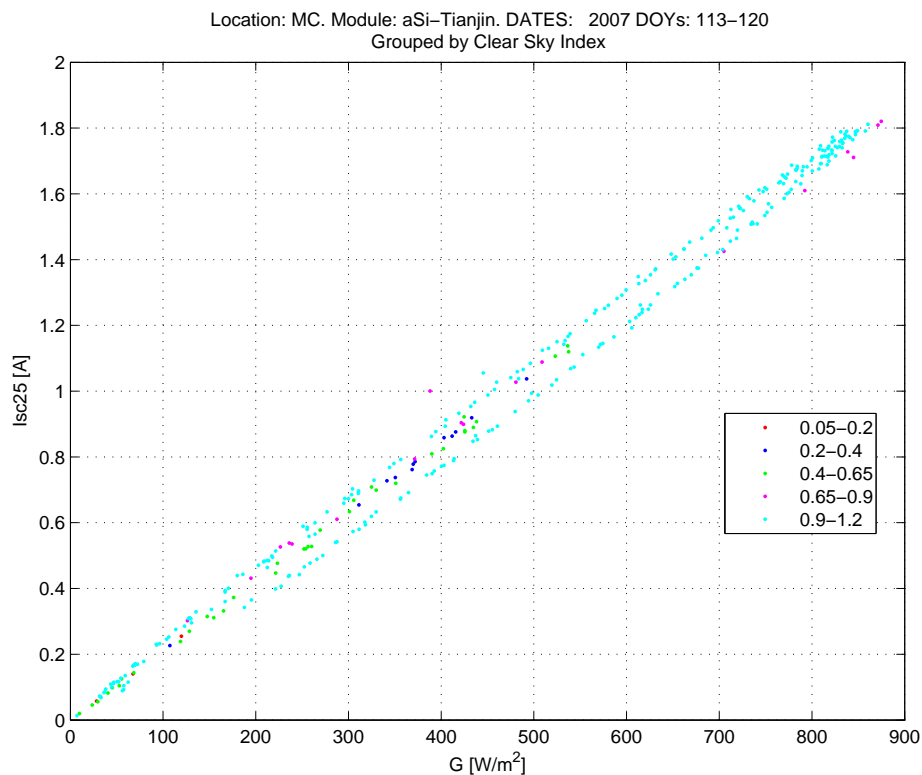


Figure 3.8: For the data of the sunny and hot days of April 2007 the short circuit current data points for clear sky conditions (pale blue points) split in two branches which form something similar to an ellipse. Although this phenomenon is not completely understood, it is related to high temperatures of the PV modules and the sensor cell.

Chapter 4

The Spectral Parameters *SPARs*

Firstly I want to introduce the acronym *SPAR* or *SPARs* (plural) for referencing the *SPectral PArameters*. They will save some valuable bits in the hard disk and a few microseconds in your brain when going through this document.

Let's recall the aim of this work: Modeling the I_{sc} production of photovoltaic modules taking into account the spectral variations of the solar irradiance. For this purpose we have at hand 2 spectral parameters: The *APE* or *Average Photon Energy* and the *Used Fraction* or *UD*. Both parameters have been already used in research works about spectral influences on *PV* devices (see [2] and [3]) and the present work is somehow a continuation of them. That is the reason why these two spectral parameters have been taken as starting points for our spectral analysis.

$$S\ PARs \begin{cases} APE \\ UD \end{cases} \quad (4.1)$$

It is important to realize at this point that when we talk about spectral parameters we have 2 different features which such parameters can describe:

1. *Chromatic* content: This is the distribution of the energy in the spectrum without regard of the magnitude of the spectral irradiance. We will be talking about *blue* and *red* spectra although the extraterrestrial and *AM1.5* spectra have already a high blue (*UV-VIS*) content. Thus the blue spectra look similar to these reference ones, with a maximum about 500nm ; while the red ones are flatter with maxima shifted to higher wavelengths.
2. *Intensity*: The absolute amount of energy we get for each wavelength or frequency value. The integration of these energies will give the total energy "carried" by the given spectrum.

We will encounter these features frequently in the future and they will be keys for the understanding of this work. Before further explaining the parameters it may be helpful to review some features and facts about the solar spectrum itself (especially if you have not understood well the features a spectral parameter can describe or you don't know which are those *reference* spectra). Please refer to the appendix A. Likewise it will be useful to have some basic information about the data used for the analysis of the spectral parameters presented in the current chapter. This you will find in the coming section.

4.1 The Data Used for the *SPARs* Analysis

The data used for the analysis presented in this chapter are exclusively *SOLIS* satellite-based data.

The data correspond to following dates of the year 2006:

1. Day of year (DOY): 152-214. June 1 - August 02.
2. Day of year (DOY): 280-324. October 7 - November 20.
3. Day of year (DOY): 331-365. November 27 - December 31.

In Fig. 4.1 the global broad band irradiance read directly from the broad band data files from *SOLIS* is compared to the integration (sum) of the global spectral irradiance read from the spectral data files

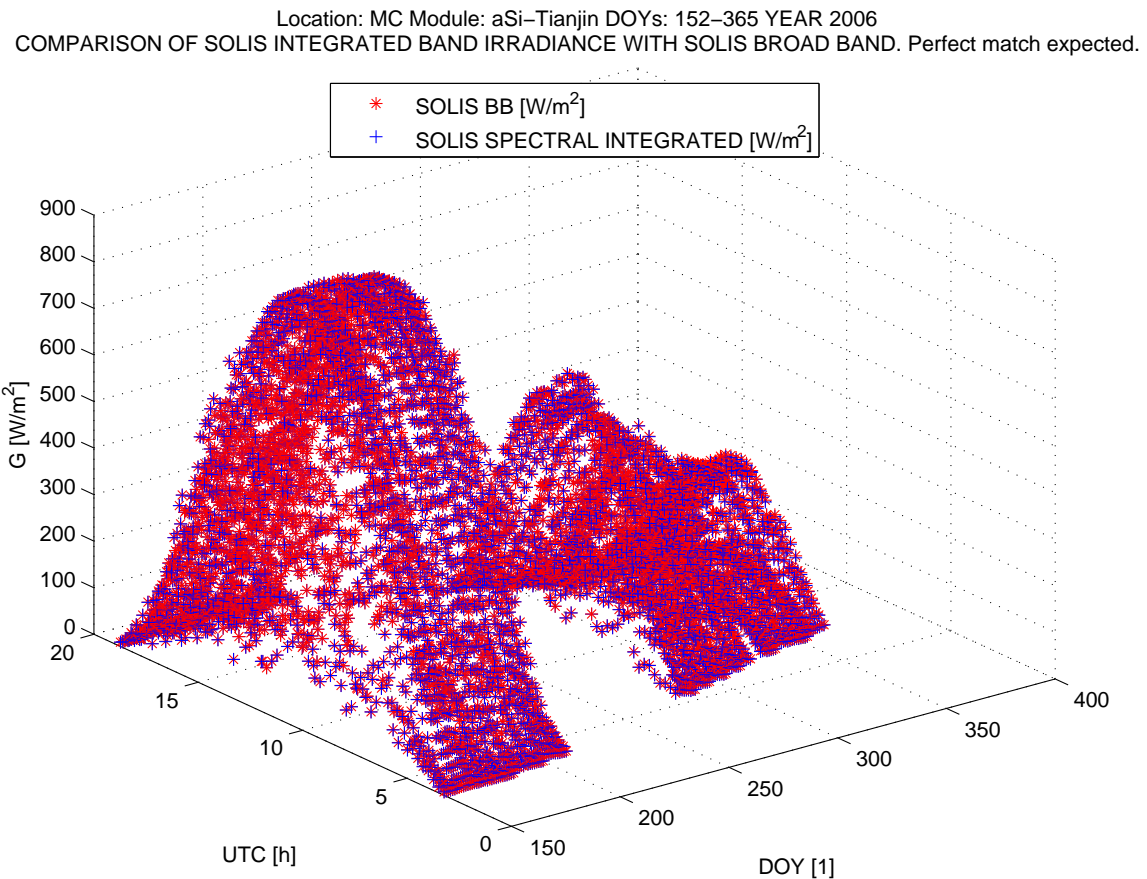


Figure 4.1: Time series of integrated spectral global irradiance and broad band irradiance

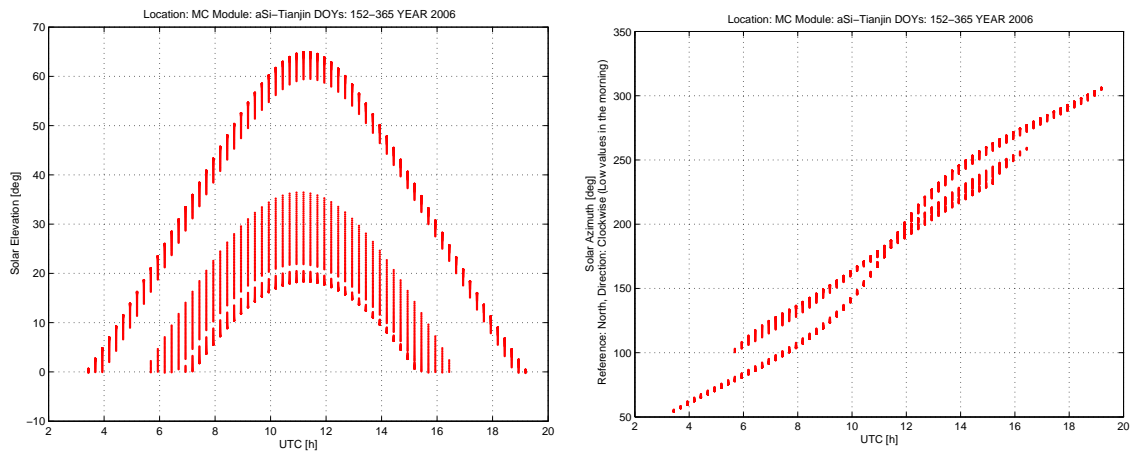


Figure 4.2: Solar Elevation γ_s vs UTC displaying seasonal variations.

Figure 4.3: Solar Azimuth φ_s vs UTC displaying seasonal variations.

from *SOLIS*. For most of the cases both values match, however it is clear that for irradiances under about $300W/m^2$ small discrepancies are frequent. It happened sometimes that the global spectral irradiance value of the 25th *SOLIS* band contained *Nan* values. This however does not represent a big problem because the values of this band contribute a very low fraction of the total irradiance. For further plots and calculations the global broad band irradiances from the broad band *SOLIS* files are used.

In Fig. 4.2 and Fig. 4.3 the Sun elevation γ_s and Sun Azimuth φ_s are plotted against *UTC*.^{*} The Sun coordinates were calculated according to the norm *DIN 5034* [16]. In these plots the seasonal variations can be recognized: Both angles reach the highest values in summer and have a wider range in the *UTC* axis. The reference for the Sun Azimuth is the north marked with 0° , east corresponds to 90° and west to 270° . In the plots of Fig. 4.4 the variation of the global broad band irradiance [†] with the solar coordinates is shown with the data grouped by Clear Sky Index k^* [‡]. In these plots the seasonal variations are also recognizable, especially in the plots including the solar azimuth angle. It is remarkable that for winter and autumn like conditions the increase of global broad band irradiance is steeper than in summer for clear sky conditions. This is related to the fact that during summer the turbidity of the atmosphere is in general higher than in winter.

4.2 Average-Photon Energy *APE*

APE is defined as the ratio of the broad band irradiance in a wavelength interval to the photon flux over the same interval, as it can be seen in equation 4.2. In this equation G_λ is the spectral irradiance density function in $W/m^2 \times nm$ and ϕ_λ is the spectral photon-flux density function in $photons/m^2 \times s \times nm$. Note that the photon flux is dependent on the corresponding spectral irradiance

^{*}*Universal Time Coordinated*. For Germany $UTC = CET - TimeZone - SummerTime$. *CET* is Central European Time, *TimeZone* is the Time Zone of the location (+1h) and *SummerTime* refers to the time advance used in summer time (1h or 0h).

[†]It is important to recall that all the irradiances referred in this document are on horizontal plane unless otherwise stated.

[‡]The k^* values were calculated from the Cloud Index n values provided by *SOLIS*. For more information on n and k^* see [6] and [12]

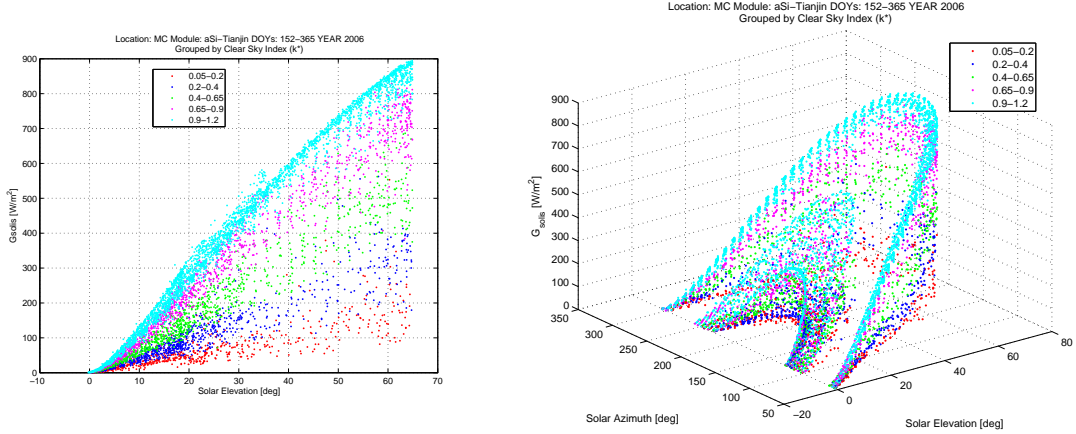


Figure 4.4: Global broad band irradiance dependence on Sun elevation (left) and Sun azimuth and Sun elevation (Right). The seasonal variations are better visualized in the last plot.

value and the photon energy at the given wavelength.

APE has units of energy (in this case Joules) and this is the energy of an average photon of a given spectrum in the wavelength window $[a, b]$. Given the order of magnitude of the *APE* values, a more appropriate unit to use is the Electronvolt. The value in *eV* is obtained from the one in Joules by dividing by the magnitude of the fundamental charge when expressed in Coulombs, $1.6e^{-19}$.

$$\begin{aligned}
 APE &= \frac{\int_a^b G_\lambda d\lambda}{\int_a^b \phi_\lambda d\lambda} \\
 \phi &= \frac{G_\lambda}{hc/\lambda} \\
 APE &= hc \frac{\int_a^b G_\lambda d\lambda}{\int_a^b \lambda G_\lambda d\lambda}
 \end{aligned} \tag{4.2}$$

APE is thought as a parameter for characterization of the solar spectra on Earth, without consideration of any properties of *PV* devices under investigation. Therefore it is cataloged as a "device independent" spectral parameter [§]. This should not be misunderstood: In practice the calculated

[§]In this chapter we will find plots of *APE* which are labeled with a given type of *PV* module. This is due to the fact that when calculating *APE* values other *device dependent* spectral parameters are also calculated.

APE values depend of course on the device or method used for obtention of the G_λ values.

Strictly speaking *APE* should always be calculated using the same integration limits a and b ; however spectral irradiance measurement devices usually have different wavelength band-width and this results in different *APE* values for the same spectrum. In any case the band-width [a, b] must be wide enough and correctly positioned in the electromagnetic spectrum in order to include the major part of the extraterrestrial solar spectrum (a band from about 300nm to 2000nm minimum).

4.2.1 Calculation of *APE* with *SOLIS* Spectral Data.

For this work *SOLIS* provide the satellite-based spectral irradiance data per band in W/m^2 , i.e. the equivalent of the integrated spectral irradiance density over the given band. In this case the upper and lower integrals in equation 4.2 turns into simple sums. For the calculation of the photon fluxes per band we use the band spectral irradiance and the energy of a photon of the average wavelength of each band. In this way the discrete form of *APE* is:

$$APE = hc \frac{\sum_{i=1}^N G_{\lambda_i}}{\sum_{i=1}^N \lambda_i G_{\lambda_i}} \quad (4.3)$$

The *APE* values calculated from the *SOLIS* data use the 26 *SOLIS Kato-bands*, which cover the interval 306.8nm – 3001.9nm. The fact that the *Kato-bands* bandwidths are variable 5nm – 175nm, increases the uncertainty in the calculated *APE* value respect to cases which handle uniform bandwidths of 1nm or less. However the latest cases mean having much more data in regions where it is not quite meaningful.

The value of *APE* calculated for the spectrum of a black body at 5780K at the Earth-Sun distance using the *SOLIS Kato-bands* is 1.43eV. Other reference values for *APE* can be found in table 4.1 [2].

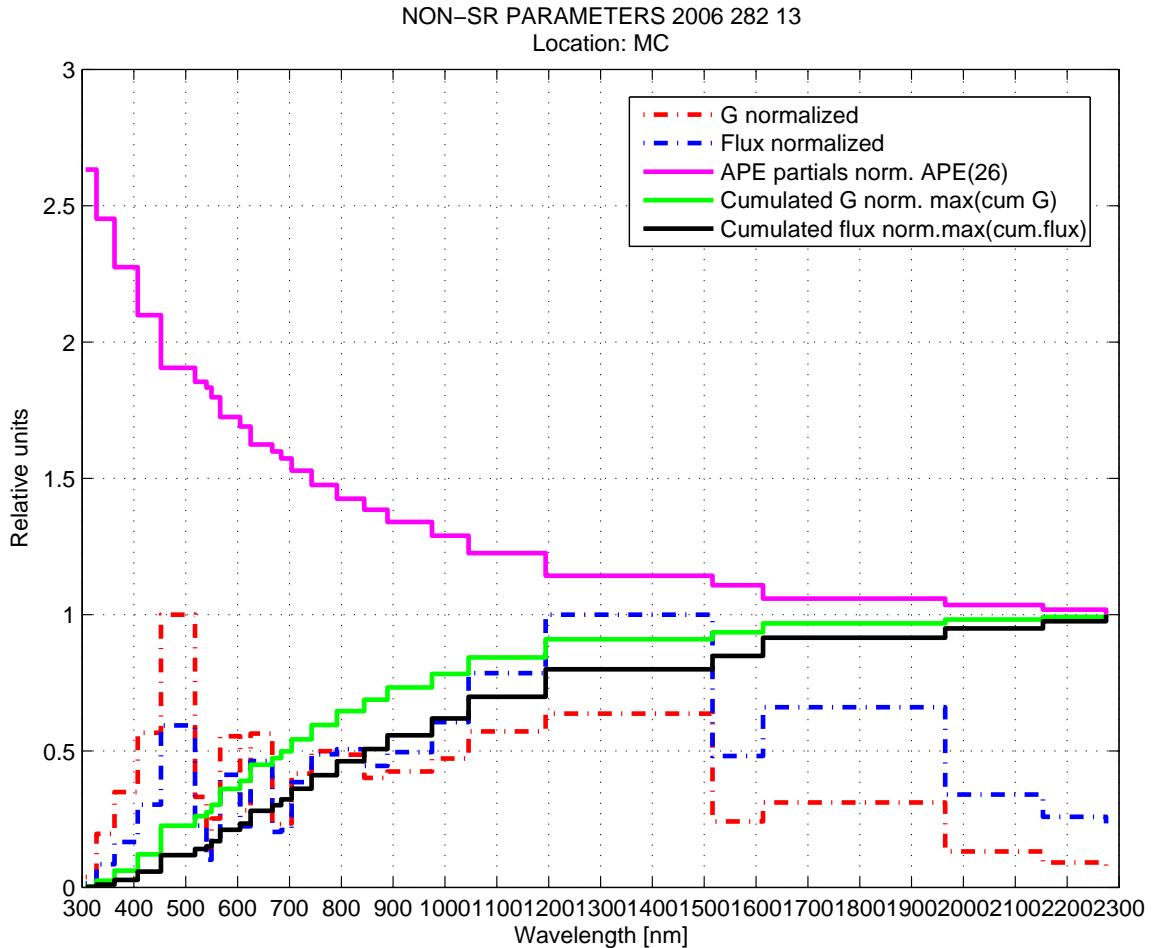


Figure 4.5: *APE* calculated up to the i^{th} band of *SOLIS*. The parameters used for its calculation are also shown. The data corresponds to the day of year (*DOY*) 282 of year 2006 at 13.186 hour. The shape of the spectral irradiance may look strange because the plotted values are the normalized values per *Kato-band* obtained directly from *SOLIS*.

Wavelength Range [nm]	<i>APE</i> [eV]
300-4000	1.43
300-2500	1.48
300-1700	1.62
300-1100	1.86

Table 4.1: Variation of the *APE* values calculated for the same AM 1.5G spectrum by integrating over different wavelength ranges, all of them starting in the *UV* region of the *EM* spectrum. [2].

4.2.2 Understanding *APE*

For a spectral parameter to be useful, it must describe changes in the chromatic content of the spectra. How does *APE* do it? The “*secret*” of *APE* lies in the fact that the energy of photons decreases with increasing wavelength. If we look at the mathematical form of *APE* in equation 4.2 and equation 4.3, we can see that the numerator and the denominator are accumulative terms which add sub-terms which can never be negative. In this way the only possibility for numerator and denominator is to increase over integration/sum.

Let’s imagine that the spectral irradiance density is a constant over wavelength. In that case to obtain the same spectral irradiance at a higher wavelength requires higher photon fluxes. In this way as we integrate, the photon flux term in the denominator increases faster than the broad band irradiance term in the numerator does. Then we can see that *APE* values calculated up to a higher wavelength value for a given spectrum are lower than when integrating over a shorter λ range with the same starting point.

But this is a special case and certainly not what we encounter in the spectra of the sunlight on Earth, which are variations of a curved shape very similar to the one of a black body at 5780K (Planck’s radiation law). Will our argument hold for this shape and for any other arbitrary shape of spectral irradiance density?

The answer is yes, we will get lower values of *APE* when integrating up to a higher wavelength. By observing the last expression in equation 4.2, we can see that:

1. The order of magnitude of the *APE* values is given mainly by the constant term hc , which is

$1e - 26.$

2. The ratio of integrals will define the behaviour of the values of *APE*: For an *arbitrary* G_λ function, the lineal term λ in the denominator will always cause the ratio of integrals to decrease when integrating up to a higher wavelength value. This is due to the fact that the terms in the upper and lower integrals differ only in this lineal term.

We have seen what happens with the *APE* values when integrating up to different λ values. We can use this explanation to outline the chromatic behaviour of *APE*. Let's take a *blue* spectrum as the cut-off of an arbitrary spectrum up to a certain value (not so far in the *IR* region), let's say 1000nm . Likewise a *red* spectrum as a cut-off of the same spectrum but up to a higher value, for example 2500nm . Seen this way, when integrating the first spectrum, the *APE* value will be higher than when integrating the second one, i.e. the blue spectra will be characterized with a higher value of *APE* than the red one.

In Fig. 4.5 on page 29, it is shown how the *APE* value is calculated up to different *SOLIS* bands for an arbitrary spectrum. The cumulated values of broad band irradiance and photon flux are displayed. Likewise the normalized curves of band spectral irradiance and photon flux are plotted. The partial *APE* values are normalized by the value calculated up to the last (26^{th}) band. In this way it is easy to see how the values of *APE* decrease when we integrate up to a higher band.

With our analysis until now we are able to state that the *APE* values will be higher for blue spectra than for red spectra which are identical up to the cut-off value of the blue one. But could we be a bit more general? At this point it should be clear that higher *APE* values will be obtained with spectra in which you get more energy with less photons. This serves also to have a more precise definition of what a blue or red spectrum is. We can use *APE* as parameter for blueness or redness. With this idea in mind, let's try to see what we can get from simple mathematical analysis, we may arrive to some more general conclusions.

APE Mathematical Analysis

For this analysis we will use two base cases in which all the possible spectral variations should be included:

1. Cases with a *fixed spectral distribution and different values of global broad band irradiance*.

What I call here spectral distribution is what characterizes the chromatic content of the spectra. It is the shape of curve of spectral irradiance density (discrete or not) without considering the magnitude. Thus only the relative magnitudes among different bands are important.

2. *Fixed broad band irradiance and different spectral distributions*.

Let's start with the first case and assume we have a reference spectral density curve from which others can be calculated just by multiplying by a positive scalar. This we can see in equation 4.4. The mathematical results are straightforward but meaningful: The *APE* value is independent of the value of the scalar constant and therefore independent of the magnitude of the broad band irradiance. If we apply the same argument to any spectral irradiance density curve G_λ (which includes already all the possible spectral variations) we arrive to the general conclusion that:

APE is a pure chromatic parameter and therefore describes only the spectral distribution of a spectral irradiance density curve, not its magnitude

$$APE_1 = hc \frac{\int_a^b a_1 G_\lambda d\lambda}{\int_a^b \lambda a_1 G_\lambda d\lambda} = hc \frac{\int_a^b G_\lambda d\lambda}{\int_a^b \lambda G_\lambda d\lambda} \quad (4.4)$$

For the case of fixed broad band irradiance and different spectral distributions the analysis is not so straightforward. In the expression of equation 4.5 the continuous and discrete versions of the case are given. The natural question is:

*Will all the different combinations $\int \lambda G_\lambda$ or $\sum \lambda_i G_{\lambda i}$ give rise to different values of *APE*? In other words, can *APE* resolve all the spectral conditions specified by a spectral irradiance density function?*

$$\begin{aligned} APE &= hc \frac{G_0}{\int_a^b \lambda G_\lambda d\lambda} \\ APE &= hc \frac{G_0}{\sum_{i=1}^N \lambda_i G_{\lambda i}} \end{aligned} \quad (4.5)$$

We must be careful to answer this question. Out of the context of solar spectra and in a strict mathematical sense the answer would be *No*. We can not uniquely represent a continuous arbitrary function in a given domain with a single scalar. However our case is not so general. The set of functions we want to represent with one number is restricted: all of them are variations of the extraterrestrial solar spectrum. The shape variations are produced by random variables as clouds and atmospherical turbidity and other periodical variations as Sun-Location-on-Earth geometry. This means only that in our case the things don't look so bad, however we still could have different spectral irradiance densities which could yield the same value of *APE*. Then the next question is:

*How could we estimate the resolution power of *APE*?*

I consider this step is complicated but necessary in order to gain understanding of the *SPARs*. Although I didn't do it, I will give some guidelines describing what I consider should be done for estimating the resolution of this parameter.

Let's assume that we have spectral irradiance data with very high accuracy and precision. Then we could try to answer whether the factors which affect the spectra on Earth produce spectra which are different but are characterized with the same *APE* value. It seems that the answer to this question is dependent on the specific location. What would we need for this analysis? We would like to characterize every wavelength (or wavelength band) with a set of possible values and their probability

distribution. We could set the higher limits for each wavelength as the values defined by the spectrum with clearest sky conditions, lowest atmospherical turbidity and highest Sun elevation. The lower limits are not zero in general because we shouldn't consider dark situations. These values would be given by long term measurements at site or in our case obtained from the satellite-based data . From this data we also find the probability distributions for each wavelength. With this information we could devise a method for calculating the probability of obtaining the same value of *APE* with different spectra. In case this probability is not zero, we should analyze which type of spectra produce the folding.

Now we should realize that we have finite uncertainty in the values of spectral irradiance, and that this uncertainty affects the probability analysis of the previous paragraph. This uncertainty depends on the wavelength bandwidths used. Wider bandwidths also cause a decrease of the precision of the photon fluxes, however this may be of no importance because these numbers are in the order of $1e + 20$.

4.2.3 Plots of *SOLIS* Spectra and *SOLIS APE*

In this section we will see the results of using the *SOLIS* spectral irradiance for calculation of *APE* and we will go through them in order to further understand the behaviour of this parameter.

In Fig. 4.6 the values of *APE* are plotted versus *SOLIS* global broad band irradiance with the data grouped by Clear Sky Index values. In this plot we will call the vertical axis the *chromatic axis* while the horizontal one will be called the *intensity axis*. About this plot we can make the following remarks:

1. *APE* is not a function of broad band irradiance, as expected.
2. The lower the broad band irradiance the higher the number of possible *APE* values. The number of meaningful values for fixed *G* could be estimated with the *APE* range and the uncertainty in the *APE* values.

3. For a given Clear Sky Index group the variation in the *APE* values is small when no irradiances below about $20W/m^2$ are considered. For irradiances below this value the *APE* values decrease very fast. This suggests influence of the Air Mass, which is related to the Sun elevation. This is confirmed in Fig. 4.7 and Fig. 4.9, where we can see that for angles under 5° the *APE* decay is very fast. For all the k^* groups the *APE* values seem to stabilize asymptotically, however this stabilization is faster under clear sky conditions.

The *SOLIS* based *APE* values suggest that for low Air Mass conditions the main influence on the spectral variations are the clouds and for high Air Mass values the main influence is the Air Mass itself. This is plausible for the *SOLIS* irradiance given that it is calculated for horizontal surface. Under this condition, at very low γ_s angles, the diffuse component of irradiance is very high and strongly affected by the path through the atmosphere. As the Sun elevation increases, the direct component of irradiance rapidly increases, which results strongly affected by the clouds presence while the path through the atmosphere is shortened.

We can contrast these results with the results found in Figures 2.12 and 2.13 of [2]. These are respectively the plots of *APE* versus global broad band irradiance and versus Air Mass. Although these plots are not grouped by k^* value, it is possible to do some basic comparisons. For example we can see that there is no clear maximum value for *APE* as in our case. In the plot against Air Mass, we find a variation of about 6% in the range of *AM* [1.1, 6.0], which corresponds approximately to Sun elevation angles of 65° and 10° respectively. In our case the corresponding variation for the clear sky condition group is about 3%. The differences are due to the fact that in [2] the spectral irradiance comes from ground measurements on tilted surface. This may attenuate the effects of clouds and distribute more or less uniformly the Air Mass effects along the broad band irradiance axis.

For finishing this analysis of the parameter *APE*, we will see some examples on how variations in the spectra reflect in the *APE* value. For doing so we will plot *SOLIS* spectra for different conditions against the mean wavelength value of each band. In Fig. 4.10 on page 39 we fixed a value of global

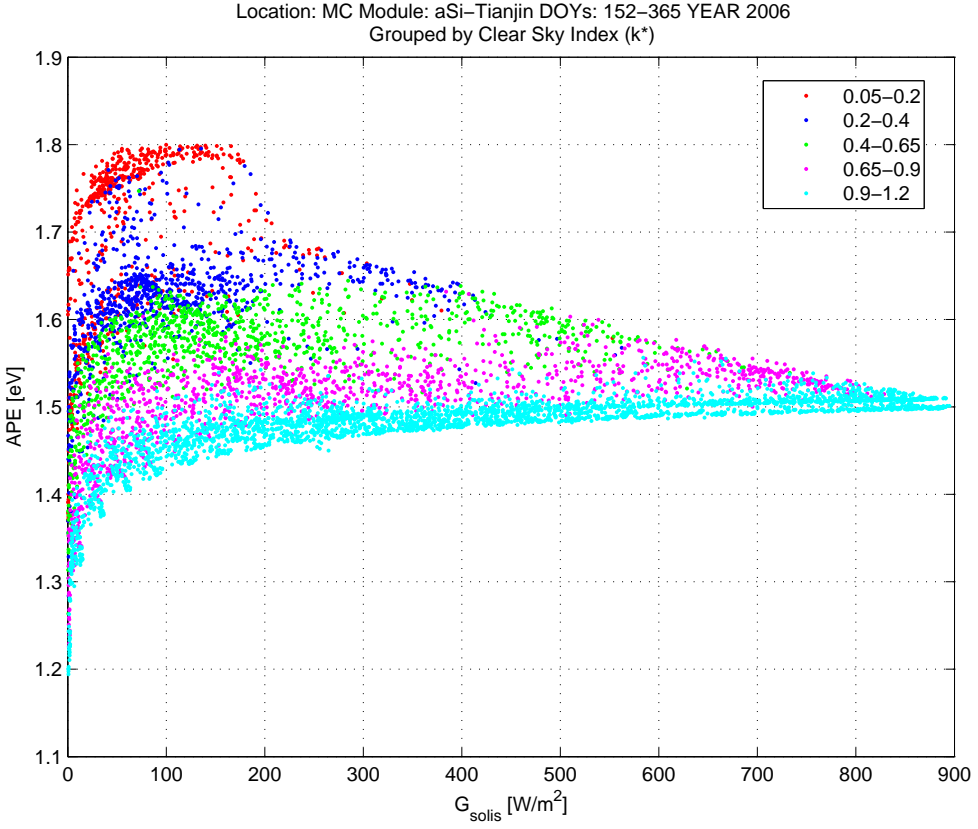


Figure 4.6: APF dependence on global broad band irradiance. Data grouped by Clear Sky Index value.

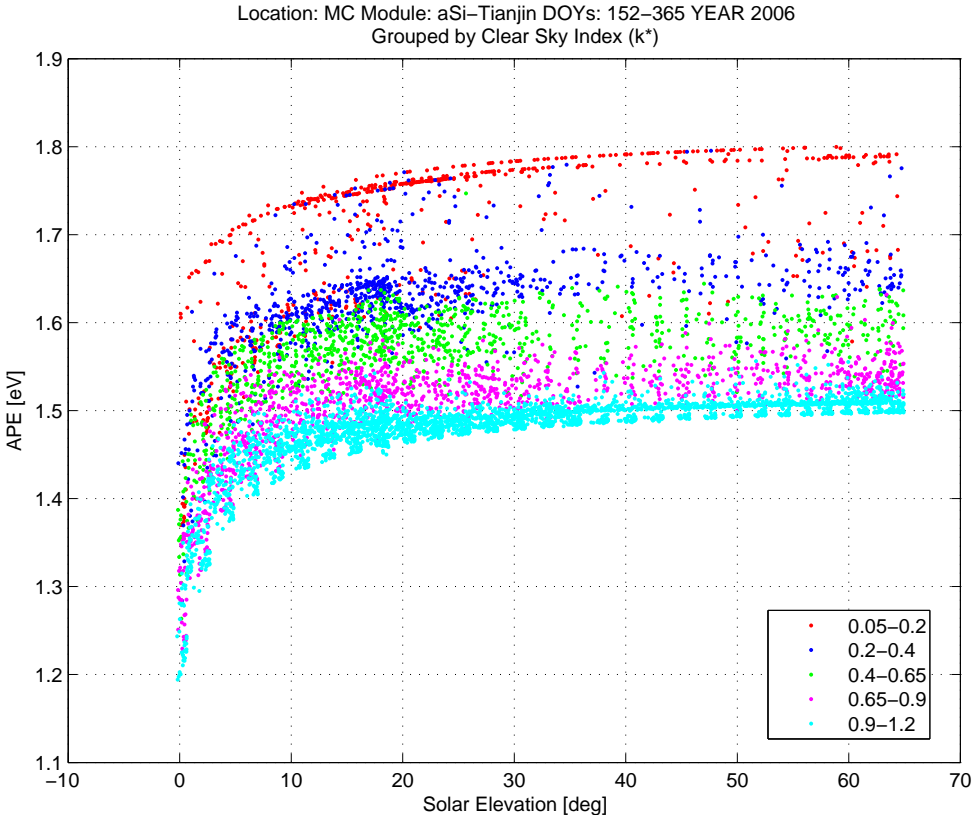


Figure 4.7: APF dependence on solar elevation angle γ_s .

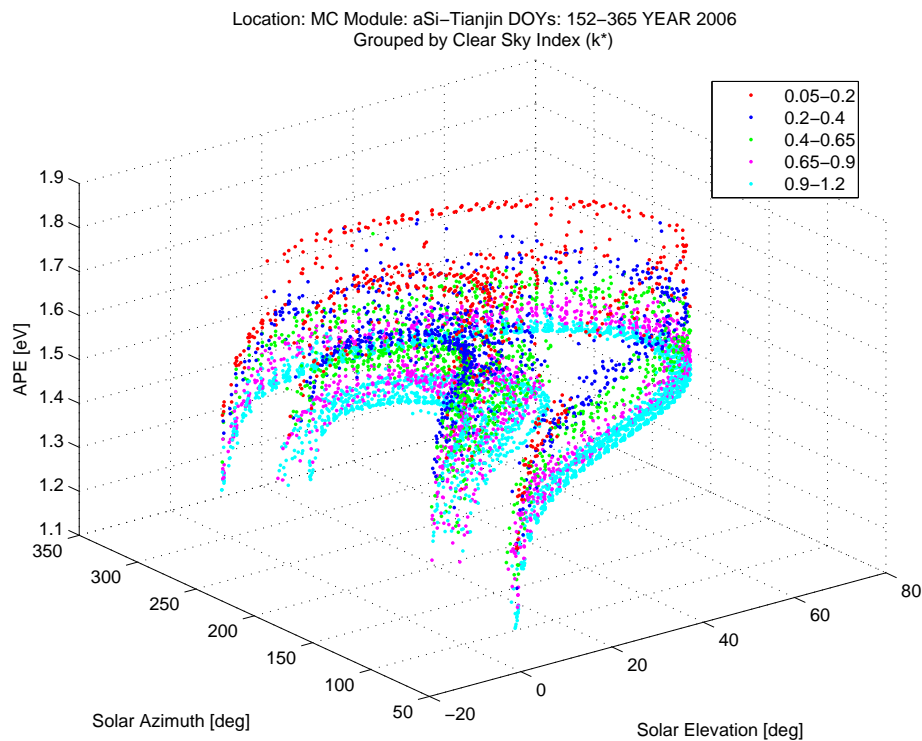


Figure 4.8: APE dependence on solar elevation γ_s and solar azimuth φ_s .

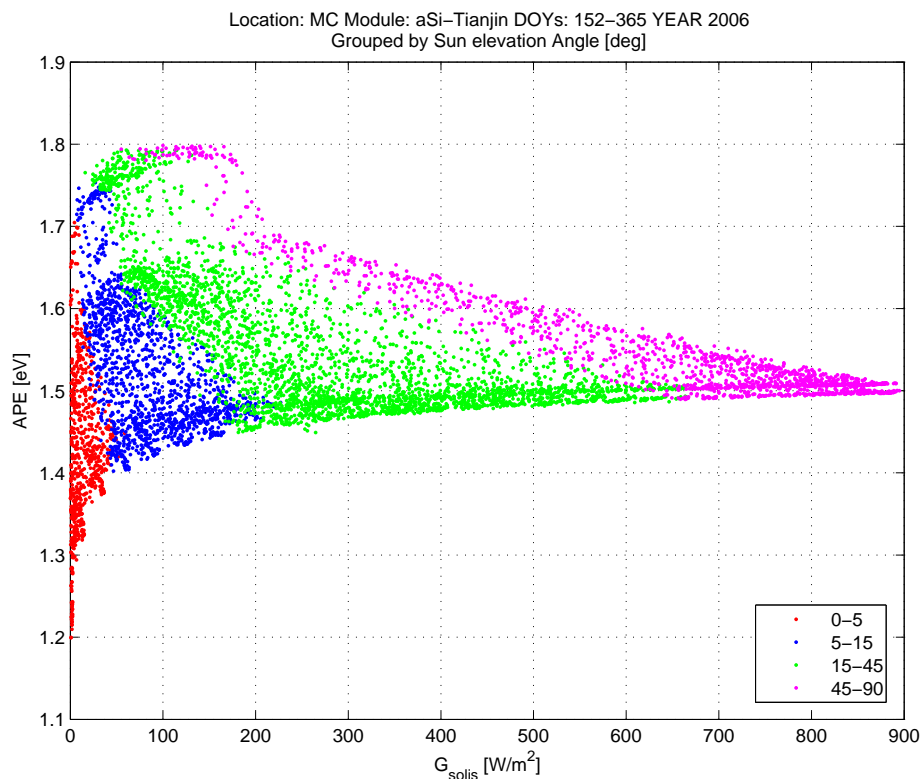


Figure 4.9: APE dependence on global broad band irradiance. Data grouped by Sun elevation angle value.

broad band irradiance and selected three situations with low, mid and high values of k^* . The value of irradiance is $100W/m^2$ because at this value we have all the k^* groups. We can see that for the spectra with lower APE values, a *red-shift* occurs in the region $300nm - 600nm$ while in the region $1300nm - 2300nm$ an increase in the band spectral irradiance values occur to compensate the shifting and to preserve the same area value under each curve for all the cases. These chromatic variations are due mainly to cloud conditions, however the effect of AM is still present but at a minor extent. The bluest spectrum occurs at very high Sun elevation and very cloudy situation while the reddest one at very low Sun elevation and clear sky conditions. It is not possible to isolate cloud effects from AM effects for fixed irradiance under outdoor conditions.

In the second spectra example we have fixed the k^* value at 1.05 ± 0.15 (see Fig. 4.11 on page 39). In this case we want to observe the effects of AM , which implies different broad band irradiance values. This time we don't have two variables affecting the spectra disguised because APE is independent of the intensity of the spectra. In this case the bluest spectrum is obtained at very high values of Sun elevation and broad band irradiance, while for the reddest completely the opposite happens. In table 4.2 and table 4.3 the reddening of the spectra with lower APE values is given. The value is given as percentage of the APE value of the bluest spectra for the cases of fixed G and fixed k^* respectively.

4.3 Used Fraction or Broad Band Photoelectrical Efficiency UD

We will include another spectral parameter in our study. The *Used Fraction UD* is mathematically defined by equation 4.6. In this equation SR_λ is the spectral response curve of a *PV* module. It is clear then that this parameter is not *device independent* as APE .

$$UD = \frac{\int_a^b G_\lambda SR_\lambda d\lambda}{\int_a^b G_\lambda d\lambda} \quad (4.6)$$

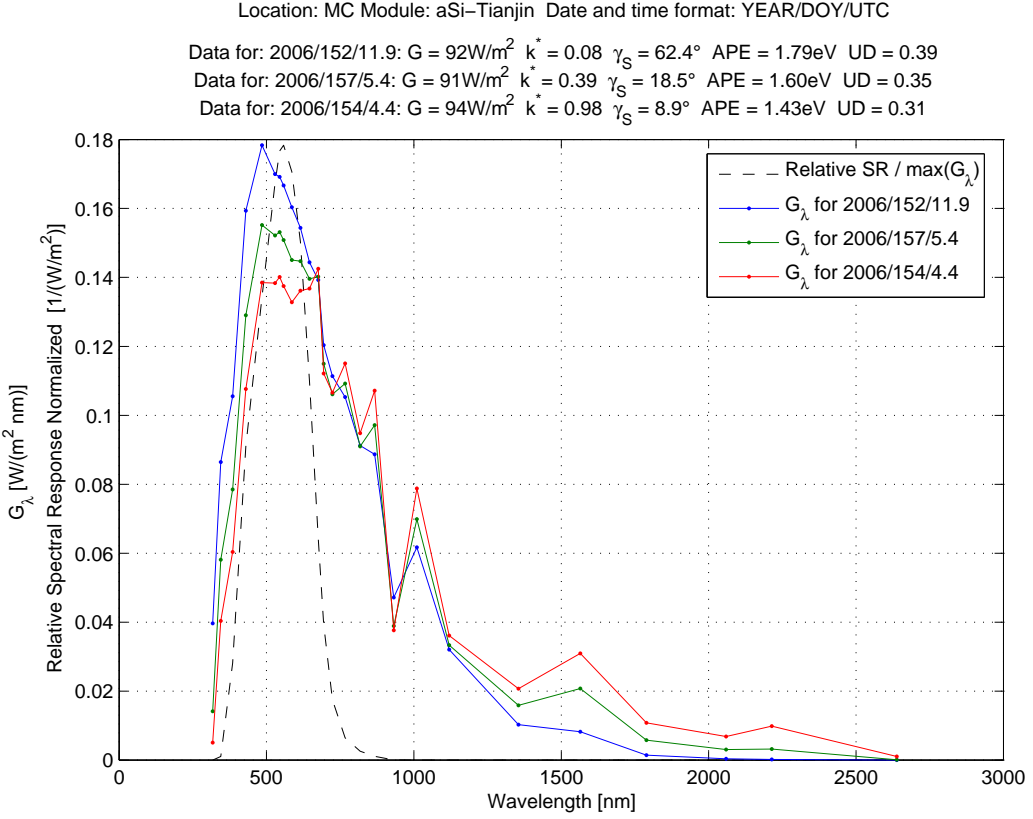


Figure 4.10: Examples of SOLIS spectra for fixed global broad band irradiance of $100 \pm 10\text{W/m}^2$ for different conditions of Clear Sky Index k^* and Sun elevation γ_s .

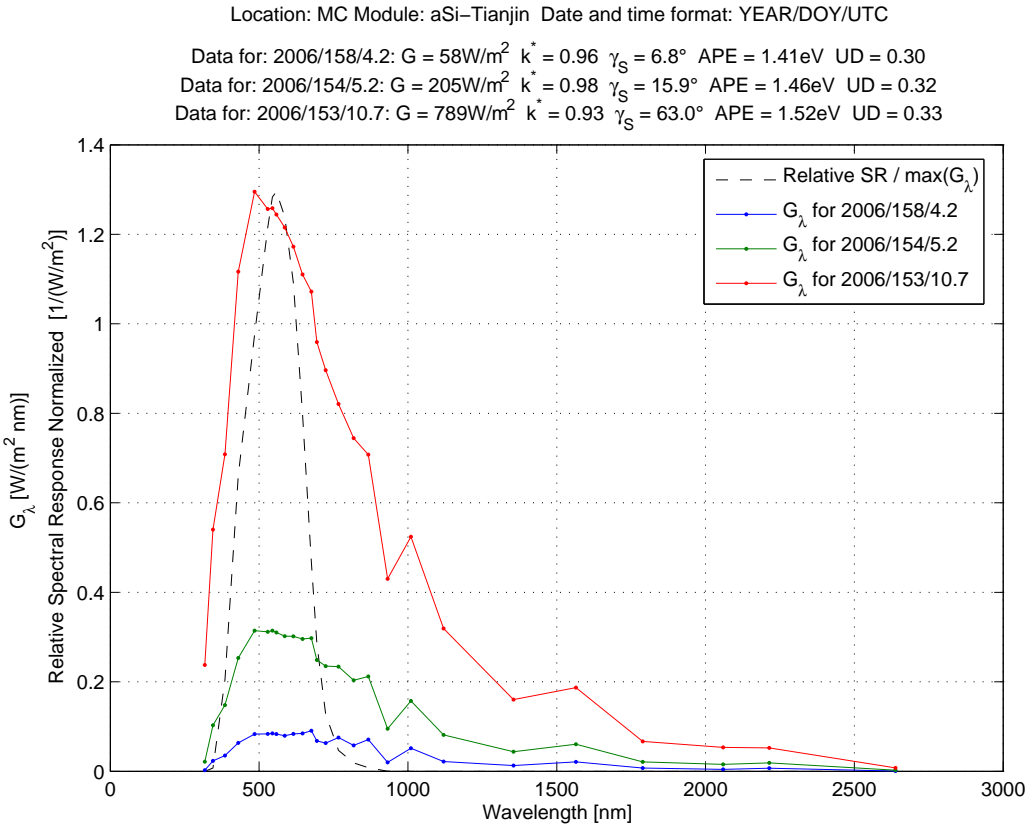


Figure 4.11: Examples of SOLIS spectra for fixed Clear Sky Index of 1.05 ± 0.15 for different conditions of global broad band irradiance and Sun elevation γ_s .

<i>Spectral Variation for Fixed Irradiance $G = 100 \pm 10 W/m^2$</i>				
$G [W/m^2]$	$k^* [1]$	$\gamma_s [\text{deg}]$	$APE [\text{eV}]$	Reddening [%]
92	0.08	62	1.79	-
91	0.39	18	1.60	10.6
94	0.98	9	1.43	20.1

Table 4.2: Reddening of *SOLIS* spectra for fixed global broad band irradiance according to *APE*.

<i>Spectral Variation for Fixed Clear Sky Index $k^* = 1.05 \pm 0.15$</i>				
$G [W/m^2]$	$k^* [1]$	$\gamma_s [\text{deg}]$	$APE [\text{eV}]$	Reddening [%]
789	0.93	63	1.52	-
205	0.98	16	1.46	3.9
58	0.96	7	1.41	7.2

Table 4.3: Reddening of *SOLIS* spectra for fixed Clear Sky Index value according to *APE*.

In words *UD* is defined as follows:

UD is the ratio of the theoretically generated electric charge in a time interval Δt to the energy incident on the area of the PV device in the same time interval. This is then the *broad band photoelectrical response* of the device under study in $A/(W/m^2)$.

When we use a relative spectral response instead of the one in A/W , we just have that *UD* is a number proportional to this *broad band photoelectrical response*.

It is important to note that employing a quantum efficiency curve (or the relative one) for the UD calculation hinders the previous interpretations. For an explanation please refer to the section 3.1.2 on page 12. The results presented in this chapter for *CdTe* were calculated on the basis of a relative quantum efficiency curve and therefore are not comparable to the ones of *a-Si* and *c-Si*.

The *Useful Fraction UF* is a parameter which is a special case of *UD*. In this case we use a step function equal to 1 for the relative spectral response curve for the bandwidth of the actual response.

In reality *UD* originated from *UF* and not the opposite, and hence the name *Used Fraction*; however the approach of both parameters is slightly different: *UF* is on the side of the irradiance and is strictly speaking the fraction of irradiance which could be converted into electrical power by a *PV* device of a given spectral response bandwidth. On the other hand, *UD* already describes the operation of the device and is not the ratio of two irradiance values. Ignoring any other influences than the spectral response, it should correspond to the electric current generated by the device. Because of that and because not all the *useful irradiance* ($G \times UF$) converts into electrical current, the name *Used Fraction* results a bit ambiguous. A more descriptive name is *Broad Band Photoelectrical Efficiency*. Nevertheless we will keep the term *Used Fraction* for the rest of the document.

Using *UD* or *UF* for spectral analysis presents advantages and disadvantages: The *UF* values for spectral responses of the same bandwidth but different modulation are equal. This sounds in principle not quite likely; however when using bands for numeric calculation the chances increase. This is exactly what happened with the amorphous Silicon and the Cadmium-Telluride spectral responses, used in this work together with the *SOLIS Kato-bands*. On the other hand using *UD* requires knowledge of the actual spectral response of the modules used, which is seldom the case. With a considerable mismatch in the spectral responses it could happen that false trends are introduced in the data. Despite this, we decided to use *UD* in our short circuit current models hoping that the chosen spectral responses match more or less well the responses of our modules. However the spectral responses used for calculations must be similar to the actual responses of the modules given that they were taken from scientific literature.

The big advantage of *UD* is that -as we will explain in the following section- there is a 1 : 1 relationship between it and the specific short circuit current I_{sc}/G , a quantity we can obtain completely from measurements or partially from measurement (I_{sc}) and *SOLIS* (G). Then it follows that:

With UD we can anticipate how our results should look like. In this way we can analyze systematically the possible causes for mismatching; even considering mismatch between the actual spectral response of the module and the response used for calculations.

Therefore we decided to perform our analysis and modeling using the UD and not the UF values.

4.3.1 Used Fraction UD Analysis

In this section we will analyze the spectral parameter UD . Let's start with the simple mathematical analysis of equation 4.7: By doing an analogy with the analysis of section 4.2.2, this shows that UD is a pure chromatic spectral parameter, i.e it only depends on the shape of the curve of the spectrum times the spectral response and not on its intensity. By means of this equation we can also see that the only difference when using the absolute or the relative spectral response of the PV device only affects the UD value by a positive constant in the numerator. This does not suppose any obstacle when modeling the short circuit current I_{sc} .

$$UD_1 = \frac{\int_a^b a_1 G_\lambda S R_\lambda d\lambda}{\int_a^b a_1 G_\lambda d\lambda} = \frac{\int_a^b G_\lambda S R_\lambda d\lambda}{\int_a^b G_\lambda d\lambda} \quad (4.7)$$

In equation 4.8 an expression for UD in terms of APE is calculated. We see that this is definitely not a function (see also Fig. 4.12 on page 43) due to the dependence on the ratio of two integrals , each being the integral of the product of two functions of wavelength λ . For the two integrals there is one common function, the spectral irradiance density. The other function is in the numerator the spectral response and in the denominator the identity function λ . With this expression it is difficult to make any general statement other than there is an tangled relationship - anything but a bijection- between both parameters due to the different approaches they use for dealing with the spectral variations.

$$UD = \frac{\int_a^b G_\lambda S R_\lambda d\lambda}{\int_a^b G_\lambda d\lambda} = \left(\frac{\int_a^b G_\lambda \lambda d\lambda}{\int_a^b G_\lambda d\lambda} \right) \left(\frac{hc \int_a^b G_\lambda S R_\lambda d\lambda}{\int_a^b G_\lambda \lambda d\lambda} \right) \quad (4.8)$$

$$UD = \frac{hc}{APE} \frac{\int_a^b G_\lambda S R_\lambda d\lambda}{\int_a^b G_\lambda \lambda d\lambda}$$

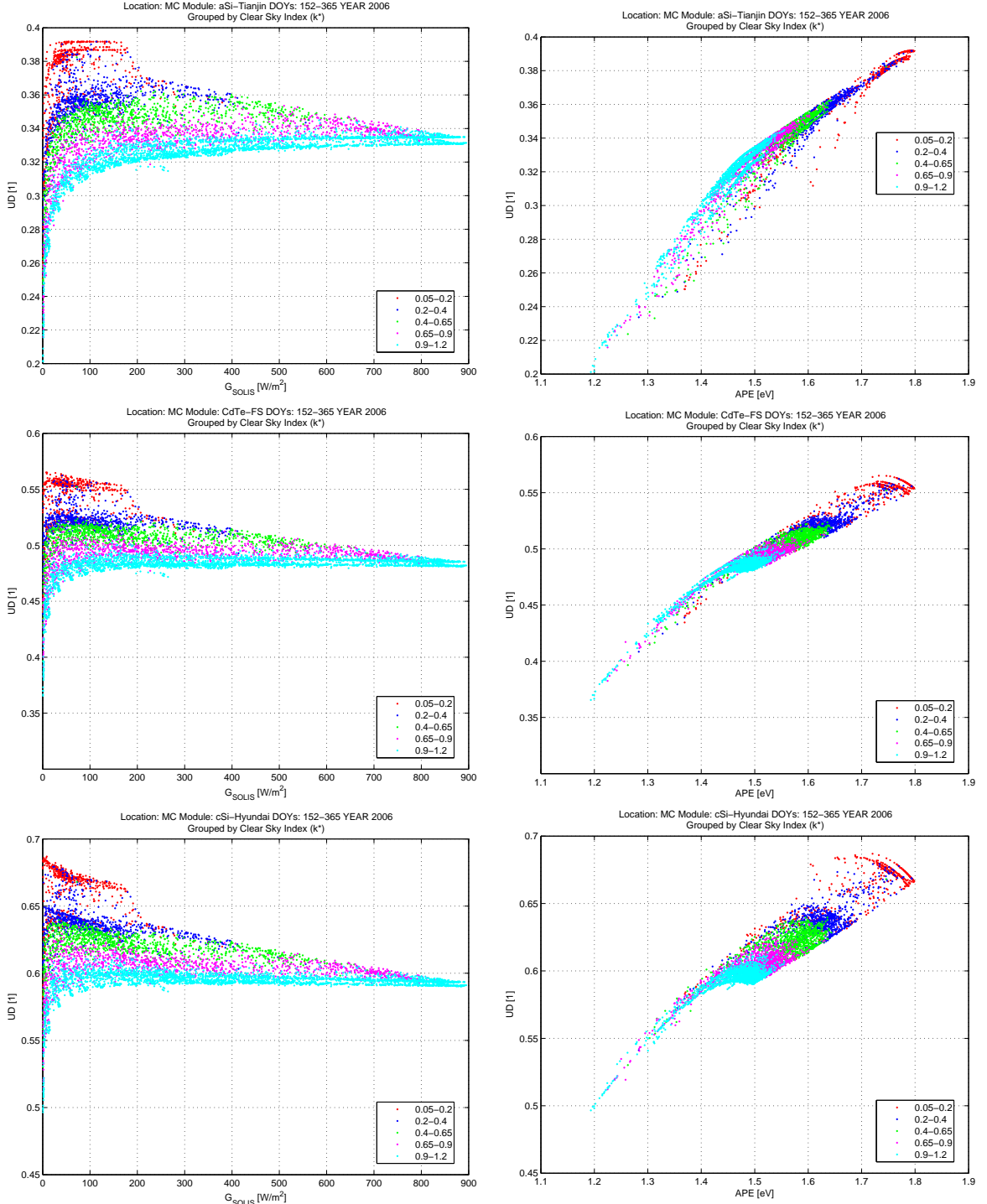


Figure 4.12: *UD* variation over *SOLIS* global broad band irradiance and *APE* for: *Bottom:* poly-crystalline Silicon spectral response (reference). *Middle:* Thin Film Cadmium-Telluride and *Top:* Thin Film amorphous Silicon. The data is grouped by *Clear Sky Index* value.

UD can not be taken as a measure of the *blueness* of the spectra themselves but of the spectra *seen* by the *PV* device. To better visualize these statements, let's go back to the spectra examples used in section 4.2.3 (see Fig. 4.10 and Fig. 4.11 on page 39). There we used different spectra at fixed broad band irradiance for analyzing the effects of clouds mainly; then we saw how these changes manifested in the *APE* values. Likewise we used different spectra at fixed k^* for observing the effect of *AM*. In those plots not only the values of *APE* for each spectrum are included but also the values of *UD* for the *a-Si* device. In Fig. 4.14 the same spectra are used but this time we display spectral irradiances normalized to one in order to facilitate the analysis. The advantage consists in that as we already saw, the parameters *APE* and *UD* depend only on the distribution of the energy in the spectra, not on the amount of energy of them. By plotting normalized spectral irradiances and superposing them, we will be able to see more closely what are the changes which account for reddening/bluening. Let's do some relevant observations:

- For both cases, fixed G and fixed k^* a flattening at low wavelengths (about $500nm$) and a peaking at higher wavelengths (about $1000nm$ and $1500nm$) occur.
- For the cases of fixed G the peaking effect is more important than the flattening. For fixed k^* the flattening effect is more evident but still remains smaller than the peaking effect (these comparisons are made in terms of area differences between the curves about $500nm$, $1000nm$ and $1500nm$.

The reddening is quantified in terms of *APE* and *UD* and the results are gathered in table 4.4 and table 4.5 on page 45. As visual aid, the graph of the spectral irradiance of a black body at $5780K$ at Sun-Earth distance is displayed; as spectral density curve per nm and also in the *SOLIS Kato-bands*. In the same graph we have the relative spectral response curves of three devices used, together with the values of the *APE* and *UD* parameters for the black body spectrum calculated with the *SOLIS* bands. The *UD* values for the black body are 0.29 for *a-Si*, 0.43 for *CdTe* and 0.54 for *c-Si*.

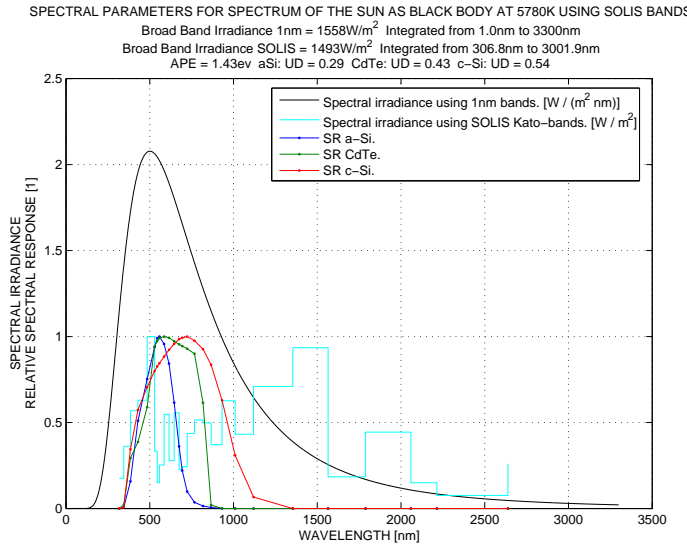


Figure 4.13: Spectrum of the Sun as Black Body: Spectral density curve and SOLIS Kato-bands. The spectral response curves for *a-Si*, *CdTe* and *c-Si* are displayed and can be related to the values of the device dependent spectral parameter *UD* in the top of the graph.

Spectral Variation for Fixed Irradiance $G = 100 \pm 10\text{W/m}^2$				Used Fraction UD [1]			Reddening [%]			
G [W/m^2]	$k^*[1]$	γ_s [deg]	APE [eV]	$a\text{-Si}$	$CdTe$	$c\text{-Si}$	APE	UD <i>a-Si</i>	UD <i>CdTe</i>	UD <i>c-Si</i>
92	0.08	62	1.79	0.39	0.55	0.66	-	-	-	-
91	0.39	18	1.60	0.35	0.52	0.63	10.6	10.3	5.5	4.5
94	0.98	9	1.43	0.31	0.48	0.59	20.1	20.5	12.8	10.6

Table 4.4: Reddening of example spectra for fixed $G = 100 \pm 10\text{W/m}^2$ according to spectral parameters *APE* and *UD*.

Spectral Variation for Fixed Clear Sky Index $k^* = 1.05 \pm 0.15$				Used Fraction UD [1]			Reddening [%]			
G [W/m^2]	$k^*[1]$	γ_s [deg]	APE [eV]	$a\text{-Si}$	$CdTe$	$c\text{-Si}$	APE	UD <i>a-Si</i>	UD <i>CdTe</i>	UD <i>c-Si</i>
789	0.93	63	1.52	0.33	0.48	0.59	-	-	-	-
205	0.98	16	1.46	0.32	0.48	0.59	3.9	3.0	0.0	0.0
58	0.96	7	1.41	0.30	0.47	0.59	7.2	9.1	2.1	0.0

Table 4.5: Reddening of example spectra for fixed $k^* = 1.05 \pm 0.15$ according to spectral parameters *APE* and *UD*.

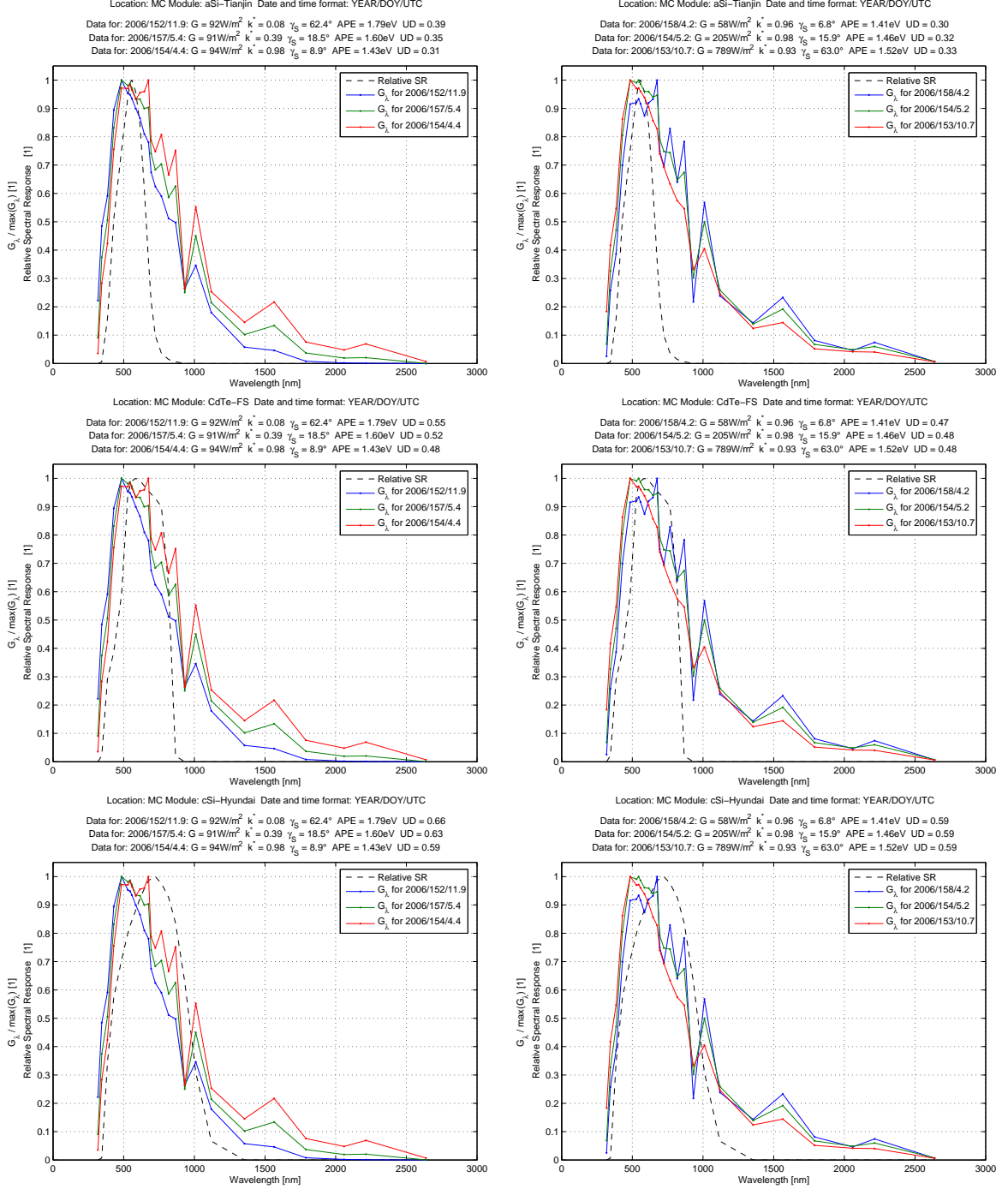


Figure 4.14: Examples of SOLIS spectra with spectral responses overlapped: Top:a-Si. Middle:CdTe. Bottom:c-Si. These are the same spectra used in section 4.2.3.

For both cases, fixed irradiance and fixed Clear Sky Index, and for the used spectral responses; it is clear that the reddening in the UD parameter decreases as the spectral response becomes wider. This phenomenon is related only to the numerator in the expression for UD (the denominator affects the absolute values of UD letting us distinguishing *blue-centered* narrow spectral responses from wider ones centered at higher wavelengths.)

For understanding the UD reddening, let's make a mind experiment: Imagine we have step relative response functions of unity value. Start with a narrow one with the same λ center as the *a-Si* response curve. This narrow SR can only distinguish the flattening while the peaking is completely ignored. This will cause that the UD reddening is very strong because the flattening occurring in more or less narrow bands is considered (big differences in the numerator in the expression for UD for each spectrum) while the peaking which is distributed in wider bands is totally ignored. As we begin to widen our step SR function, we begin to consider at low extents the peaking, so the UD reddening must decrease. Because the widest SR function we have (*c-Si*) reaches only $1350nm$, much of the peaking is still not considered, which causes that the reddening fraction is still greater than zero. This phenomenon is what we observe in the results of table 4.4, where the wider the SR curve, the lower the reddening percentage. In the case we extend the step SR curve to the the same wavelength range of the spectra, our UD values will tend to unity for any spectra, demonstrating that UD does not describe intrinsically the *blueness* of the spectra. At this point the closest thing to an intrinsically descriptor is *APE*, so we will consider it as reference.

In real life we don't have step functions as spectral response curves. This time the spectral responses not only cut the spectra but weight them. This makes things a bit more complicated. Although the three SR curves are more sensitive at low wavelengths (*flattening predilection*), in this range *c-Si* is less sensitive than *a-Si*. This causes that *c-Si* area differences at low wavelengths lose weight in comparison to the area differences at higher values. This reflects in even lower reddening values for the *real c-Si SR* curve than for the ideal step function.

It is worth to note that the case of the ideal step spectral response functions is the one corresponding

to the parameter *UF*.

To close this discussion, let's compare the *UD* reddening values with the *APE* values: The *UD* values for *a-Si* are the most similar to the *APE* ones, being lower or higher. This indicates that for the *APE* calculations the most important reddening information is found at lower wavelengths ($450\text{nm} - 650\text{nm}$) where the response of *a-Si* is close to unity.

SUMMARY: We have two main effects altering the *UD* reddening:

1. The *SR* bandwidth: The wider the curve the lower the resolved reddening.
2. The modulation of the curve: The less sensitive the curve is at lower wavelengths, the lower the resolved *UD* reddening.

4.4 Modified Irradiances

The *modified irradiances* are the result of the multiplication of the global broad band irradiance *G* and a pure chromatic parameter as *UD* or *APE*. This type of parameters comprehend the two components of a spectral parameter: the *chromatic content* from the side of *APE* or *UD* and the *intensity component* from the side of the *G*. The idea of using such parameters comes from the work of Beyer [3], where the *Useful Fraction UF* is used to calculate the *Useful Irradiance UF \times G*.

It is natural to use the spectral parameter *Used Fraction (UD)* for calculation of a modified irradiance as spectral parameter for modeling I_{sc} .

Why?

The answer is simple: By looking at equation 4.9 we realize that $G_{ud} = G \times UD$ should correspond to the electric current generated by the incident light; in the case of using a spectral response in A/W. When using a relative spectral response we simply have a number proportional to the generated

current. To distinguish G_{ud} from the actual measured short circuit current, we will call G_{ud} **Broad Band Photoelectrical Response**.

The relationship between the modified irradiance G_{ud} and I_{sc} is a bijection; i.e a 1 : 1 relationship.

Note that given that different spectra can have the same G_{ud} value, these spectra also generate the same electric current.

$$G_{ud} = \int_a^b G_\lambda S R_\lambda d\lambda \quad (4.9)$$

In the case of the parameter *UF* it is also natural to calculate a modified irradiance; however in this case we can not expect a 1 : 1 matching between this new parameter and the short circuit current given that only the bandwidth of the spectral response is considered. With spectral parameters not considering the spectral response at all, like *APE*, also a non-bijective relationship is expected. Recall that *APE* describe variations in the spectra which could not be significative for the *PV* device (In this case we expect to have in certain cases several values of *APE* for a single I_{sc} value). In any case, for both cases the results should be poorer than with *UD*, although we could also expect improvement respect the traditional model I_{sc} vs G given the similarity of the plots of *UD*, *UF* and *APE* against G .

From this discussion we can see that the plot of I_{sc} vs G should look like the one of G_{ud} vs G . In the case of using the spectral response of the *PV* device in *A/W*) and zero uncertainty in the values of G and I_{sc} both plots should be identical. When using the relative spectral response the splitting is exaggerated because the relative curve is the actual curve multiplied by a positive scalar greater than 1. We know that the order of magnitude of the short circuit current of photovoltaic modules is $10^1 A$ while the one of G_{ud} about $10^2 W/m^2$. Therefore when we plot both quantities against G (about $10^2 W/m^2$ also) the same effects look dramatic when using G_{ud} (See figure Fig. 4.15 on page 50). This is really important to note, because it shows that:

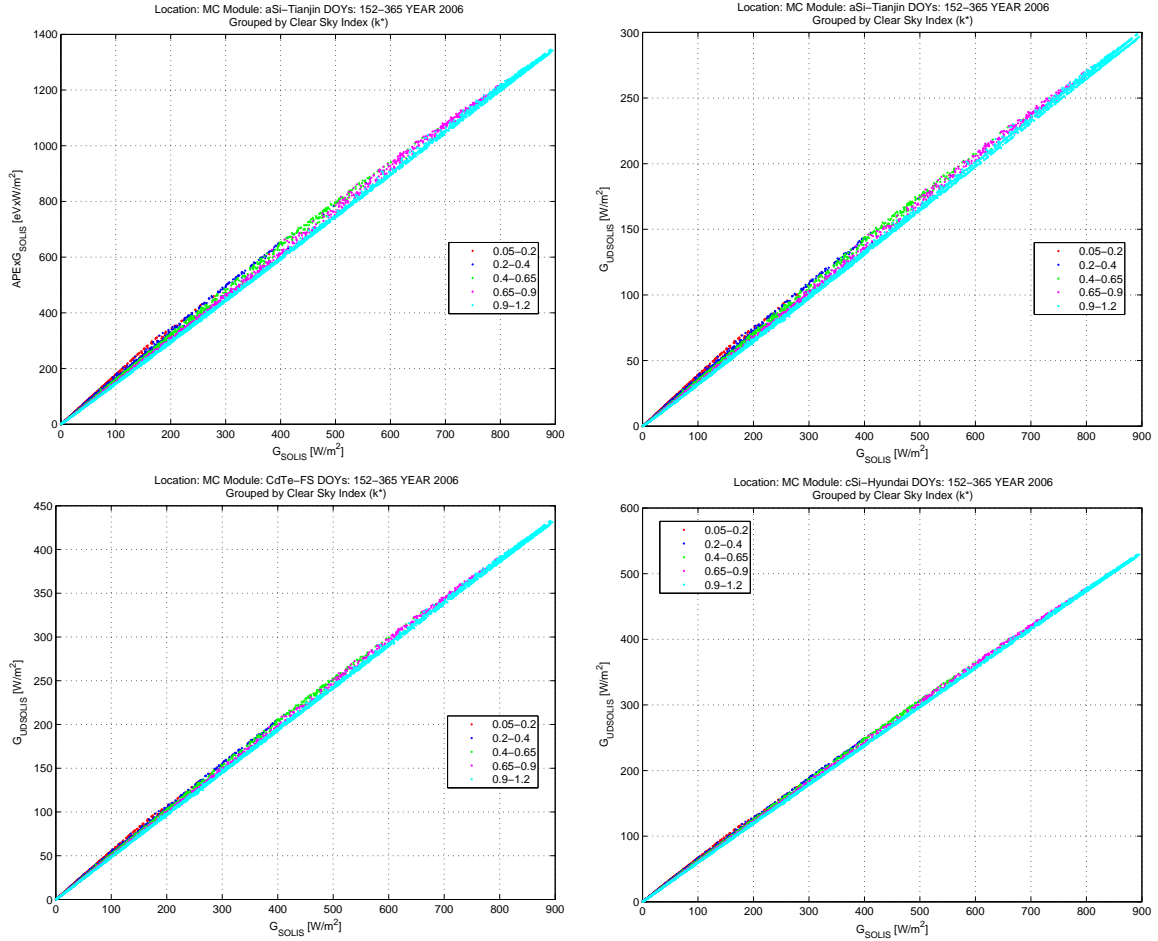


Figure 4.15: *SOLIS* modified irradiances $APExG$ and $G_{ud} = UDXG$ vs global broad band irradiance. G_{ud} is shown for *a-Si* (upper right corner), *CdTe* (lower left corner) and *c-Si* (lower right corner).

By describing a PV device[¶] solely with its spectral response, the spectral effects in the short circuit current values are small enough to be well approximated by a straight line.

This fact is important because it tell us that:

we are dealing with small variations and therefore the uncertainty in our measurements and irradiance calculation models must be minimized.

[¶]Devices with spectral responses similar to the ones of the devices studied in this work.

4.4.1 Modified Irradiances and Linearity

The first thing we have to recall is that linear model $I_{sc} vs G$ works well in general for any type *PV* device, however for devices with lower energy efficiency (income/output) due to spectral response the model does not work as well as for more efficient technologies - but works.

However we better wonder why the linear relationship works so well. In first place we have to realize that G is somehow a spectral parameter, a poor one but still spectral. Why? From our analysis of the previous section it is clear that we could have the same value of irradiance for many different spectral conditions; however the number of possibilities reduces with increasing irradiance. What does it mean? That the set of spectral situation with the same G value is finite. This is a consequence of two factors: The constant nature of the extraterrestrial spectrum and the numerous but finite set of atmospherical, cloud and geometrical conditions affecting the value of G measured on Earth's surface. Therefore G is a spectral parameter which groups big numbers of spectral conditions in each value. The spectral resolution of G is enough for high irradiances. However we must realize what high irradiances imply on Earth's surface:

1. Clear sky
2. High fraction of direct irradiance component.
3. Perpendicular or nearly perpendicular incidence of direct irradiance on surface (low incidence angles). In general this implies high Sun elevation angles but depends on the tilting of the light sensitive surface.

Now let's apply all these conditions and we will see that we are close to only depend on the shape of the extraterrestrial spectrum, where the relationship *spectrum - broad band irradiance* becomes bijective. So this confirms that G is a spectral parameter, but not because of its mathematical definition (an integral over λ) but because of the special conditions imposed by the nature of the Sun and of the complex variations in the atmosphere of our planet.

The previous discussion shows that we don't need spectral parameters which resolve all the thinkable variations in a given range, the problem is then:

how much resolution power do we need?

The answer to this question is not only related to factor exposed above, but when we think about I_{sc} in how much are the *PV* devices affected by the spectral variations. The results of table 4.4 on page 45 and table 4.5 on page 45 suggest that within *SOLIS* less resolving power is required for *CdTe* and *c-Si* than the power offered by *SOLIS APE*. For *a-Si* a similar resolving power is required.

What is behind the calculation of a modified irradiance?

When we multiply broad band irradiance by a chromatic spectral parameter like *APE* or *UD*, what occurs can be summarized like this:

- The data is splitted into groups. These groups are the k^* groups observed in the plots of *APE* and *UD*.
- Each group looks like a straight line when plotted against G ; all with intercept tending to zero and each line with a different slope. These facts can be observed in Fig. 4.15 on page 50.

So it seems we can consider spectral irradiances to be linear functions of G for a fixed k^* group. Let's take a closer look: In order to obtain true straight lines the requirement is that for each k^* group the values of the chromatic parameter are randomly distributed about a constant value when plotted against G . However this is not completely true for our parameters. We have that for Sun elevation angles under 5° the parameter values of *UD* and *APE* decay very fast. This means a strong reddening relative to the rest of the data of the respective k^* group, which seems to be due to high *AM* values mainly. For higher Sun elevation values, the *AM* effects manifest as a small slope in the plot of the chromatic parameter against broad band irradiance for each group. For *APE* there is

an increase (*blueing*) in the values. In the case of *UD* this slopping effect is also influenced by the spectral response of the *PV* device. For *a-Si* *blueing* is observed while for *CdTe* and *c-Si* reddening occurs. The strongest variations occurring account for small slopes about $\pm 10^{-4}$.

In this way, when we multiply the *SPAR* value by the corresponding value of G , we will be introducing small *non-linearities*, especially at Sun elevations under 5° . At higher Sun elevations the effects are negligible because the G values are in the order of $[10^2, 10^3]$ while the *SPAR* values are around $[10^{-1}, 10^0]$, so that the non-linearities are smoothed. The smoothing effect is smaller under 5° where we have values around $[10^{-1}, 10^0]$ and 10^1 for *SPAR* and G respectively. In any case, the data under 5° was not used in the modeling of the short circuit current, given that this Sun elevation value was calculated as the horizon line for the site of the measurements ^{||}

In table 4.6 and table 4.7 on page 55 the results of the fits $SPAR \times G$ as functions of G are shown. With this statistical analysis we want to check the linearity of the modified irradiances. All of them display a linear behaviour, which improves in the following order:

1. Lowest linearity: $APExG$ and G_{ud} for *a-Si*
2. G_{ud} for *CdTe*
3. Highest linearity: G_{ud} for *c-Si*. Also within each model the quality of the fits becomes better as the Clear Sky Index average value of the groups increases.

These results are -as it should be- in agreement with what we found in the reddening analysis of the *SPARs*: The results for *APE* and *a-Si* are very similar (high reddening/lower linearity) while *CdTe* is in the middle and *c-Si* on the other extreme (low reddening/high linearity).

The improvement of linearity in the $UD \times G$ models with increasing area of spectral response is understood because in the limit of infinitely wide and sensitivity equal to unity for relative response

^{||}The limit value under which we can have shadow effects for direct irradiance due to buildings, trees or any other obstacle nearby.

curve, our parameter G_{ud} converges to the parameter G (for the case of relative spectral response). In the case of $APExG$ there is no such limit because APE intrinsically describes the spectra.

The fact that the fits $SPARxG$ vs G worsen for increasing cloudy conditions is due to greater absolute uncertainty in calculating small spectral irradiances values coupled to smaller ranges of broad band irradiance.

As stated at the beginning of this section, we see that the results shown here help to understand how the *spectral effects* altering power production appear within a *PV* device which is solely described as a spectral response curve.

In table 4.6 and table 4.7 we have the fit parameters for the calculated modified irradiances. The parameter a -the slope- represents the value of $SPAR$ for each k^* group, which is assumed constant over G . We can use these a values to estimate the relative dispersion of the straight lines $SPARxG$ vs G . In the case of $SPAR = G_{ud}$ these values allow us to see the relative dispersion of the straight lines I_{sc} vs G (the spectral effects). The higher the dispersion among groups, the worse the fit I_{sc} vs G will be. As expected $a\text{-Si}$ displays the highest dispersion and $c\text{-Si}$ the lowest (see table 4.8 on page 55).

4.5 Proposed Spectral Models

After analyzing the spectral parameters APE and UD and their respective modified irradiances, we can proceed to propose the models with which we will model our short circuit current measured data.

1. **Model I_{sc} vs G :** Consists in a single linear fit. It is the reference model which does not take into account the spectral effects resolved by the parameters APE and UD . Here we have the option to use the global broad band irradiance values from ground measurements or the ones calculated with *SOLIS*.

$\langle k^* \rangle$		$APE \times G = a \times G + b$					$a\text{-Si}: G_{ud} = a \times G + b$				
		a [1]	b [eVxW/m ²]	R^2 [1]	$RMSE$ [eVxW/m ²]	$RMSE$ %	a [1]	b [W/m ²]	R^2 [1]	$RMSE$ [W/m ²]	$RMSE$ %
0.11	1.68	+2.3	0.996	6.3	5.6		0.37	+0.4	0.997	1.3	5.2
0.31	1.63	+0.6	0.999	5.4	3.0		0.36	+0.0	0.999	1.1	2.8
0.52	1.58	-0.1	0.999	6.5	2.1		0.35	-0.2	0.999	1.4	2.0
0.79	1.54	-2.6	1.000	7.4	1.6		0.34	-0.9	1.000	1.7	1.6
0.99	1.51	-6.3	1.000	5.1	0.8		0.34	-1.9	1.000	1.4	1.0

Table 4.6: Fit parameters for device-independent model $APE \times G$ vs G and for the device-dependent model $UD \times G$ vs G for $a\text{-Si}$. The relative $RMSE$ values are calculated by dividing by the mean modified irradiance of the corresponding k^* group. No filters applied to *SOLIS* data.

$\langle k^* \rangle$		$CdTe: G_{ud} = a \times G + b$					$c\text{-Si}: G_{ud} = a \times G + b$				
		a [1]	b [W/m ²]	R^2 [1]	$RMSE$ [W/m ²]	$RMSE$ %	a [1]	b [W/m ²]	R^2 [1]	$RMSE$ [W/m ²]	$RMSE$ %
0.11	0.52	+1.0	0.998	1.5	4.2		0.64	+1.3	0.998	1.6	3.7
0.31	0.51	+0.8	0.999	1.2	2.1		0.62	+1.3	1.000	1.2	1.7
0.52	0.50	+0.8	1.000	1.4	1.5		0.61	+1.3	1.000	1.5	1.2
0.79	0.49	+0.4	1.000	1.8	1.2		0.60	+1.0	1.000	1.8	1.0
0.99	0.48	+0.0	1.000	1.4	0.7		0.59	+0.8	1.000	1.2	0.5

Table 4.7: Fit parameters for device-dependent models $UD \times G$ vs G for $CdTe$ and $c\text{-Si}$. The relative $RMSE$ values are calculated by dividing by the mean modified irradiance of the corresponding k^* group. No filters applied to *SOLIS* data.

$\langle k^* \rangle$		Relative Increase of a Fit Parameter for Fits G_{ud}		
		$a\text{-Si}$ %	$CdTe$ %	$c\text{-Si}$ %
0.11	12.1	8.3	8.5	
0.31	9.1	6.2	5.1	
0.52	6.1	4.2	3.4	
0.79	3.0	2.1	1.7	
0.99	—	—	—	

Table 4.8: Calculation of relative dispersion of k^* groups due to spectral effects. The dispersion is ideally the same in the plots G_{ud} vs G and I_{sc} vs G . The reference group is the one with the highest k^* average value.

2. **Model I_{sc} vs G_{ud} :** Is the model using the *broad band photoelectrical response* of the PV device or *Used Fraction*. It consists in a single linear fit. This model could offer best matching due to the ideal 1 : 1 linear relationship between both quantities. We have at hand G_{ud} values calculated from SOLIS broad band irradiance or ground measurements. The UD values are calculated with the SOLIS spectral irradiance.
3. **Model I_{sc} vs $G k^*$ groups:** In this model several single linear fits are performed, one for each Clear Sky Index group. This model assumes that the spectral effects manifest as splitting of the I_{sc} data plotted against G , into several straight lines. Each line is defined by points of similar k^* value. This assumption comes from the results of this chapter, in which G_{ud} displays the behaviour described above and from the correspondence between this parameter and I_{sc} . This model does not consider directly the spectral composition of the irradiance but the cloud conditions which modify it. Again we have the two choices for irradiance, measurement and SOLIS. The k^* values are taken from SOLIS.
4. **Model I_{sc} vs $G_{ud} k^*$ groups:** It is in principle a redundant model because we fit what should be a single straight line with several of them. It is allowed because of the clear stratification of the UD parameter in k^* groups. If improvement is obtained over models 2 and/or 3, it permits analyzing why. For example, in case it is better than models 2 and 3, it would mean that both things -fitting by k^* groups and using G_{ud} instead of G are not completely redundant. If improvement is got over model 3, it would suggest that the k^* values are not sufficient or adequate for describing the spectral variations to which the PV device is sensitive. In the case of improvement over model 3, it could indicate mismatching between the actual spectral response and the one used for calculation of UD . Given that there is total certainty on this aspect, it would point to deficiencies in the spectral irradiance values.
5. **Model I_{sc} vs $APExG k^*$ groups:** In this model the use of a modified irradiance and the k^* groups is not redundant. The absence of a 1 : 1 relationship between I_{sc} and $APExG$ indicates so. If improvement is obtained over model 3, this could be a suggestion that the

inclusion of APE as spectral parameter improves the matching with I_{sc} , even when this a device-independent parameter. Probably improvement can be found for some modules but worsening for others. Improvement over models 2 and/or 4 would suggest very low matching of spectral responses.

Chapter 5

RESULTS: The Short Circuit Current Models

In this chapter we model the short circuit current measured for *a-Si* and *c-Si* with the 5 models proposed in the previous chapter (see section 4.5). The procedure is simple: Using the measured short circuit current values and the selected irradiance parameters (G , G_{ud} , etc) for fitting the data. Then comparison of the modeled data with the original measured data is done. The results presented in this work correspond to the typical error analysis of a fitting procedure: the analysis of the modeled data (\hat{y}) and the original data (y). However the code written is able to use the fit parameters obtained with a given set of data and model I_{sc} values for other set of irradiance parameters. It performs the error analysis of the modeled data with measured data, which must be of course available. In Fig. 5.1 on page 60 a diagram of the information flow for the case of using a single set of data is presented. In this diagram we see that we have two sources of data: The ground measurements and the *SOLIS-Satellite* combination. When we go through it, we see how due to the possible combinations of data from both sources, the 5 proposed spectral models turn into 10. Likewise the inclusion of a temperature model before the spectral models become evident.

In this chapter we will go through diagram 5.1, paying special attention to how spectral effects are

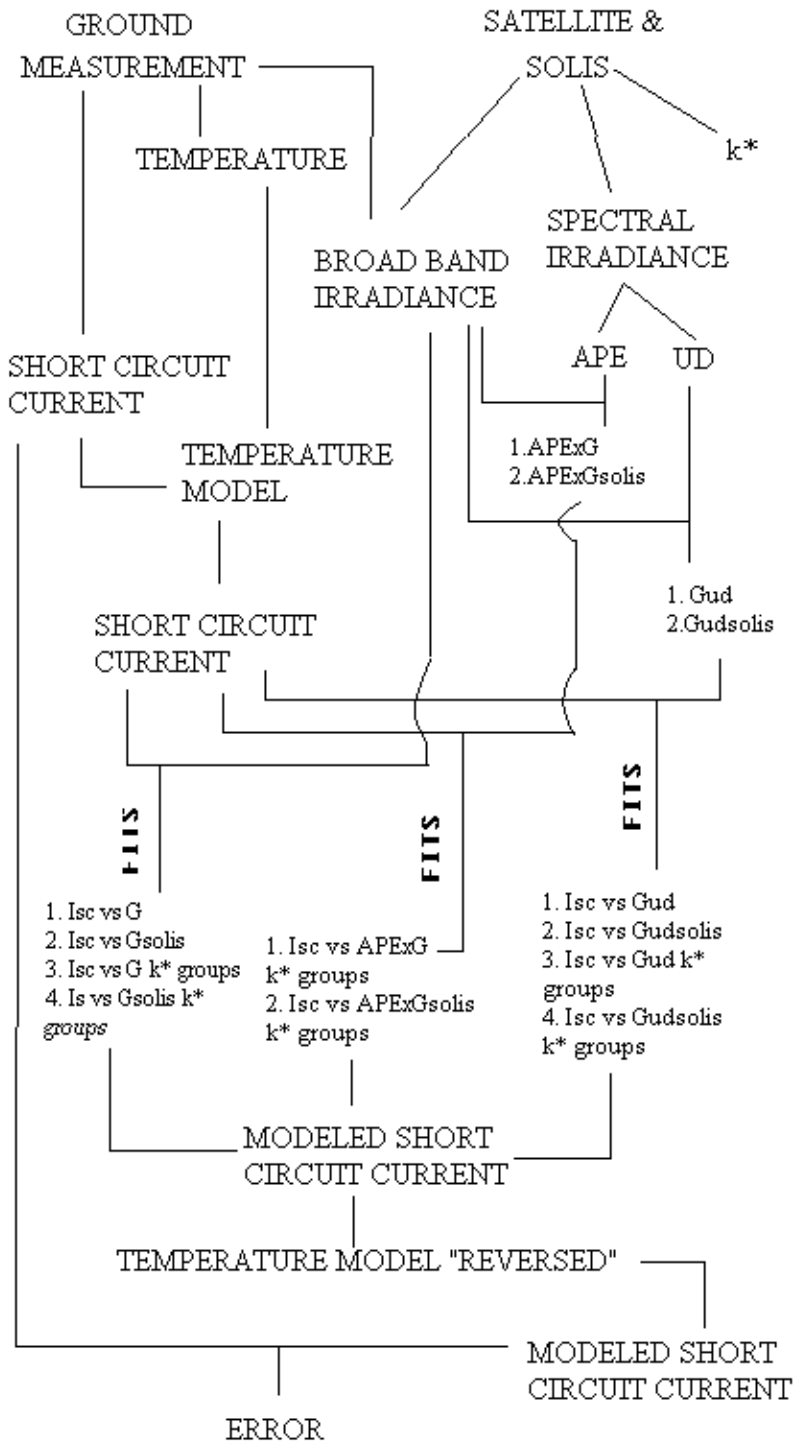


Figure 5.1: Flow of data in the process of modeling short circuit current according to the scheme devised in this work. This diagram corresponds to the case of using a single set of data I_{sc} - Irradiance Parameters for fitting and error analysis. The computer code can handle two complete sets of data: one for fitting and the other for error analysis.

manifest in our data before applying the spectral models. In this way we will be able to expect something about the results of the modeling.

5.1 I_{sc} Temperature Model

It is well known that the temperature of a *PV* cell affects its power production. The higher the temperature the lower the power production. This is related to the fact that for higher temperature and fixed broad band irradiance the open circuit voltage decreases while the short circuit current increases. These changes are modeled as fractional variations of a reference value. They depend on both factors:

1. The temperature difference between the reference point and the actual temperature of the device.
2. A constant characterizing the *PV* device valid for the entire operational range of temperatures.

These constants are known as the temperature coefficients and are normally obtained by variation of temperature with all the other *STC* conditions fixed. Usually they are provided by the producers of the devices.

The temperature coefficients are typically in the order of $+10^{-4}/^{\circ}\text{C}$ for current and $-10^{-3}/^{\circ}\text{C}$ for voltage. This means that the changes in open circuit voltage values are about ten times bigger than the changes in short circuit current. This reflects as an overall decrease in the power production. In equation 5.1 the temperature model for I_{sc} is shown. The model for U_{oc} looks exactly the same.

$$I_{sc}(T_2) = I_{sc}(T_1) [1 + \alpha(T_2 - T_1)] \quad (5.1)$$

The way in which we apply this model is: We fix the reference temperature of 25° (the *STC* temperature) and calculate all the values of I_{sc} at this reference temperature using the measured cell

temperature of the irradiance sensor,* and the temperature coefficients provided by the producers of the modules used.

The values of I_{sc} calculated at the temperature of 25°C are denoted by I_{sc25} .

5.1.1 Results of the Application of the Temperature Model

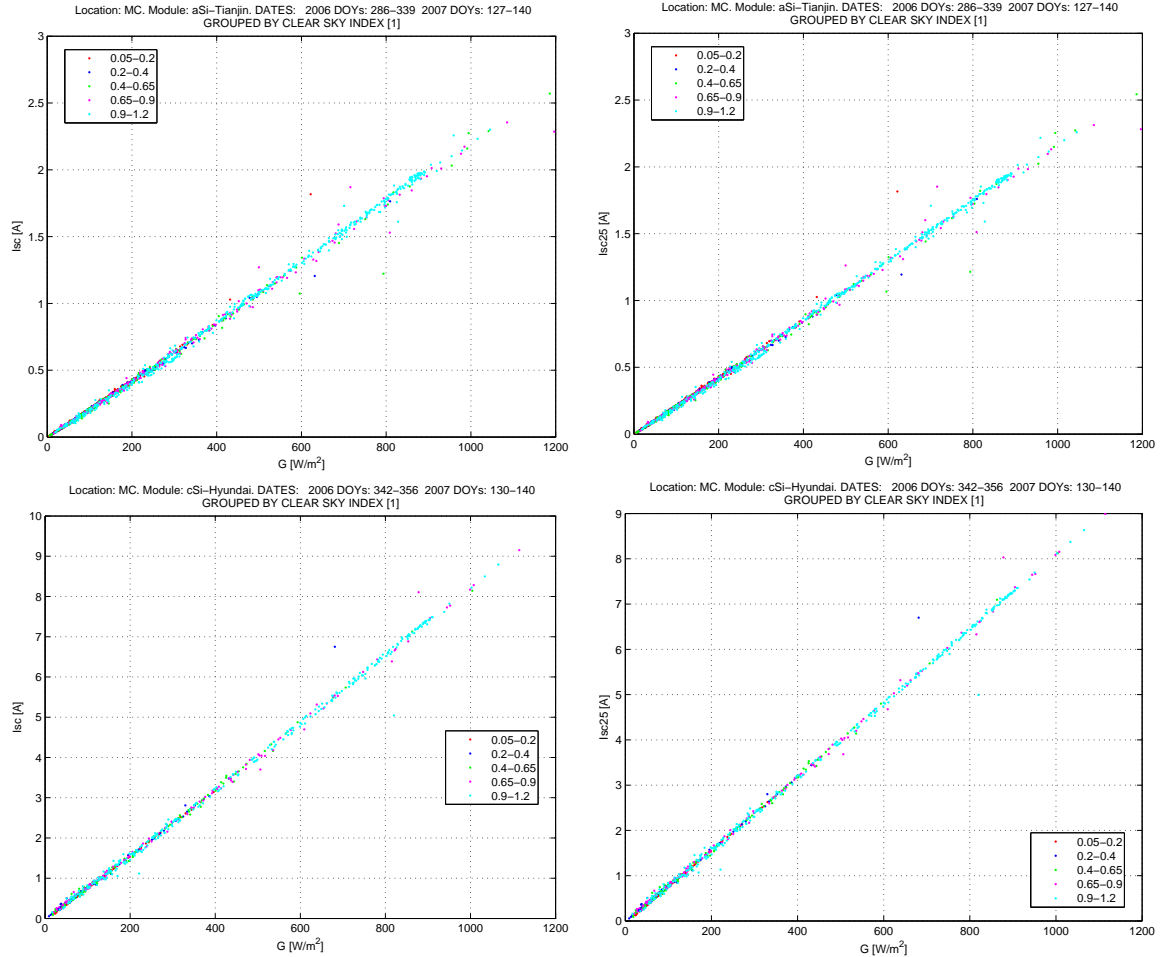


Figure 5.2: Effects of the temperature *correction* of the measured short circuit current values on the linearity of I_{sc} and measured G . Top: *a-Si*. Bottom: *c-Si*. The temperature *corrected* values are denoted by I_{sc25} .

*Note that this is an approximation in which the temperature of the PV module is the measured temperature of sensor cell.

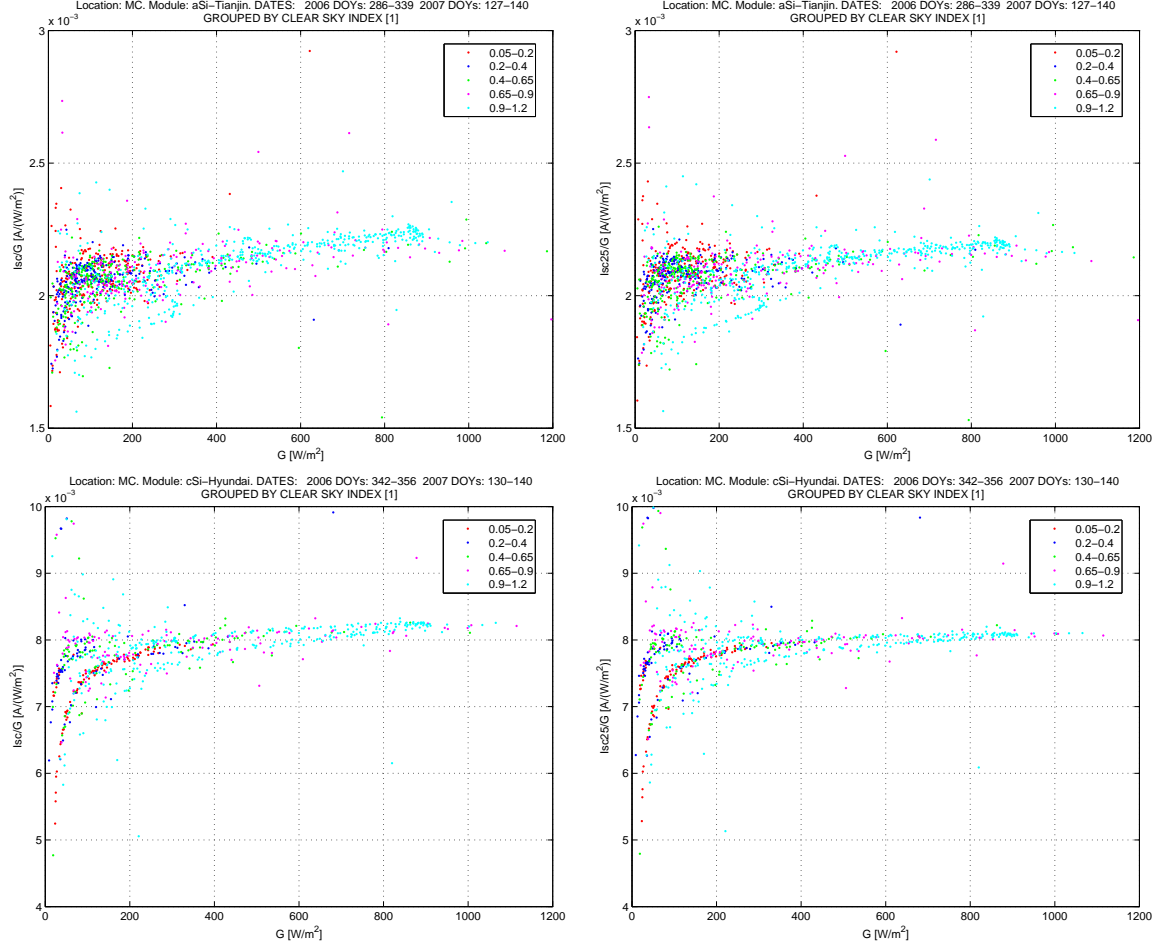


Figure 5.3: Effects of the temperature *correction* of the measured short circuit current values on the linearity of I_{sc} and measured G . Top: *a-Si*. Bottom: *c-Si*. The temperature *corrected* values are denoted by I_{sc25} .

By comparing Fig. 5.2 on page 62 with Fig. 5.5 on page 66 and Fig. 5.3 on page 63 with Fig. 5.6 on page 67 two things become evident:

1. The temperature *correction* improves the linearity of the short circuit current and broad band irradiance for the measured G data. For the G_{solis} values the effects are negligible.
2. The effects are difficult to observe in plots of short circuit current against global broad band irradiance. In plots of specific short circuit current (I_{sc}/G) vs G the effects become evident for high irradiance values which imply the highest temperature deviations from $25^{\circ}C$.

Note that when plotting values of specific short circuit current against any variable, the dispersion of the data increases as the irradiance values decrease. This is due to a nearly constant absolute uncertainty in the short circuit current values for the whole irradiance range, together with a dependence on the uncertainty of I_{sc}/G on the inverse of the G value (assuming no uncertainty in the G value.)[†]

In Fig. 5.2 it can be seen that after the temperature correction a non-linear trend remains for clear sky conditions. For cloudy conditions no trend can be recognized because of the high data dispersion. This trend can be due to different things:

1. Temperature effects not accounted in the correction: Due to systematic error in the temperature measurements, probably related to the assumption that the temperature of the small PV cell in a cage behaves the same as the temperature of the modules. Also the possible underestimation of the temperature coefficient of the sensor cell used for *correcting* the measured G values.
2. Spectral effects related to Sun elevation variations.

[†]

$$\Delta\left(\frac{I_{sc}}{G}\right) = \sqrt{\left(\frac{\Delta I_{sc}}{G}\right)^2 + \left(\frac{I_{sc}\Delta G}{G^2}\right)^2} \quad (5.2)$$

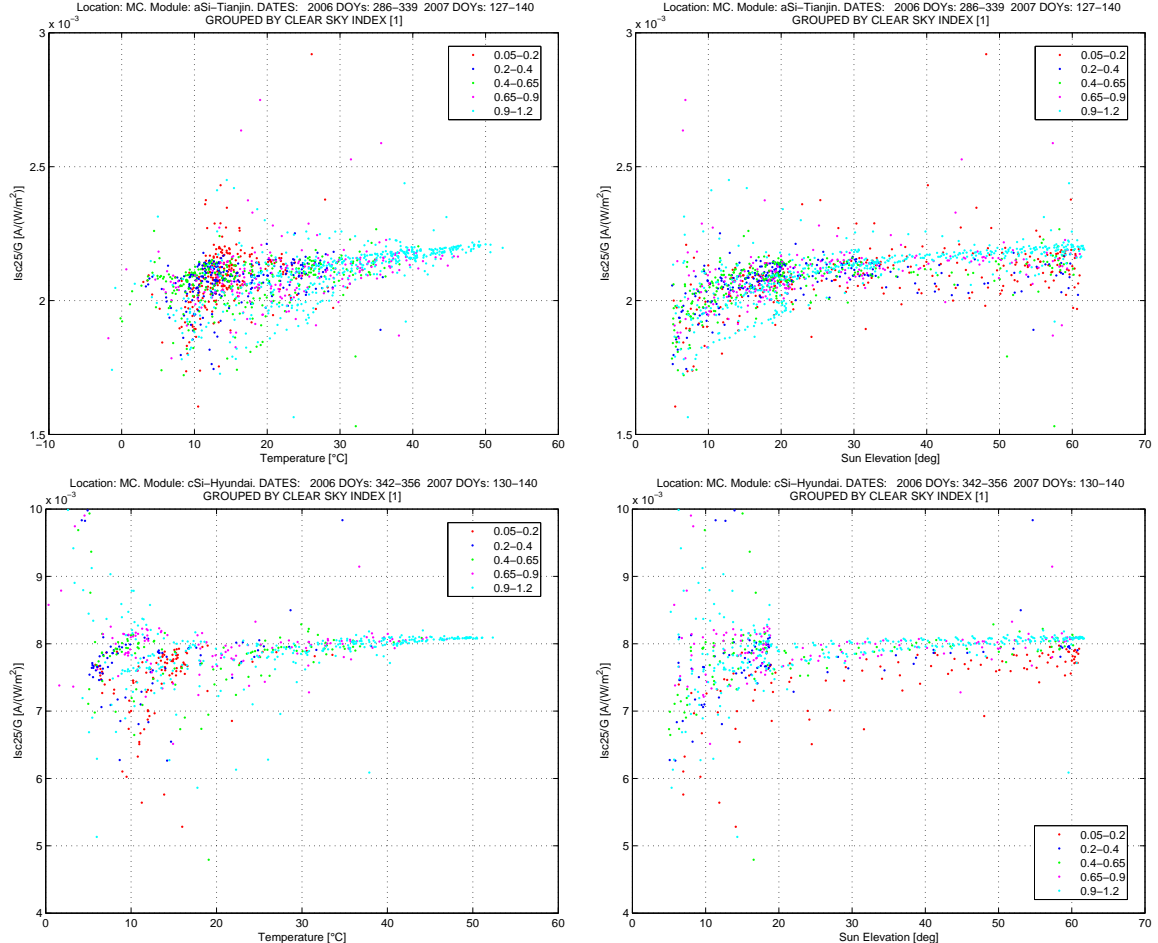


Figure 5.4: Effects of temperature and Sun elevation on the linearity of I_{sc25} and G measured data.
Top: *a-Si*. Bottom: *c-Si*.

In Fig. 5.4 we plot the temperature corrected specific short circuit current against temperature and Sun elevation. We see that the trends of figure Fig. 5.2 are present, which complicates recognizing at what extent the trend is due to temperature effects or Sun elevation effects. We can note that these three variables are related: For clear sky conditions increase in the Sun elevation manifest as increase in the broad band irradiance and in the module's temperature.

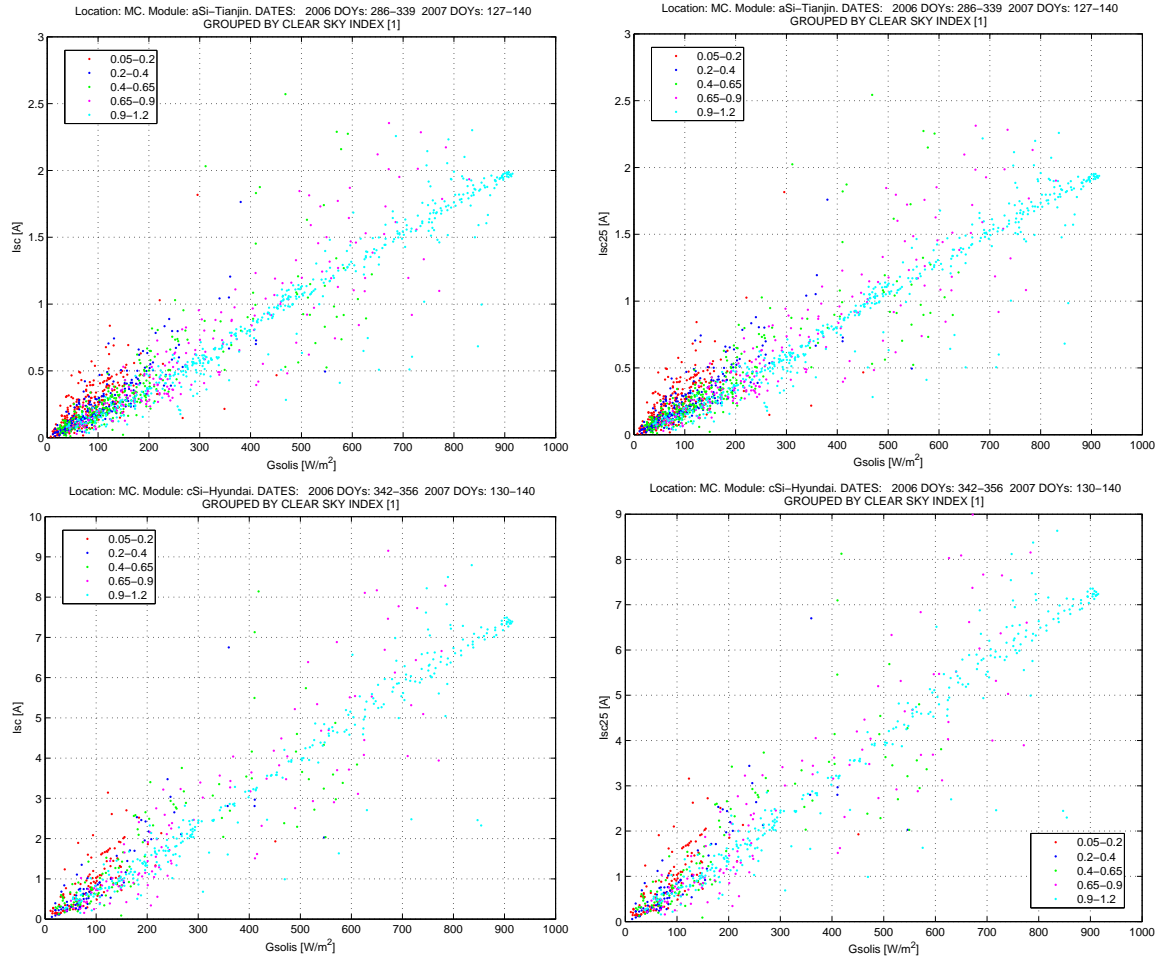


Figure 5.5: Effects of the temperature *correction* of the measured short circuit current values on the linearity of I_{sc} and G_{solis} . Top: *a-Si*. Bottom: *c-Si*. The temperature *corrected* values are denoted by I_{sc25} .

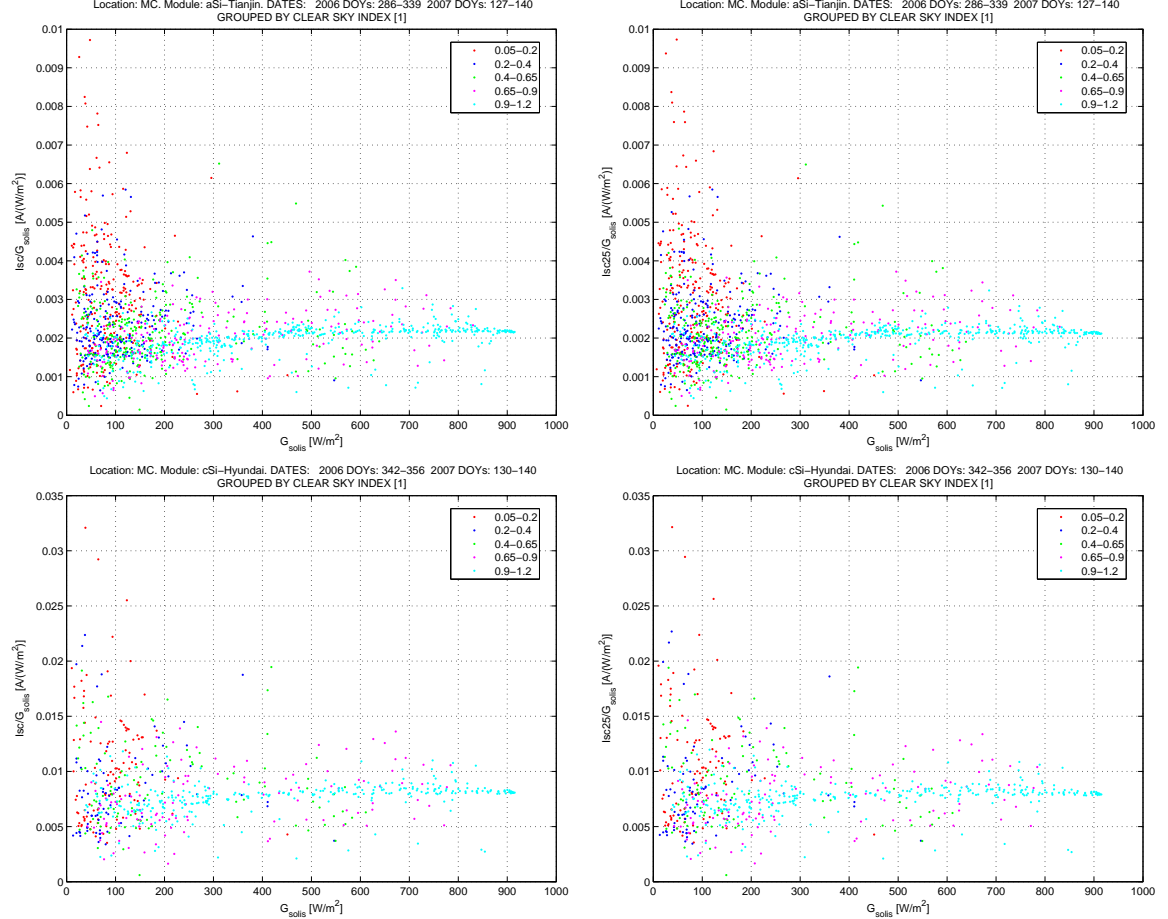


Figure 5.6: Effects of the temperature *correction* of the measured short circuit current values on the linearity of I_{sc} and G_{solis} . Top: *a-Si*. Bottom: *c-Si*. The temperature *corrected* values are denoted by I_{sc25} .

5.2 Spectral Effects

At this point is necessary to realize that:

The plots of temperature-corrected specific short circuit current against global broad band irradiance should be equal to the plots of *Used Fraction* against irradiance. This holds when *UD* has been calculated with the actual spectral response of the PV device.

This is due to the equivalence of G_{ud} and I_{sc} . When using the relative spectral response the plots should differ in the values on the vertical axis but should keep the same proportions.

Before proceeding to compare these plots, we must perform the comparison of UD vs G and UD vs G_{solis} . For both devices they show that **relative to the measured irradiance, the *SOLIS* values are underestimated for cloudy conditions**. This is confirmed when we plot the *SOLIS* global irradiance against the measured irradiance (see Fig. B.2 on page 97). The Clear Sky Index values used for classification of the data into cloudy and no-cloudy conditions, were calculated from the satellite-measured Cloud Index. Therefore we can expect that this underestimation is due to errors in the calculation of the Cloud Index and the radiative transfer model (*RTM*) or only the first. Note that this underestimation of broad band irradiance may affect or not the calculated values of the spectral parameters UD and APE , depending on whether the underestimation is equally distributed in all *Kato-bands* (values are not affected) or not (values are affected). This underestimation is a first obstacle for distinguishing the spectral effects.

Now let's start the comparisons:

In Fig. 5.3 on page 63 we have the plots of I_{sc25}/G vs G for *a-Si* and *c-Si* and in Fig. B.3 on page 98 the plots of UD vs G (please keep in mind that the values of UD are calculated using the *SOLIS* spectral irradiance). The clearest fact is that the plots of specific short circuit current don't exhibit the stratification in k^* groups observed in the UD plots. For *c-Si*, after application of the Sun elevation filter, no fast decay of the values UD is seen for low irradiances; however a fast decay

of I_{sc25}/G can be appreciated. For *a-Si* the fast decay is observed in both type of plots. For the *c-Si* two different branches of I_{sc25}/G are recognized at low irradiances which I can not explain. Respect to the variations along the horizontal axis, the clear sky group is the only one which can be analyzed because it has a wide broad band irradiance range and the dispersion is not critical. From the plots of *UD* vs G and G_{solis} a slope[‡] of about $+10^{-5} m^2/W$ is calculated for *a-Si* and of $-10^{-5} m^2/W$ for *c-Si*. The calculation of the corresponding slopes in the plots I_{sc25}/G vs G give values of about $+10^{-7} m^2/W$ for both devices. It is interesting the change in sign of the slope for *c-Si*. This may be due to the uncorrected temperature effects. However a mismatch in the spectral responses may affect this trend also.

In Fig. 5.6 on page 67 we have the plots of I_{sc25}/G_{solis} vs G_{solis} . In this case the dispersion of the data for cloudy conditions is approximately 5 times bigger than in the case of measured irradiance. Despite of this fact one could say that the stratification of the k^* groups can be recognized at some extent, because for overcast situations there are very high values of I_{sc25}/G_{solis} which are clearly not superposed with any other k^* group. For the case of using *SOLIS* irradiance, the analysis of the slopes gives a positive slope for *a-Si* (about $10^{-7} m^2/W$). For *c-Si* the slope is nearly zero and difficult to determine whether positive or negative. In this case the changes in the slopes may be due also to mismatch of spectral response and uncorrected temperature effects, which for the *SOLIS* case are smaller.

In brief in none of the cases we can clearly observe the main spectral effect predicted with the plots $G_{udsolis}$ vs G_{solis} : the stratification of the k^* groups.

In another attempt to unmask the spectral effects, we can plot the specific short circuit current I_{sc25}/G and I_{sc25}/G_{solis} against the spectral parameters *UD* and *APE*. In the case of *UD*, what we ideally expect is to obtain a straight line with slope 1 and 0 intercept. Because we are using relative spectral responses, the slope should be dramatically reduced. In Fig. 5.7 on page 73 we see these plots, where no straight line can be clearly recognized due to high dispersion. In Fig. 5.8 bins of data have been made according to the Clear Sky Index groups. The order of magnitude of the values

[‡]an approximation calculated in the range $200W/m^2 - 800W/m^2$

in the vertical axis let us estimate the magnitude of the proportionality constant between the spectral response in A/W and the relative spectral response: $SR_{relative} \sim 10^2 SR$. Despite the binning, no trend can be defined due to the extreme dispersion and the tiny variations. However the binning suggests that for low UD values, dominated by clear sky conditions and temperatures above $25^\circ C$, the values of I_{sc25}/G are overestimated. This may be due to the uncorrected temperature effects we see in Fig. 5.4 on page 65. In the case of I_{sc25}/G_{solis} increasing trends are outlined, and this suggests that indeed the overestimation of I_{sc25}/G for low APE values is due to temperature effects.

When plotting I_{sc25}/G and I_{sc25}/G_{solis} against APE the same trends are outlined. This can be seen in Fig. B.6 on page 101 and Fig. B.7 on page 102. In Fig. 5.9 on page 75 we see the dependence of UD on APE and we understand why the trends are kept. It is remarkable also, that in comparison to the same plots in chapter 4 (Fig. 4.12 on page 43), the *comet tails* for APE values under about $1.45eV$ are gone. This is a clear effect of the filtering of the data under 5° Sun elevation used for the I_{sc} model analysis.

Assuming a good correspondence between the satellite based k^* values and the ground measurements, the plots of temperature corrected short circuit current against measured irradiance grouped by k^* value (see Fig. 5.2 on page 62) should display the spectral effects clearly, which is not the case. Then how high should be the precision of the short circuit current measurements so that we are able to distinguish the spectral effects? According to the results of table 4.8 on page 55, for $a\text{-Si}$ we expect 12% increase in I_{sc} values at fixed irradiance when the conditions turn from clear sky to overcast. For $a\text{-Si}$ 8%. However for the site of measurements we have both cloud conditions at maximum $200W/m^2$. At this irradiance we have electric currents of about $0.5A$ for $a\text{-Si}$ and $1.5A$ for $c\text{-Si}$. This means the minimum required precision for detecting the biggest spectral variations are about $0.05A$ and $0.15A$ respectively, which shouldn't be a problem for a decent measurement. However this is rarely the case, usually we have extreme cloud conditions at lower irradiances. At $100W/m^2$ the precision required would be $0.02A$ for $a\text{-Si}$ and $0.08A$ for $c\text{-Si}$; at $50W/m^2$ $0.01A$ and $0.04A$ and so on. For the smallest variations (in terms of k^* groups), the required precision would be about 4 times higher; i.e. about $0.003A$ and $0.01A$ at $50W/m^2$. Besides there are precision require-

$\langle k^* \rangle$	<i>a-Si: $I_{sc25} = (a \times G + b)$ Groups k^*</i>				<i>a-Si: $I_{sc25} = (a \times G_{solis} + b)$ Groups k^*</i>			
	<i>a</i>	<i>b</i>	R^2	<i>RMSE</i>	<i>a</i>	<i>b</i>	R^2	<i>RMSE</i>
	[A/(W/m ²)]	[A]	[1]	[A]	[A/(W/m ²)]	[A]	[1]	[A]
0.11	0.0023	-0.020	0.976	0.031	0.002	+0.06	0.42	0.15
0.31	0.0021	-0.001	0.998	0.012	0.002	+0.00	0.70	0.13
0.51	0.0021	-0.007	0.993	0.034	0.002	+0.03	0.71	0.22
0.79	0.0022	-0.008	0.994	0.041	0.002	-0.09	0.83	0.22
1.00	0.0022	-0.032	0.998	0.025	0.002	-0.09	0.92	0.16

Table 5.1: *a-Si*: Fit parameters of temperature-*corrected* short circuit current against global broad band irradiance, fitting separately Clear Sky Index groups. The variation of the slope *a* gives the variation of the temperature-*corrected* short circuit current values due to spectral effects associated with clouds. Left: Using measured irradiance. Right: Using *SOLIS* irradiance.

$\langle k^* \rangle$	<i>c-Si: $I_{sc25} = (a \times G + b)$ Groups k^*</i>				<i>c-Si: $I_{sc25} = (a \times G_{solis} + b)$ Groups k^*</i>			
	<i>a</i>	<i>b</i>	R^2	<i>RMSE</i>	<i>a</i>	<i>b</i>	R^2	<i>RMSE</i>
	[A/(W/m ²)]	[A]	[1]	[A]	[A/(W/m ²)]	[A]	[1]	[A]
0.11	0.0080	-0.043	0.999	0.015	0.008	+0.24	0.49	0.49
0.31	0.0086	-0.071	0.985	0.130	0.009	+0.04	0.67	0.62
0.51	0.0081	-0.034	0.999	0.052	0.008	+0.22	0.67	0.91
0.79	0.0081	-0.038	0.998	0.110	0.009	-0.28	0.82	0.95
1.00	0.0081	-0.058	0.998	0.113	0.008	-0.19	0.93	0.64

Table 5.2: *c-Si*: Fit parameters of temperature-*corrected* short circuit current against global broad band irradiance, fitting separately Clear Sky Index groups. The variation of the slope *a* gives the variation of the temperature-*corrected* short circuit current values due to spectral effects associated with clouds. Left: Using measured irradiance. Right: Using *SOLIS* irradiance.

ments on the values of measured broad band irradiance. The bigger the uncertainty in the G values, the higher the required precision for I_{sc} . Because our estimations have been made on the basis of a 100% accurate G measurement, the I_{sc} measurements must be even more precise.

Because we measure broad band irradiance with a crystalline cell, we push even higher the precision standards for the I_{sc} measurements of *a-Si*. As we go down in irradiance values, the fluctuations in the electric current output of the devices are expected to increase, so we may find a point where no spectral effects can be recognized because of these random fluctuations due to the statistical nature of the interaction of irradiance with matter and the fact that we are measuring several cells which are in reality not identical.

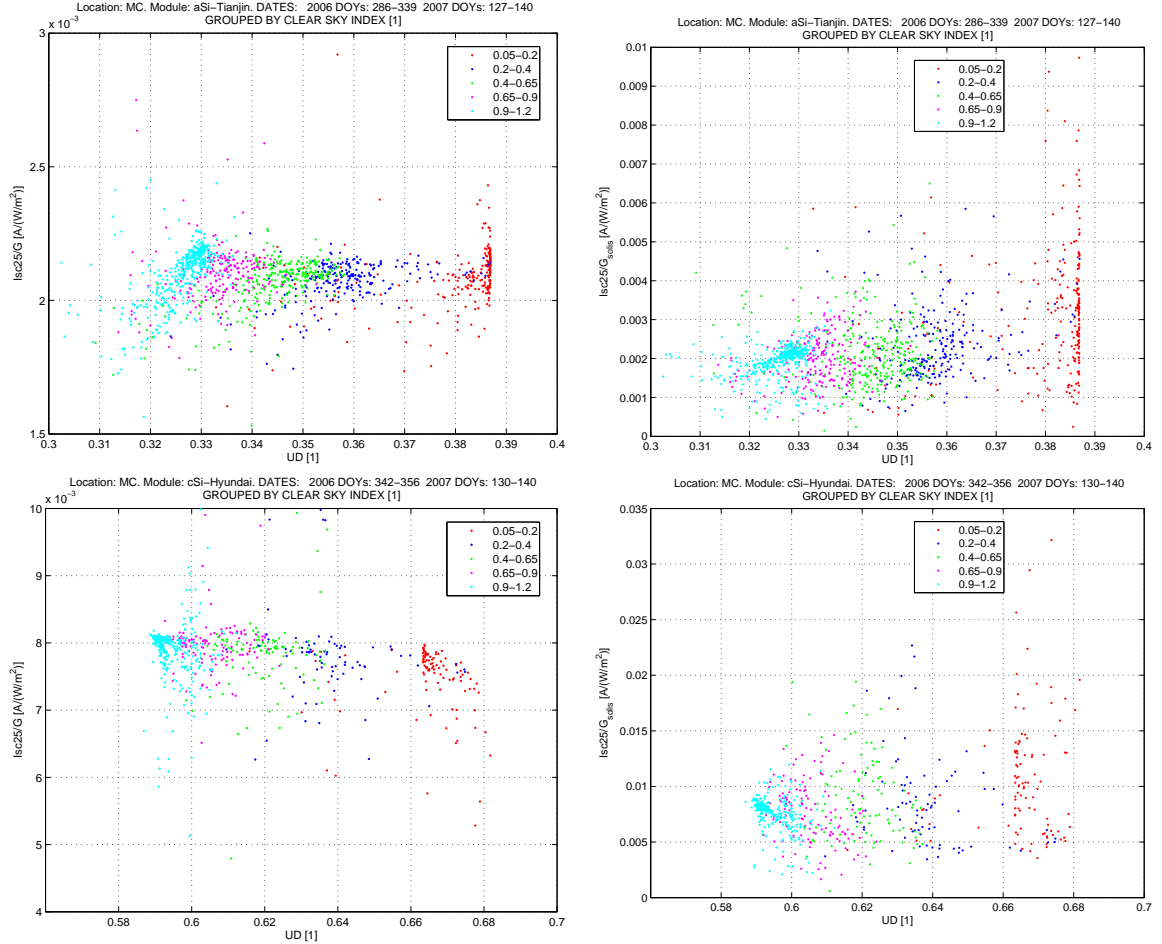
In tables table 5.1 and table 5.2 on page 71 the results of the fits I_{sc25} vs G and I_{sc25} vs G_{solis} for k^* groups are shown [§]. The slopes of these fits should be proportional to the ones found in table 4.6 and table 4.7 on page 55. However in the new tables we can not recognize any trend or even significant change in the values of these slopes. This may suggest that the precision of our measurements is not sufficient. Nevertheless a mismatch of the spectral responses (actual and used for *UD* calculation) and non-corrected temperature effects may account for these observations. Because we did not estimate the uncertainties in the measured I_{sc} and G values, we cannot say whether the measurement precision may mask completely the spectral effects. This cannot be overlooked in future work. However we know that the uncertainties in the I_{sc} and G values depend not only in the precision of the measurements but also on the error introduced by the interpolation of the data.

INNER SUMMARY:

Up to now the results of this section confirm that we cannot recognize clearly the spectral effects:

1. Stratification of Clear Sky Index groups is not observed, not in the $I_{sc25}/G_{(solis)}$ vs $G_{(solis)}$ nor in the $I_{sc25}/G_{(solis)}$ vs *UD* or *APE* plots. In the first type of plots the great increase in the dispersion of the variable $I_{sc25}/G_{(solis)}$ for low irradiances overlap all the k^* groups . The

[§]Note that these statistical results are not the ones used for the evaluation of the quality of the models G with k^* and G_{solis} with k^* . The evaluation of the models is performed using the complete set of data, no matter if the fitting was done by groups or not.

Figure 5.7: I_{sc25}/G and I_{sc25}/G_{solis} vs UD .

dispersion is also due to spectral variations related to Sun elevation variations. In the second type of plots the increased dispersion is distributed along the entire x-axis (UD or APE) and the uncorrected temperature effects are mostly present at low values of the spectral parameters (clear sky conditions). In these plots the data points in the upper part, which clearly define a limit line correspond to the data points with the highest irradiance values of each of the k^* groups.

2. The more subtle spectral effects related to Sun elevation variations are even more difficult to isolate because of the correlation between Sun elevation and module temperature together

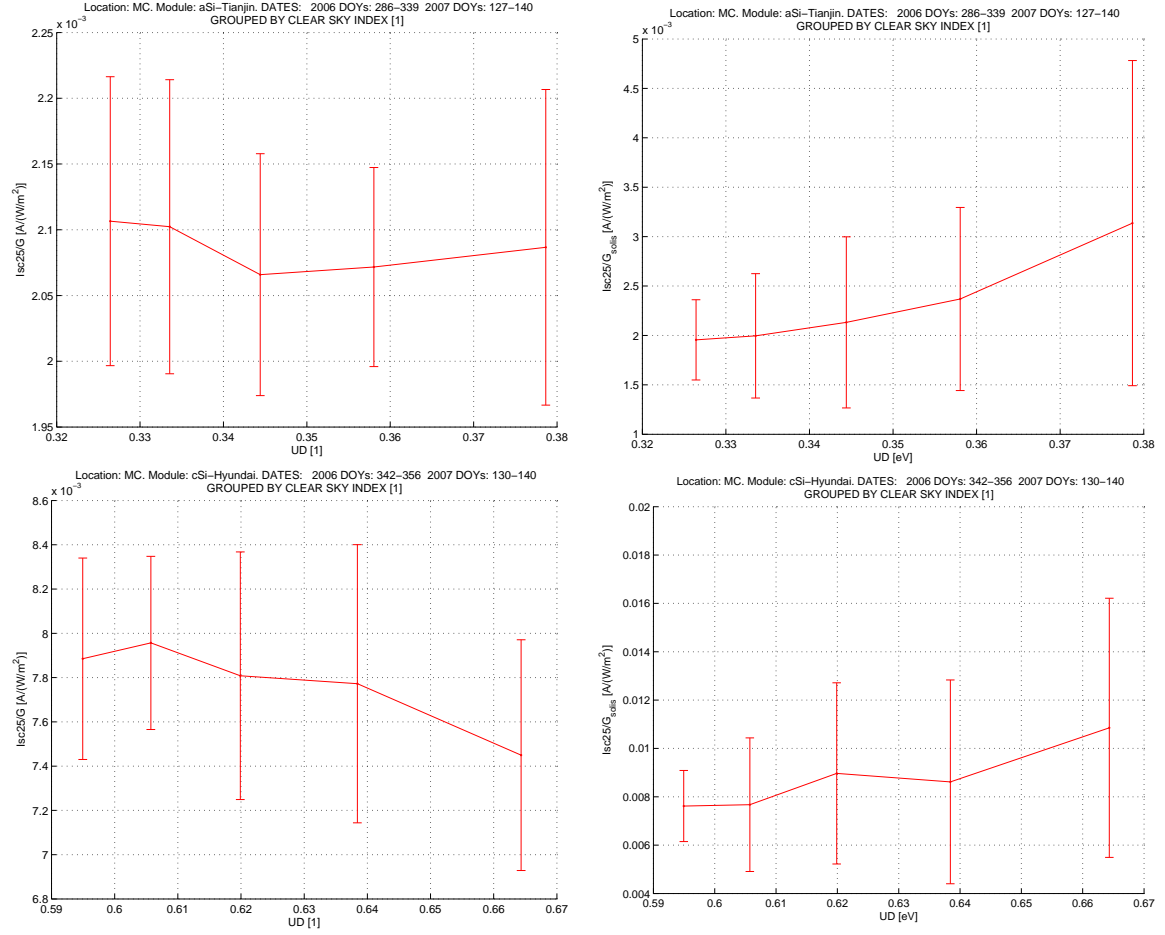


Figure 5.8: I_{sc25}/G and I_{sc25}/G_{solis} vs UD . Bins of data have been made according to the Clear Sky Index groups. The error bars correspond to the standard deviation of the bin.

with uncorrected temperature effects at high temperatures and irradiances.

END OF INNER SUMMARY

Now we will try to find factors which may account for the fact that we are unable to observe spectral effects. Because we have already discussed the influence of uncertainty in measurements, we will focus on other or related causes.

In Fig. 5.10 on page 76 the plots of temperature corrected short circuit current (I_{sc25}) against G_{ud} and $G_{udsolis}$ are presented. According to our discussion about the *Used Fraction* parameter UD , we

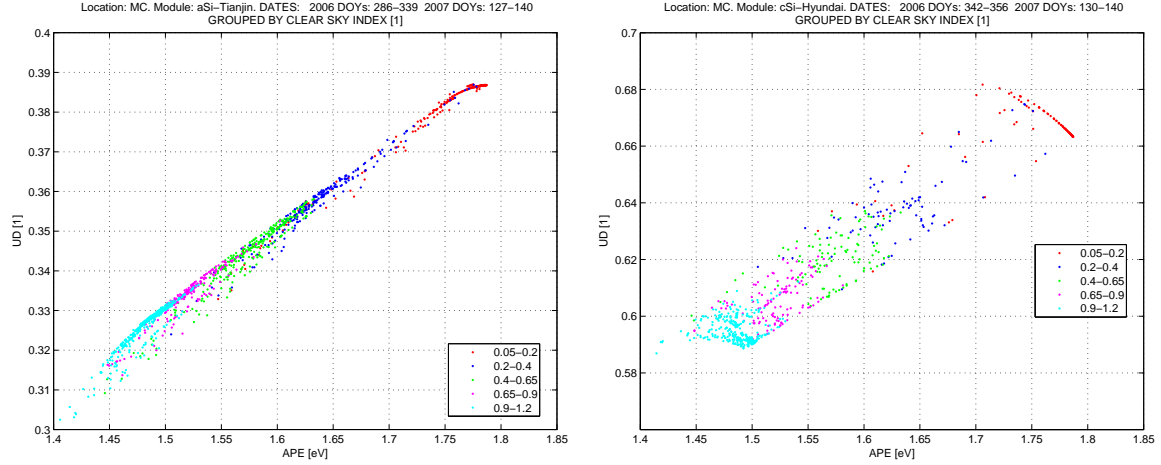


Figure 5.9: UD vs APE for the data used in the I_{sc} model analysis. Left: $a\text{-Si}$. Right: $c\text{-Si}$. Differences with the plots in Fig. 4.12 on page 43 are mainly due to the filtering of data under 5° Sun elevation.

expect to obtain a single straight line in each of these plots. Clearly our expectation is not fulfilled; however the splitting in the results is again magnified by the use of relative spectral responses with values between 0 and 1. In order to gain understanding we have to start by analyzing separately the cases of G_{ud} and $G_{udsolis}$.

In the case of G_{ud} the short circuit current values for cloudy conditions are under the values for clearer conditions for a fixed G_{ud} value. This is interpreted as an overestimation of the values of G_{ud} for cloudy conditions. Most probably this overestimation arises in the UD value than in the G value. On the side of G we could have non-corrected temperature effects. Nevertheless these effects are present most notably at high irradiances and high temperatures. So it looks like the UD values are overestimated for cloudy conditions. This can have 2 different reasons:

1. Arise directly from mismatching of the actual spectral response of the PV device and the spectral response used for UD calculations.
2. It may be related to the systematic underestimation of SOLIS broad band irradiance for cloudy conditions. As stated before, this underestimation may affect the values of UD if this phenomenon is caused by a systematic error in the calculation of the cloud index n : An erroneous

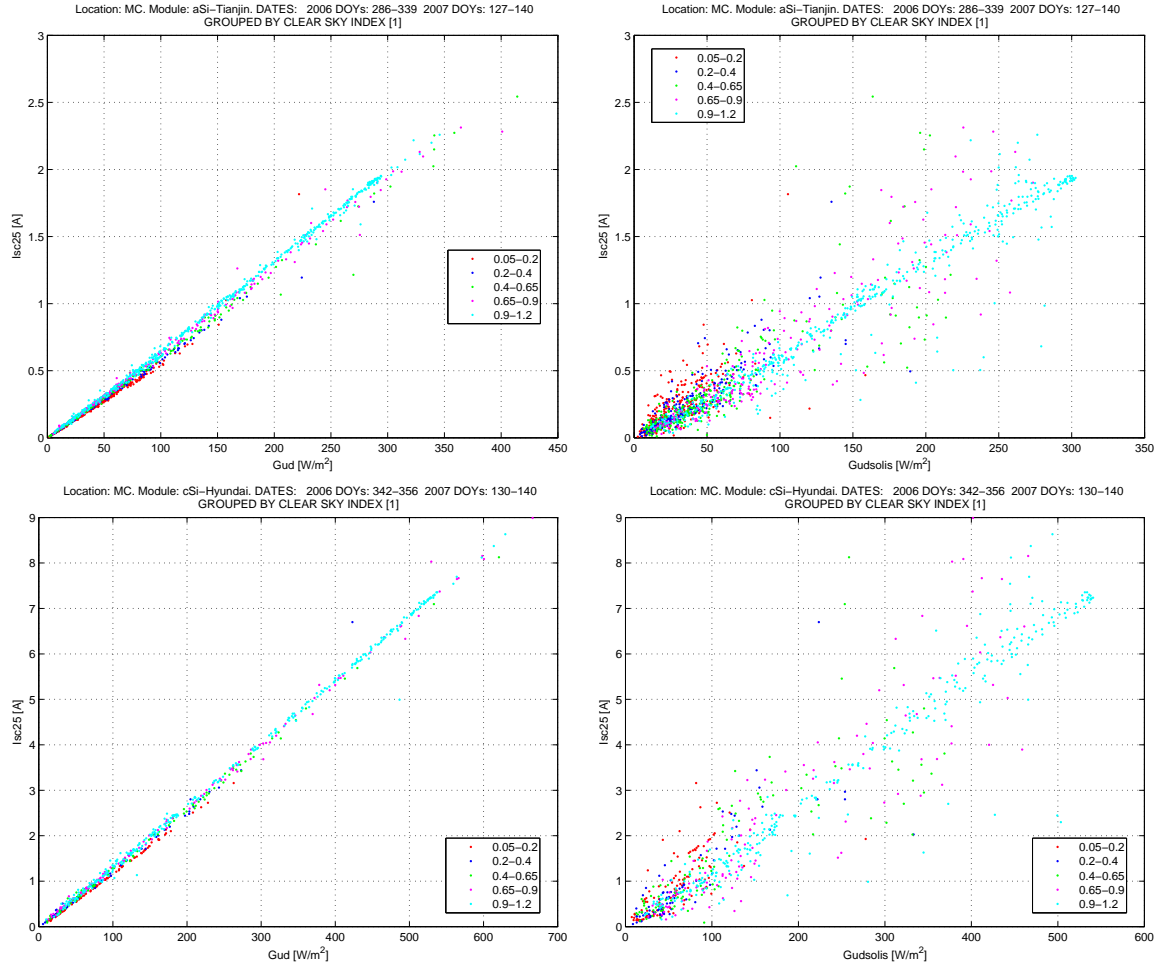


Figure 5.10: I_{sc25} vs G_{ud} and $G_{udsolis}$. Top: *a-Si*. Bottom: *c-Si*.

n value results in in a wrong *SOLIS* spectral distribution and therefore in a wrong *UD* value. So it may happen that too high values of n are calculated for cloudy conditions and therefore higher *UD* values are obtained. However I can not assure that the reductions in the *SOLIS* broad band irradiance values are always associated with an increase or even a change in *UD*.

In the case of $G_{udsolis}$ despite the high dispersion, the contrary effect can be distinguished although only for extreme cloud conditions : Under overcast conditions higher values of short circuit current are obtained than under clear sky conditions for a fixed $G_{udsolis}$ value. This is interpreted as underestimation of $G_{udsolis}$ values for cloudy conditions. How is this understood? The underestimation of

G_{solis} respect G is a fact and the measured G is expected to be better correlated to the short circuit current measurements. Moreover the previous case strongly suggests that an erroneous increase in the UD values is got for cloudy conditions. In this way the underestimation of the $G_{udsolis}$ values is the result of the superposition of the underestimation of G_{solis} and the overestimation of UD . This suggests that the overestimation of UD is minor compared to the underestimation of G_{solis} under cloudy conditions.

This hypothesis is reasserted by the plots of Fig. B.4 on page 99. In these plots we see that the cases G_{ud} vs G and $G_{udsolis}$ vs G_{solis} are consistent and in accordance with our expectations. Differently, the case $G_{udsolis}$ vs G is not what we expect. The first case is still consistent with our expectations despite it makes use of the *SOLIS* spectral data for the UD calculations. However the third cases collapses when we mix *SOLIS* broad band irradiance values with the corresponding measured values. Therefore this is the case we expect to find when modeling measured I_{sc} with pure *SOLIS* modified irradiance.

In any case it must be deeper investigated what are the reasons for the underestimation of the *SOLIS* broad band irradiance values for cloudy situations; with special attention on how the *SOLIS* spectral irradiance results affected.

5.3 Application of the I_{sc} Spectral Models

In this section the term I_{scca} is used. It stands for *calculated short circuit current* and refers to the modeled values which are finally used for the statistical analysis. These values are obtained after application of the temperature and the spectral models in the following order:

1. **Temperature Model:** For calculation of the I_{sc25} values.
2. **Spectral Model:** Calculates the values of temperature *corrected* short circuit current accounting for spectral effects (I_{sc25ca}).

3. **Temperature Model:** For going *back* from the modeled - temperature *corrected* values to the modeled values at the original temperature values (I_{scca}). These values are compared with the measurements.

In this way the chain of short circuit current values looks like this:

$$I_{sc} \rightarrow I_{sc25} \rightarrow I_{sc25ca} \rightarrow I_{scca}$$

Now we can proceed with the discussion about the application of the spectral models:

Despite we could not distinguish the spectral effects predicted with the *SOLIS* spectral irradiance data together with the relative spectral responses of the modules, we will apply the proposed models to observe what the results are. We expect that given clear spectral effects were not measured but only predicted, the models including *UD* and *APE* will collapse.

We have 10 models for each *PV* module. 5 correspond to the models which use ground measurements of global broad band irradiance and the other 5 to the ones using *SOLIS* broad band irradiance. From the 10 models 8 of them use information about the spectral composition of the light (by means of *SOLIS*-Satellite based k^* groups and /or the spectral parameters *UD* and *APE*) except the two reference models I_{sc} vs G and I_{sc} vs G_{solis} .

The results for *a-Si* using measured irradiance are found in table 5.3 and in table 5.4 when using *SOLIS* irradiance. The corresponding results for *c-Si* are in table 5.5 and table 5.6 on page 80.

For the case of using measured broad band irradiance, all the models except one give the same results when we consider only the first significant figure in the statistical error parameters. The exception is the model I_{sc} vs G_{ud} , which gives worse results. It is surprising that the the models I_{sc} vs G_{ud} with k^* groups and I_{sc} vs $APE \times G$ with k^* groups don't collapse. This occurs because the non-existent spectral variations in I_{sc} introduced by the parameters *UD* and *APE* are clearly grouped in k^* groups (see Fig. 5.11); therefore fitting each group separately is consistent. This suggests that indeed no spectral effects can be resolved with precision of the measurements of I_{sc} and G and the

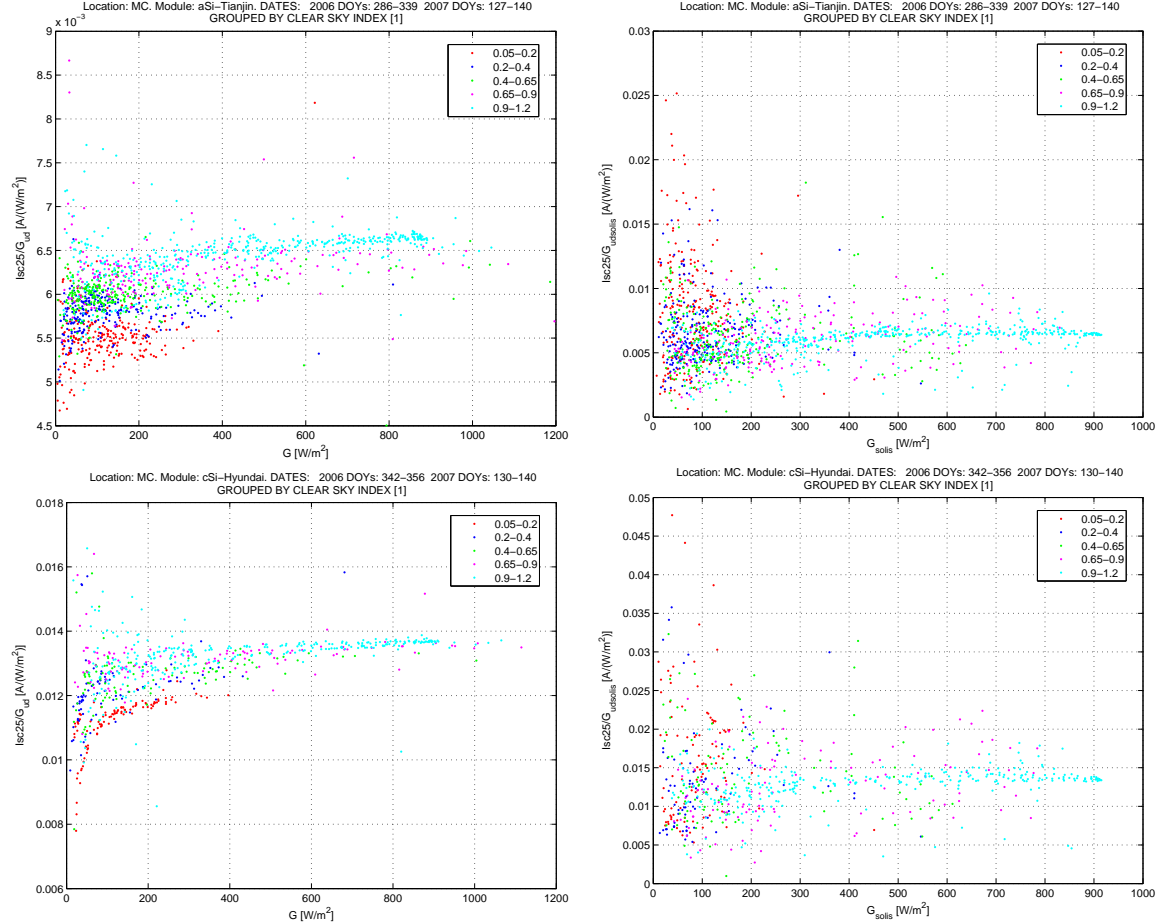


Figure 5.11: I_{sc25}/G_{ud} vs G and $I_{sc25}/G_{udsolis}$ vs G_{solis} . Top: *a-Si*. Bottom: *c-Si*. Because no spectral effects were found in the measured data, the use of G_{ud} , which assumes their existence, introduce artificial spectral dependencies. This is patent when measured broad band irradiance is used. For the case of *SOLIS* irradiance the high dispersion of the data masks these artificial variations (compare with plots of I_{sc25}/G_{solis} vs G_{solis} in Fig. 5.6 on page 67).

<i>a-Si. BASED ON MEASURED IRRADIANCE</i>					
$\langle I_{sc} \rangle = 0.571A$					
Model	$\langle I_{sc} \rangle$ [A]	Bias [A]	Std.Error [A]	RMSE [A]	RMSE %
G	0.571	0	0.031	0.031	5.4
G_{ud}	0.571	0	0.040	0.040	7.0
G with k^*	0.571	0	0.029	0.029	5.1
G_{ud} with k^*	0.571	0	0.031	0.031	5.4
$APExG$ with k^*	0.571	0	0.030	0.030	5.3

Table 5.3: Goodness of the fits for all the models used for I_{sc} for *a-Si*, using the ground measured values of broad band irradiance.

<i>a-Si. BASED ON SOLIS IRRADIANCE</i>					
$\langle I_{sc} \rangle = 0.57A$					
Model	$\langle I_{sc} \rangle$ [A]	Bias [A]	Std.Error [A]	RMSE [A]	RMSE %
G	0.57	0	0.19	0.19	33.0
G_{ud}	0.57	0	0.18	0.18	31.5
G with k^*	0.57	0	0.18	0.18	31.5
G_{ud} with k^*	0.57	0	0.18	0.18	31.5
$APExG$ with k^*	0.57	0	0.18	0.18	31.5

Table 5.4: Goodness of the fits for all the models used for I_{sc} for *a-Si*, using the *SOLIS* values of broad band irradiance.

<i>c-Si. BASED ON MEASURED IRRADIANCE</i>					
$\langle I_{sc} \rangle = 2.47A$					
Model	$\langle I_{sc} \rangle$ [A]	Bias [A]	Std.Error [A]	RMSE [A]	RMSE %
G	2.47	0	0.10	0.10	4.0
G_{ud}	2.47	0	0.12	0.12	4.9
G with k^*	2.47	0	0.10	0.10	4.0
G_{ud} with k^*	2.47	0	0.10	0.10	4.0
$APExG$ with k^*	2.47	0	0.10	0.10	4.0

Table 5.5: Goodness of the fits for all the models used for I_{sc} for *a-Si*, using the ground measured values of broad band irradiance.

<i>c-Si. BASED ON SOLIS IRRADIANCE</i>					
$\langle I_{sc} \rangle = 2.47A$					
Model	$\langle I_{sc} \rangle$ [A]	Bias [A]	Std.Error [A]	RMSE [A]	RMSE %
G	2.47	0	0.74	0.74	30.0
G_{ud}	2.47	0	0.74	0.74	30.0
G with k^*	2.47	0	0.72	0.72	29.1
G_{ud} with k^*	2.47	0	0.72	0.72	29.1
$APExG$ with k^*	2.47	0	0.72	0.72	29.1

Table 5.6: Goodness of the fits for all the models used for I_{sc} for *c-Si*, using the *SOLIS* values of broad band irradiance.

calculations based on *SOLIS* spectral irradiance; not even for *a-Si*. The relative statistical error is about 5.2% for *a-Si* and 4% for *c-Si*, however the absolute error is 3.3 times bigger for *c-Si* (due to the considerably smaller data set used for this module).

For the case of the models using *SOLIS irradiance* all the models, with no exception give the same results up to the first significant digit of *RMSE*, including the model I_{sc} vs G_{ud} with single fit. This shows that the non-existent variations introduced by the *UD* are insignificant in comparison to the huge data dispersion got when plotting measured short circuit current against a spectral parameter including *SOLIS* broad band irradiance.p to the first significant digit, the relative *RMSE* is 33% for *a-Si* and 28% for *c-Si*. The absolute *RMSE* for *c-Si* is 3.5 times the value for *a-Si*.

Chapter 6

CONCLUSIONS

In the endeavour of modeling short circuit current data with the consideration of spectral effects, we have gone through several stages: First the understanding of the spectral parameters *APE* and *UD*. These parameters were calculated with *SOLIS* spectral irradiance. In this process the satellite-based *Clear Sky Index k** showed to be a helpful parameter. Subsequently spectral models for the short circuit current were proposed, which employ these parameters. Afterwards, we occupied ourselves with recognizing the spectral effects in our two different sets of data: The one using measured values of short circuit current and global broad band irradiance, and the other using instead *SOLIS* broad band irradiance. After that analysis we applied the proposed models and finally arrived to this point, where we will give an overall view of the observations made throughout the work. We will see also the conclusions which can be drawn, which are meant to be guidelines for further research on the topic.

6.1 The Spectral Parameters *UD* and *APE*

By using the *SOLIS* spectral irradiance data for the calculation of the parameters *Used Fraction - UD* and *Average Photon Energy - APE*, we can conclude that:

1. *APE* is a spectral descriptor of the variations in the solar extraterrestrial spectrum due to atmospherical factors on Earth. With a single number a variety of spectral conditions can be resolved. *APE* would not be a good spectral descriptor in situations where the spectra can have any arbitrary variations; however as we said our case has a base case: the extraterrestrial spectrum. *APE* is a *device independent* parameter in the sense that its values depend only on the precision and accuracy of the spectral irradiance measurements/models employed for their calculations.
2. Differently, *UD* is a *device dependent* parameter because it is calculated using the spectral response of a *PV* device together with spectral irradiance data. *UD* is also a single positive real number strongly linked to the efficiency of the cell (P_{out}/P_{in}).
3. Despite the different approach in their definition, both parameters display a similar behaviour respect the global broad band irradiance, which is the reference parameter for modeling of short circuit current. This behaviours are far from being functional relations for low irradiance values; however as the irradiance increases, a tendency in that direction can be recognized.
4. The spectral variations resolved by these parameters are well correlated to the satellite-based *Clear Sky Index*. Because this index is calculated exclusively on the basis of the satellite derived *Cloud Index - n*, it suggests that the cloud variations are the main factor to which these parameters are sensitive. In this way, grouping the data by *Clear Sky Index* constitutes a useful tool for recognizing the influences of other factors like the ones related to Sun elevation and later on, when using measured data, effects due to the temperature of the *PV* devices. The grouping is so good that it seems to allow the definition of functions $UD(G)$ and $APE(G)$ for each group.
5. Strong variations of the parameters are observed for Sun elevations under 5° , when high Air Mass and high fraction of diffuse irradiance converge. The variation consists in a steep decay from 5° to 0° . However at such low angles the uncertainties in the *SOLIS* irradiance data and the *Clear Sky Index* values dramatically increase.

6. The amount of different spectral conditions that these parameters can resolve is undetermined because it depends on the number of spectral situations which can be found on Earth's surface, which is also undetermined. However the resolution power increases as the bandwidth of the spectral data used for their calculation is decremented. In the case of *SOLIS*, the bandwidths are not constant and are supposed to better resolve at wavelengths with considerable contributions in spectral power. In general *APE* can resolve more conditions than *UD*, however this varies for different *PV* materials. It has been observed that *a-Si*, with a higher relative response at the peak of the extraterrestrial spectrum, resembles *APE* more than *c-Si*, with a wider but slightly poorer relative response at the peak's location.
7. *UD* is interpreted as the ***Broad Band Photoelectrical Efficiency*** of a *PV* device at an incident power (irradiance): *generated current / incident power*. *UD* depends only on the spectral response of the device and the spectral distribution of the incident light. Because it may happen that the same power can be obtained with different spectra, the broad band photoelectrical response of a device changes in general with spectral variations. In general, for existing *PV* devices, *UD* increases as the conditions become cloudier. Therefore at fixed broad band irradiance it is expected that the device produce more current under cloudy conditions.
8. Care must be taken in the calculation of *UD*; it must be made with the spectral response curve (actual or relative) of the device and not with the quantum efficiency if the interpretation of *UD* as the *broad band photoelectrical efficiency* of this work is to be followed. Although one curve can be calculated from the other, the results obtained are not equivalent and therefore not comparable. Unfortunately I calculated *UD* for *CdTe* with the quantum efficiency curve and therefore these values cannot be compared to the ones of *a-Si* and *c-Si*.
9. *UD* variations for fixed cloud conditions depend on the spectral response of the device. For *only-blue* sensitive devices like *a-Si* the variation is negligible. For devices with broader responses (more sensitivity in *IR* range), a slight decay in the efficiency is observed as the Sun elevation increases. For cloudy conditions this variation is steeper. These changes are

associated with increasing broad band irradiance given the correlation between its increase and the increase in the Sun elevation angle.

10. *a-Si* exhibits more sensitivity to the significative spectral variations due to cloud conditions than *c-Si*. The opposite occurs when we talk about the smaller variations due to effects associated with Sun elevation (without considering very low Sun elevation values).
11. *APE* variations are noticeable for changing cloud conditions; the variation with Sun elevation related factors is small in comparison.

6.2 Modified Irradiances

The quantity $G_{uf} = UFxG$ or *Useful Irradiance* is the basis of this idea. When using *UD* instead of *UF*, we have $G_{ud} = UDxG$ or the ***Broad Band Photoelectrical Response*** of a *PV* device under the given irradiance. When using the true spectral response of the *PV* device, this quantity should match the short circuit current. Because the actual spectral responses and the relative ones are just scaled curves, the percentage variations obtained in the G_{ud} values in this work correspond to the expected variations in I_{sc} of the devices from which the curves were measured.

Extension of the idea to the parameter *APE* does not imply a functional relationship between *APExG* and I_{sc} , given that *APE* is a device independent parameter. *UD* for *a-Si* displayed a nearly linear relationship with *APE* when data for angles under 5° is not considered. For *c-Si* the dispersion of the data is much higher.

6.3 Spectral Effects on *PV* Devices

6.3.1 Predictions Based on *SOLIS* Spectral Irradiance

The *SOLIS* spectral data used together with the spectral responses of the *PV* devices predict the existence of variations in the I_{sc} values due to variations in their efficiency under different spectral

conditions. The magnitudes of these variations from clear sky to overcast conditions are*:

- ***a-Si***: +12%
- ***c-Si***: +8%

The intermediate cloud conditions also display increase respect the clear sky condition, especially for the *thin film* technology *a-Si* (see table 4.8).

6.3.2 Spectral Effects on the Measured Data

Ideally we should observe the same variations when we replace G_{ud} by the measured I_{sc} . In this case we should have the following correspondence:

- Plots UD vs $G \leftrightarrow I_{sc}/G$ vs G
- Plots G_{ud} vs $G \leftrightarrow I_{sc}$ vs G

However the expected variations cannot be observed, not for *a-Si* nor for *c-Si*. This occurs either when we use the global broad band irradiance values from ground measurements or from *SOLIS*. It was expected that despite the interpolation of the measured data to the *SOLIS* data times, the spectral effects could be observed, at least using the measured values of I_{sc} and G .

The results suggest that in the case of using ground measured broad band irradiance, there are temperature effects which affect data which have been already temperature *corrected*. This occurs for data of the group with the highest average value of k^* with high values of irradiance (above $500W/m^2$). This may have 3 explanations:

1. Underestimation of the temperature coefficient used by the measurement device for calculation of the *temperature corrected* values of global broad band irradiance.

*The values were calculated based on the increase of the slope of the line $G_{ud}(G)$ from a fixed Clear Sky Index group to other. The reference group corresponds to clear sky conditions.

2. The temperature of the sensor cell is assumed to be the temperature of the modules.
3. Insufficient accuracy in the temperature coefficients used for the *temperature corrections* of the short circuit current values of the modules.

For this work a *ready to go* set for measurements of characteristic curves of *PV* modules was used, which employs a *combi* sensor for irradiance and temperature. The irradiance sensor is a *mono c-Si* cell and the temperature sensor is a *PT-1000*. The weaknesses of these measurements are the fact that the irradiance sensor is subject to spectral and temperature effects in the same fashion as the devices investigated. The other inaccuracy is that temperature is not measured directly on the modules but on the sensor cell.

In accordance with the predictions in the variations in the G_{ud} values, estimations about the precision required in the short circuit current values were made. This precision should allow the observation of the spectral variations due to cloud conditions in the plots of I_{sc} vs G . In the case of 100% precision in the G values, precisions of $3mA$ and $10mA$ at $50W/m^2$ were estimated for *a-Si* and *c-Si* respectively. In reality higher precisions are required given that we have uncertainty in the G values. Furthermore the uncertainties in both values increase when interpolating data, pushing to higher precisions in the measurements.

As usual in outdoor characterization of *PV* devices, distinguishing the influences due to different factors was difficult or not possible. Under clear sky conditions and at high Sun elevations, it was not possible to distinguish the effects due to low Air Masses and temperature. For low Sun elevations and given that *SOLIS* and measured data correspond to horizontal surface, we have combined effects of high Air Mass, high diffuse fraction and related to albedo which can not be discriminated. The overall effect seen as decrease in the spectral parameters *UD* and *APE* for low Sun elevations and reduction in the ratio I_{sc}/G , may be explained as the dominance of the reddening trends due to increased Air Mass over the other factors.

Using the *SOLIS beam* irradiance component of irradiance (broad band and spectral), may be used for gaining understanding on the effects at low Sun elevations. However a first attempt indicated

that the *SOLIS* model for diffuse and beam irradiance does not work well at low Sun elevations.

6.4 SOLIS

The *SOLIS* global broad band irradiance data has the attribute that is not sensitive to variables as temperature and therefore don't display bias which we had in the measured data. However the overall error is of considerable magnitude respect to the error of the ground measured irradiance.

The *RMSE* values of *SOLIS* for broad band irradiance for 10 minutes intervals is about 30%. It happened that the overall error in modeling I_{sc} with *SOLIS* data is very close to this value. Besides, if we assume that the spectral variations modeled with the spectral irradiance of *SOLIS* are close to the reality, we end up with the conclusion that *SOLIS* broad band irradiance cannot resolve fluctuations in measured values of I_{sc} which are about 10% (due to spectral effects). Even if we use hourly values the panorama does not improve because the *SOLIS* error reduces only to about 20% and also the spectral variations are smoothed when averaging data for one hour. Therefore according to my view, resolving spectral effects with *SOLIS* irradiance would require a huge improvement in its reliability at short time intervals (*RMSE* about 5%), which could be quite challenging nowadays. However in the case that *SOLIS* irradiance is definitely used for modeling short circuit current, and assuming that the precision of these values is high enough; it may happen that the models including spectral effects give better results for long term measurements. This is especially likely for locations with permanent cloudy situations and may be due to reduction in the bias of the fit.

An alternative approach for modeling I_{sc} for sites with measurements of global broad band irradiance would be simply the model called in this work I_{sc} vs G with k^* [†]. For this work the k^* values were calculated from the satellite *Cloud Index - n* values. However another possibility remains: Derive the k^* values from the measurements of global broad band irradiance and the values of the same quantity for clear sky conditions modeled with the *Clear Sky Module* of *SOLIS*. This approach may be more reliable than the previous one, because for situations of low irradiance the reflectivity

[†] k^* is defined as the ratio of global broad band irradiance and the clear sky global broad band irradiance.

measurements used by the satellite for calculation of the n values fails. Equally improvements in the spatial resolution may be obtained with this new approach.

6.5 Final Comments and Suggestions

- **Recognizing spectral effects** with ground measured broad band irradiance is a must before modeling the data.
- **Knowledge of the spectral response** of the modules under investigation is required. In this way we would know exactly how the things we expect look like. This might mean measuring them given that they are quite difficult to find, except for rare cases. The other approach would be to find modules for which the responses are available and buy or rent them for the research. This may be more practical, economical and less time consuming.
- **Validation** of the *SOLIS* spectral irradiance cannot be postponed if this work is going to be continued. It is a requisite for a scientific and methodic work. This validation may clarify aspects of this work which up to now remain in the level of speculation.

Appendix A

Short Recapitulation on the Solar Spectrum

The variable atmospherical conditions (clouds, aerosols, humidity, Ozone concentration, etc) affect not only the amount of energy we receive on a certain location on Earth's surface but the distribution of this energy in the spectrum. Reflection, absorption and scattering phenomena take place in the atmosphere. All of them affect the solar irradiance received on Earth. Absorption and scattering are the processes which mainly produce the variations of the solar spectra we measure on Earth, all of them from a unique spectrum which remains nearly constant in time: the extraterrestrial spectrum. The reflection processes produce intensity attenuation; the absorption processes produce absorption peaks in the spectra and the scattering processes cause wavelength shifts of them and also attenuation of intensity. The main absorbers in Earth's atmosphere are O_3 , H_2O , O_2 , CO_2 and clouds. The scattering is due to aerosols*, air molecules, water droplets, etc. There are 2 principal types of scattering:

- Rayleigh Scattering: is a wavelength-selective scattering produced mainly by small size par-

*Aerosols are minute particles that contribute to the visibility reduction and reddening of sunrises and sunsets. Upper atmosphere aerosols scatter sunlight while lower atmosphere aerosols change the absorption and reflection properties of clouds. Aerosols are classified in volcanic, desert dust and human-made (sulfate aerosols).

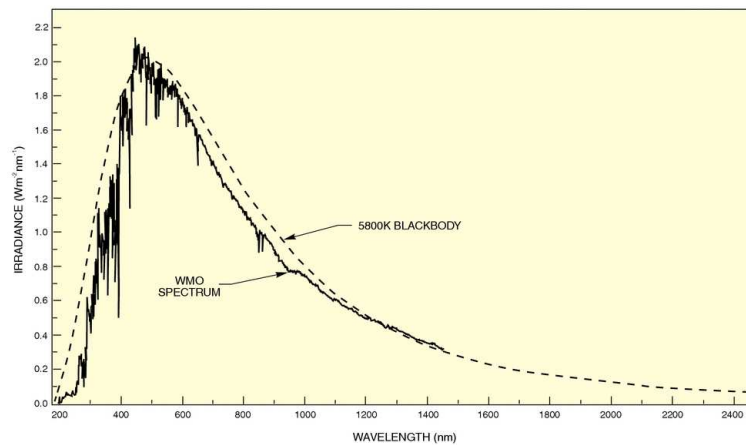


Figure A.1: Spectral irradiance density of: a) Black body at 5800K. b) Sun at Earth's outer atmosphere (dashed line) [17].

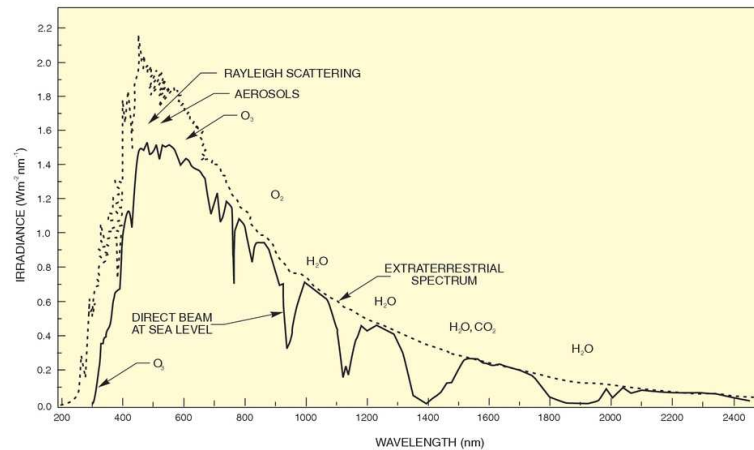


Figure A.2: Spectral direct irradiance density of: a) Sun at Earth's outer atmosphere (dashed line) b) Sun at Earth's surface (sample). Location at sea level. The main atmospherical absorption and scattering effects are displayed. [17].

ticles.

- Mie Scattering: non-selective scattering produced by bigger size particles as the ones in clouds.

Sun Elevation [°]	AM	Absorption [%]	Rayleigh Scattering [%]	Mie Scattering [%]	Total Attenuation [%]
90	1.00	8.7	9.4	0-25.6	17.3-38.5
60	1.15	9.2	10.5	0.7-29.5	19.4-42.8
30	2.00	11.2	16.3	4.1-44.9	28.8-59.1
10	5.76	16.2	31.9	15.4-74.3	51.8-85.4
5	11.5	19.5	42.5	24.6-86.5	65.1-93.8

Table A.1: Attenuation processes in the Earth's atmosphere and their attenuation contribution as function of Air Mass [7]

In table A.1 a list of the different principal attenuation processes in the atmosphere as function of the Air Mass ($AM = 1/\sin\gamma_s$) and their contributions is shown.

A.1 Standard Spectra

It will be useful to bear in mind some of the spectra which are currently used as reference or for indoor characterization of *PV* modules.

Two organizations can be referenced which publish standard spectra: The *CIE* (Committee International d'Eclairage or International Commission on Illuminance) and the *ASTM* (American Society for Testing and Materials). In table A.2 several standard spectra are characterized according to these two sources.

Spectrum	Standard	Power Density [W/m ²]		
		Total	250nm-2500nm	250nm-1100nm
Extraterrestrial	WM0	1367		
AM 0	ASTM E 490	1353	1302.6	1006.9
AM 1	CIE Pub. 85 Tab. 2		969.7	779.4
AM 1.5D	ASTM E 891	768.3	756.5	584.7
AM 1.5G	ASTM E 892	963.8	951.5	758.6

Table A.2: Power density of standard spectra. The *ASTM* spectra are given for a 37° tilted surface, turbidity of 0.27 and ground albedo of 0.2; representative values for the continental contiguous states of the USA. [17].

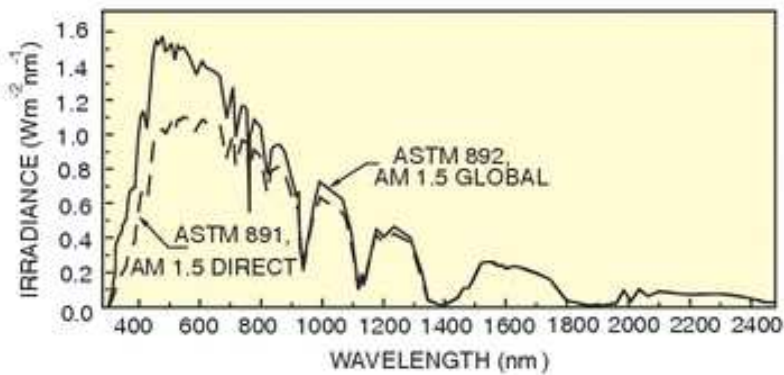


Figure A.3: Spectral irradiance density of: a)ASTM 1.5D spectrum (dashed line). b)ASTM 1.5G spectrum. [17].

Appendix B

Other Plots for the Data Sets Used for the Short Circuit Current Modeling

In this chapter several additional figures corresponding to the sets of data used for the discussion of chapter 5 are found. We have two different sets, one for *a-Si* and the other for *c-Si*.

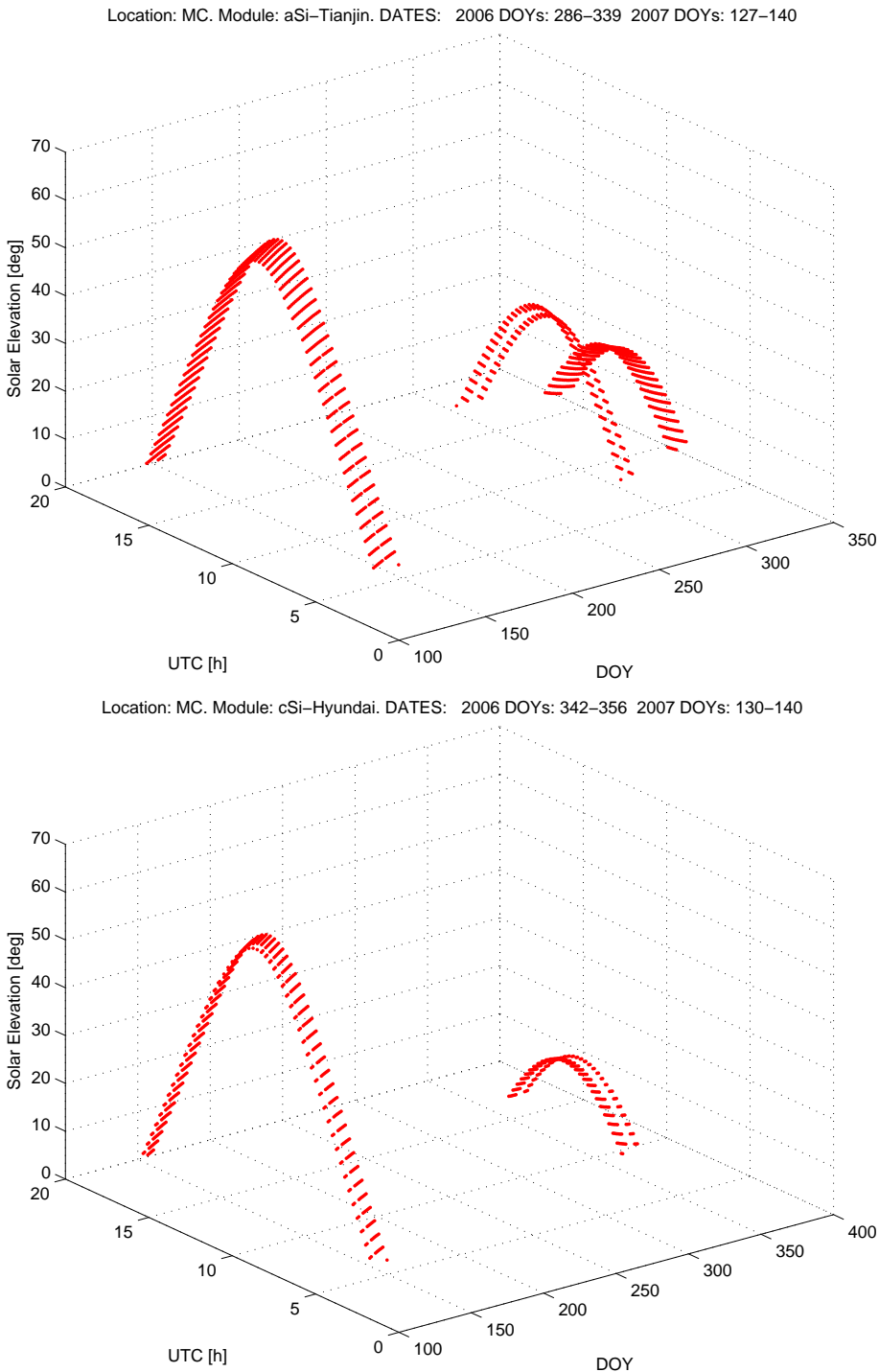


Figure B.1: Time series of calculated Sun Elevation γ_s . Top: *a-Si*. Bottom: *c-Si*.

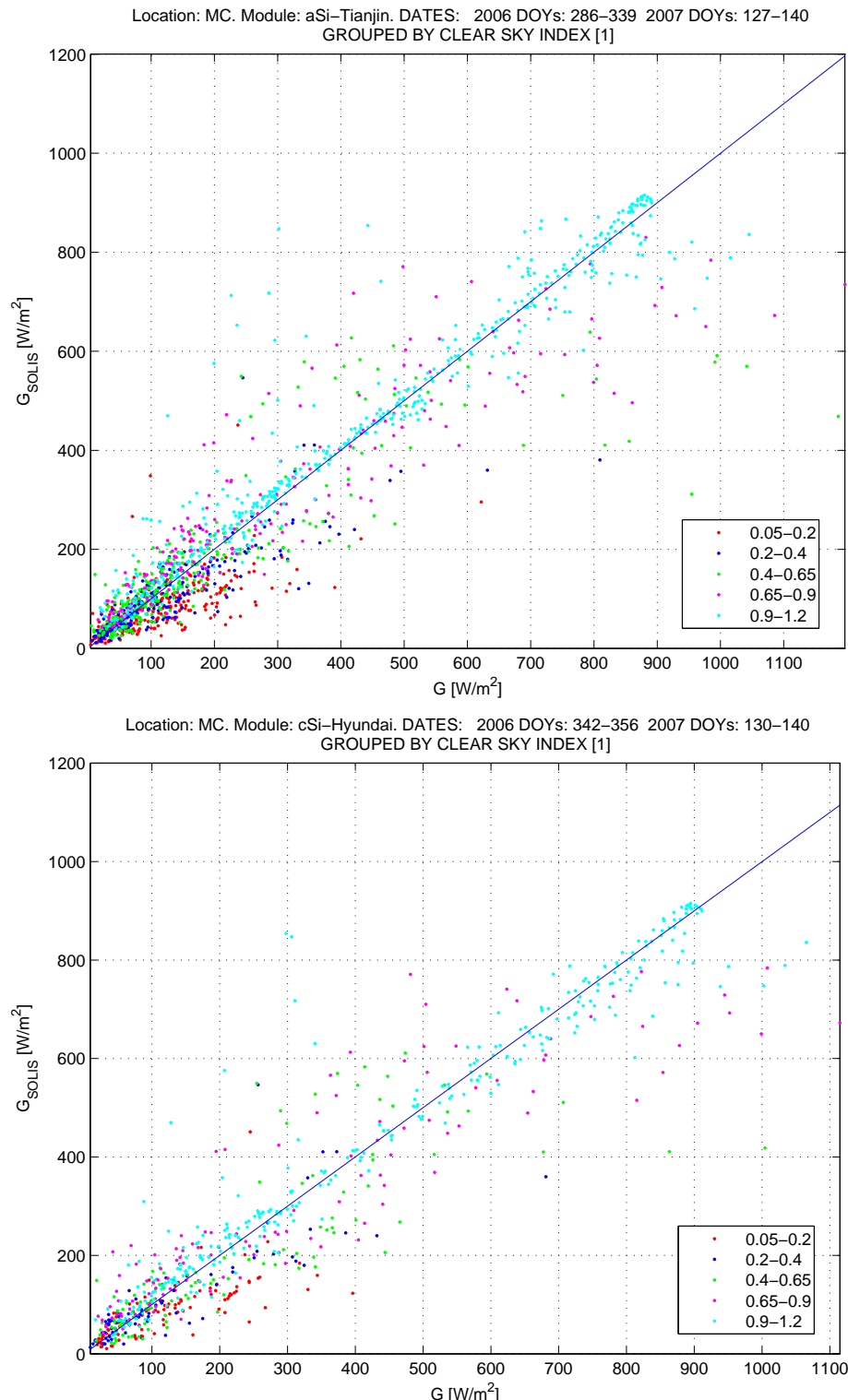


Figure B.2: *SOLIS* global broad band irradiance against ground measured global broad band irradiance for the data used in the I_{sc} model analysis. Top: *a-Si*. Bottom: *c-Si*.

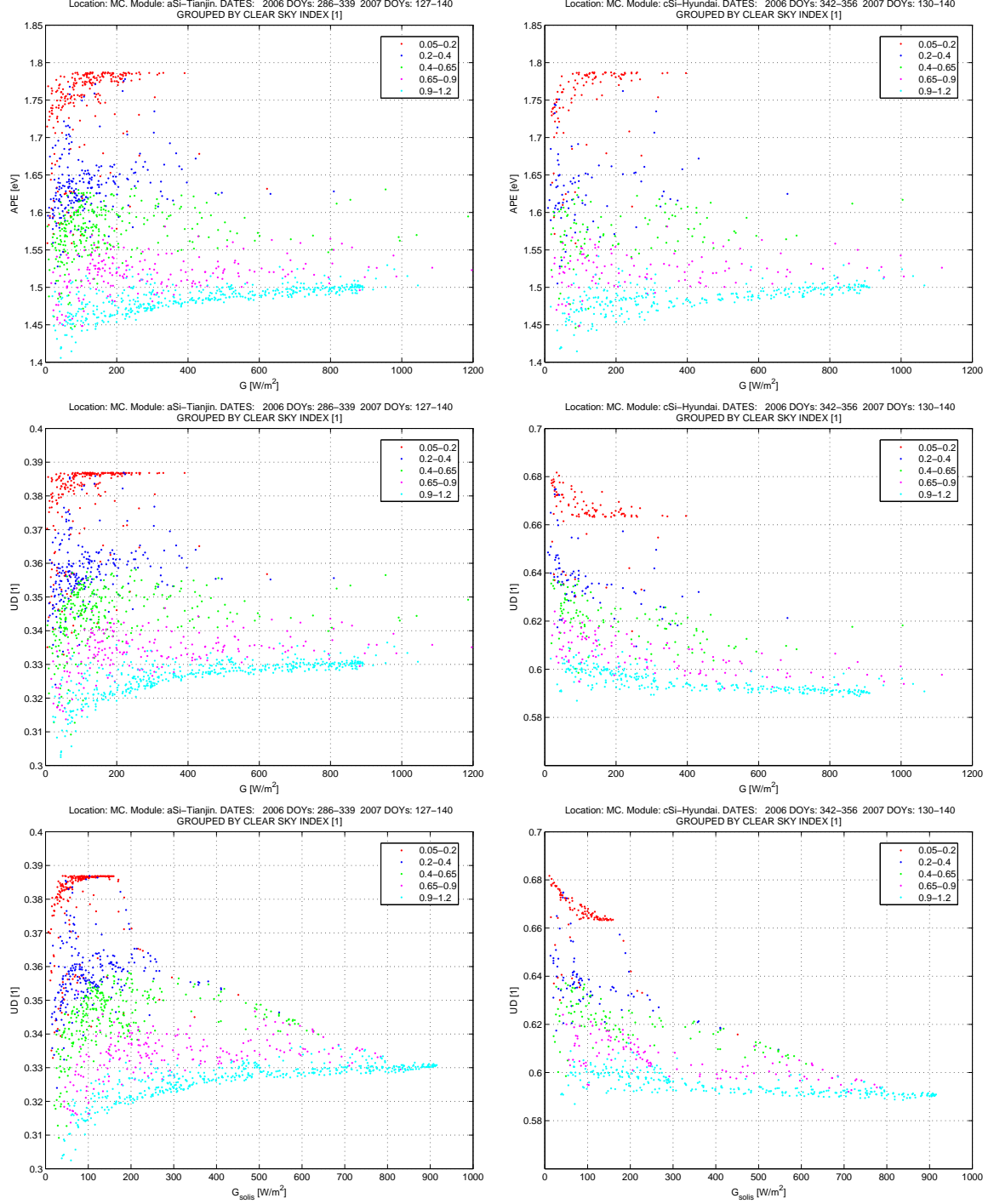


Figure B.3: Spectral parameters APE and UD for the sets of data used in the I_{sc} modeling analysis. Left: *a-Si*. Right: *c-Si*. Top: APE vs G . Middle: UD vs G . Bottom: UD vs G_{solis} . The parameters are calculated using the *SOLIS* spectral irradiance.

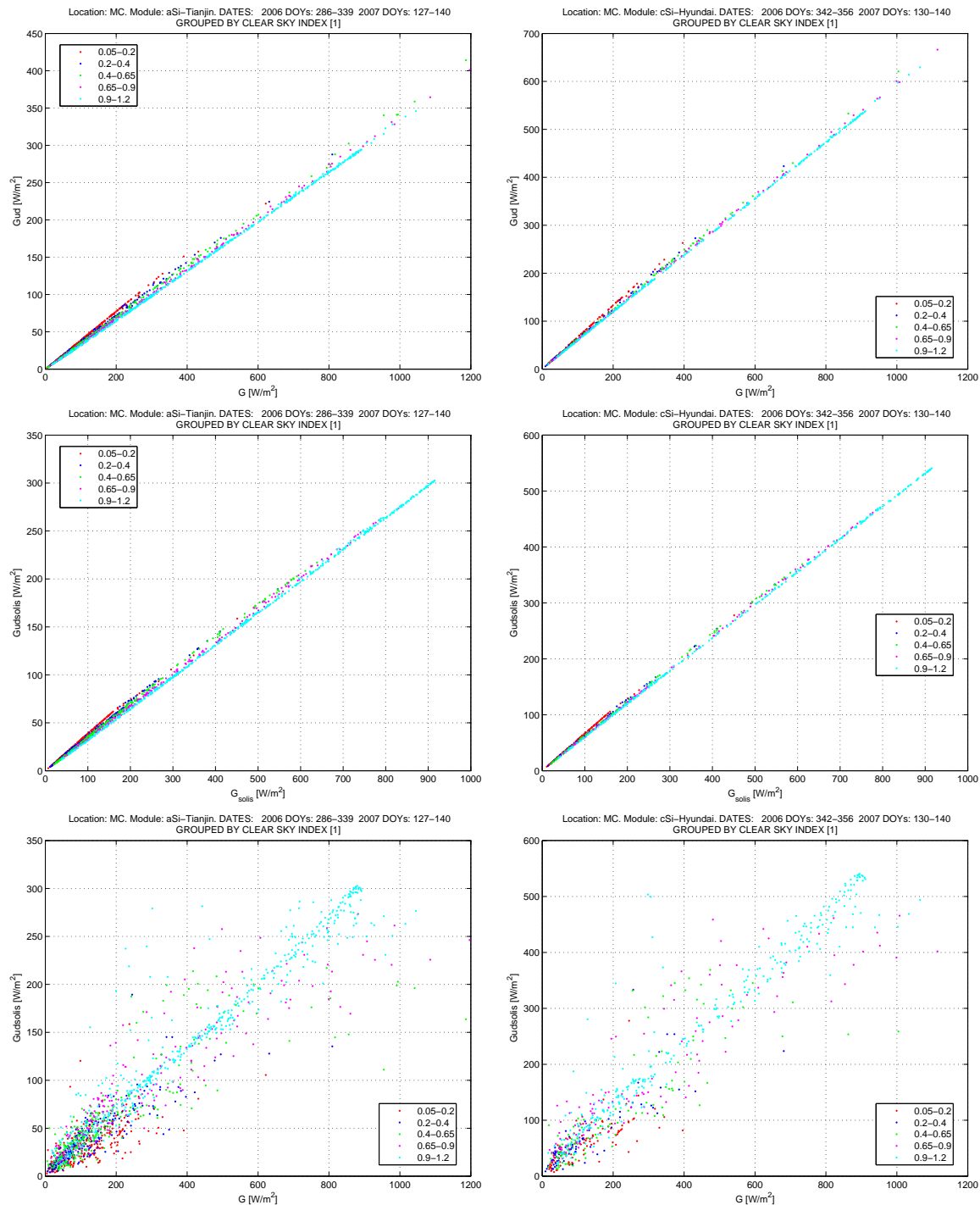


Figure B.4: Used Irradiance against global broad band irradiance. Top: G_{ud} vs G , Middle: $G_{udsolis}$ vs G_{solis} , Bottom: $G_{udsolis}$ vs G . Left: *a*-Si, Right: *c*-Si.

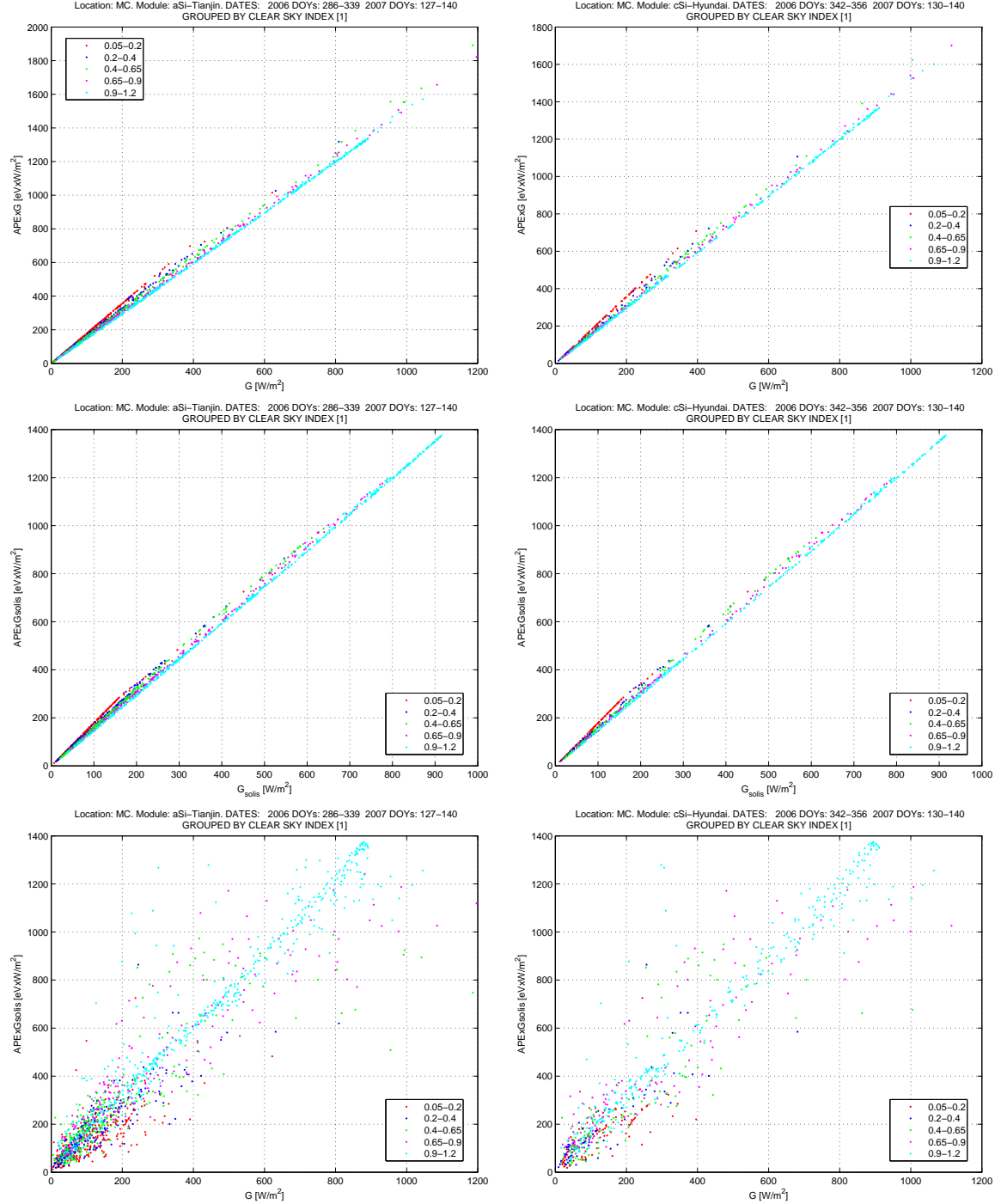


Figure B.5: Modified irradiance $APExG$ against global broad band irradiance. Top: $APExG$ vs G , Middle: $APExG_{solis}$ vs G_{solis} , Bottom: $APExG_{solis}$ vs G . Left: a-Si, Right: c-Si.

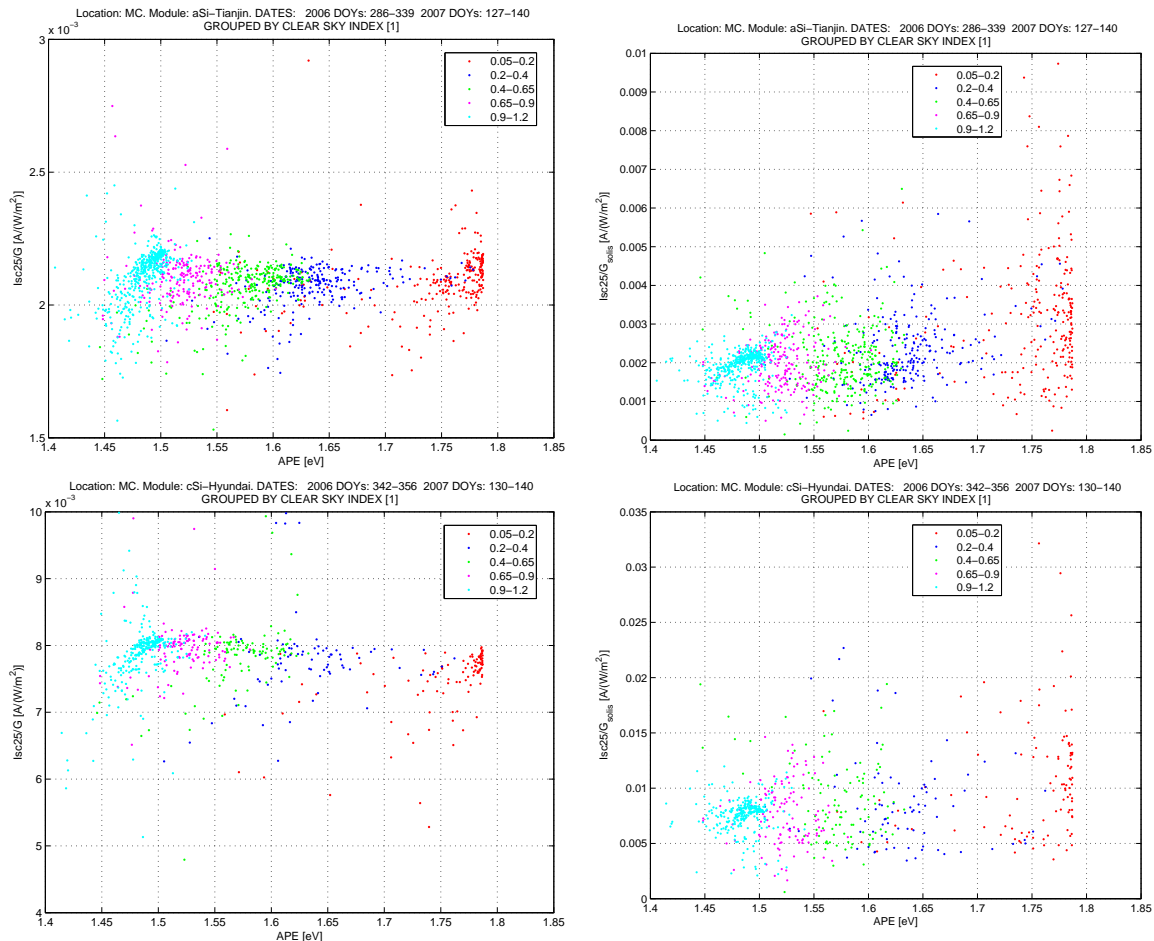


Figure B.6: I_{sc25}/G and I_{sc25}/G_{solis} vs APE.

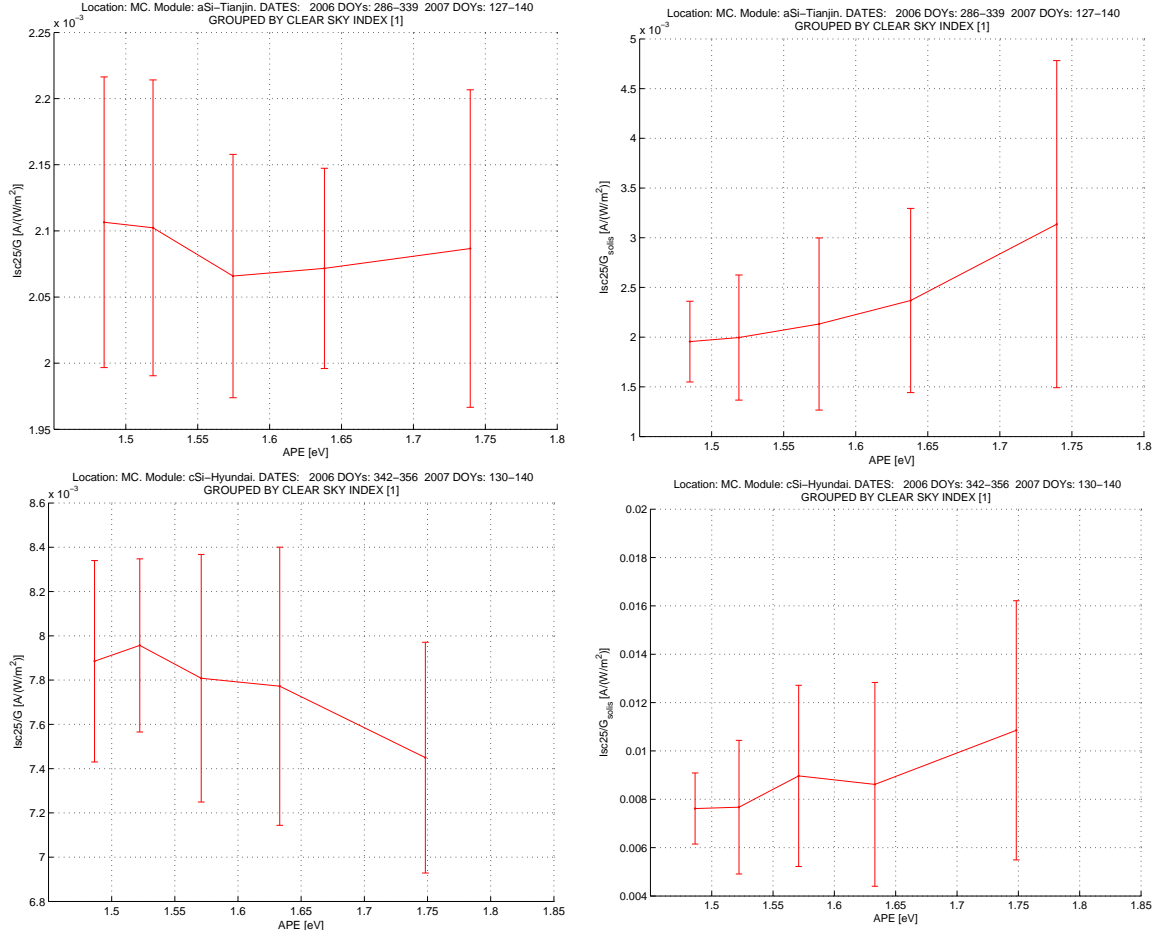


Figure B.7: I_{sc25}/G and I_{sc25}/G_{solis} vs APE . Bins of data have been made according to the Clear Sky Index groups. The error bars correspond to the standard deviation of the bin.

Appendix C

Abbreviations

In this appendix, the list of the main abbreviations used in this document is presented.

- AM : Air Mass. Calculated as the inverse of the sine of γ_s .
- APE : *Average Photon Energy*.
- G : Ground measured global broad band irradiance.
- G_{solis} : *SOLIS* global broad band irradiance.
- G_{ud} : *UD* times G .
- $G_{udsolis}$: *UD* times G_{solis} .
- G_λ : Spectral broad band irradiance. All are *SOLIS* values.
- γ_s : Sun elevation.
- I_{sc} : Short circuit current measured values.
- I_{sc25} : Short circuit current values calculated at $25^\circ C$ PV cell temperature from measured values.

- I_{scca} : Short circuit current values calculated from models.
- I_{sc25ca} : Short circuit current values calculated at 25°C PV cell temperature from modeled values.
- k^* : Clear Sky Index.
- λ : Wavelength.
- n : Cloud Index.
- ϕ_λ : Photon flux at wavelength λ .
- φ_s : Sun azimuth.
- **SOLIS**: *Solar Irradiance Scheme*.
- **SPARs**: Spectral parameters
- SR_λ : Spectral response of a PV device.
- T : PV device temperature.
- UD : Broad band photoelectrical efficiency.
- UF : *Useful Fraction*

Bibliography

- [1] BERNHARD MAYER, E. A. *libRadtran: Library for Radiative Transfer Calculations*. Downloadable at: <http://www.libradtran.org/>, December 2006.
- [2] BETTS, T. R. *Investigation of Photovoltaic Device Operation under Varying Spectral Conditions*. PhD thesis, Loughborough University, 2004.
- [3] BEYER H.G., E. A. *Modellierung der Abhaengigkeit des Kurzschlussstroms von a-Si Modulen von der Meteorologischen Situation. 18. Symposium Phtovoltaische Solarenergie. OTTI. Ostbayrisches Technologie Transfer Institut e.V.* (2003).
- [4] FIELD, H. *Solar Cell Spectral Response Measurement Errors Related to Spectral Band Width and Chopped Light Waveform*. 26th IEEE Photovoltaic Specialists Conference, 1997.
- [5] FIRST SOLAR. First Solar Documetation Kit. Next Generation Thin-Film PV Modules: Module Characterization: Spectral Response PD-5-422, first ed. 4050 E. Cotton Center #6-68. Phoenix, AZ 85040, USA, July 2005.
- [6] HAMMER, A. *Solarspezifische Solarstahlungsinformationen aus Meteosat-Daten*. PhD thesis, Carl von Ossietzky Universitaet Oldenburg, 2000.
- [7] HASELHUHN RALF, E. A. *Photovoltaische Anlagen*. Deutsche Gesellschaft fuer Sonnenenergie, 2002.

- [8] KENNY R.P., E. A. *Spectral Effects on the Energy Rating of Thin Film Modules*. European Comission Joint Research Centre Renewables Energies-Environment Institute, Date not specified .
- [9] KENNY R.P., E. A. *Energy Rating of PV Modules Based on PVGIS Irradiance and Temperature Database*. Preprint Proceedings 21st European Photovoltaic Solar Energy Conference and Exhibition in Dresden, Germany, October 2006.
- [10] KENNY R.P., E. A. *Energy Rating of Diverse PV Module Technologies Through Indoor and Outdoor Characterisation*. European Comission Joint Research Centre Renewables Energies-Environment Institute. European Solar Testing Installation ESTI, Ispra, Italy, . Date not specified.
- [11] KROENI R., E. A. *Energy Rating of Solar Modules*. Final Report PV P+D, DIS47456 / 87538, February 2005.
- [12] LORENZ ELKE, E. A. *Deliverable D4.2 Improved Difusse Irradiance Model*. Under the project: *Intelligent Performance of PV System Operation Based on Satellite Data*, October 2004.
- [13] MUELLER RICHARD, E. A. *Documentation of the SOLIS software package for solar irradiance retrieval. Program version v1.01 beta*. Under the project: *Energy-Specific Solar Radiation Data from Meteosat Second Generation: The Heliosat-3 Project*, March 2004.
- [14] MUELLER RICHARD., E. A. *Rethinking Satellite-Based Solar Irradiance Modelling*. *Rem. Sens. Environ.* (2004), 160–174.
- [15] PV-ENGINEERING GMBH. PVPM 1000C Peakleistungs- und Kennlinienmessgert. Benutzerhandbuch, second ed. Reinickendorfer Str. 2 58642 Iserlohn, Germany, July 2004.
- [16] QUASCHNING, V. Regenerative Energie Systeme. Carl Hansen Verlag, 1999.
- [17] SPECTRA-PHYSICS. *Introduction-to-Solar-Radiation*. <http://www.newport.com/Introduction-to-Solar-Radiation> by Oriel, Corion and Richardson Gratings products.

- [18] WILSON H.R, E. A. *Energetic Relevance of Solar Spectral Variation on Solar Cell Short Circuit Current.* *Solar Energy* 42, 3 (1989), 273–279.